CONF-9405328--Abstr.

UCRL-ID-114972-2

SERS Internship
Spring 1994 Abstracts and Research Papers

Barry Goldman

May 6, 1994

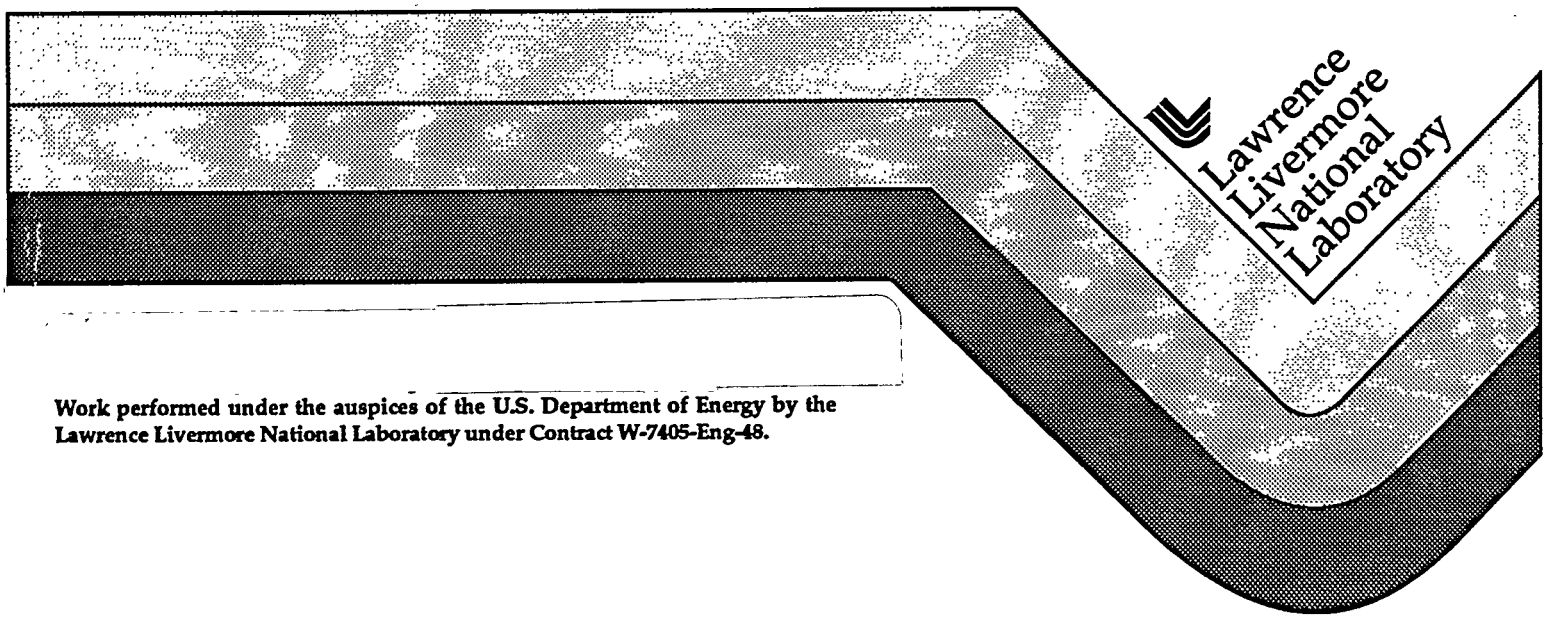

Work performed under the auspices of the U.S. Department of Energy by the Lawrence Livermore National Laboratory under Contract W-7405-Eng-48.

SCIENCE & ENGINEERING

SERS

RESEARCH SEMESTER

Lawrence Livermore National Laboratory

Spring 1994

ABSTRACTS FOR STUDENT SYMPOSIUM

May 6, 1994

Sponsored by:

The U.S. Department of Energy
Office of Energy Research

DISCLAIMER

DISCLAIMER

Portions of this document may be illegible in electronic image products. Images are produced from the best available original document.

SCIENCE & ENGINEERING

SERS

RESEARCH SEMESTER

Spring 1994 Student Symposium Abstracts

Table of Contents

The Effect of Increased Levels of Carbon Dioxide on Chlorophyll Fluorescence and Photosynthetic Pigments in *Pinus ponderosa*

David Anschel
State University of New York at Buffalo
Division of Health and Ecological Assessment

ABSTRACT

Levels of atmospheric carbon dioxide have been increasing at an unprecedented rate in modern times. In response to this situation, we have initiated a long-term study of a forest species' response to elevated carbon dioxide levels. Specifically we have been looking at effects upon photosynthesis utilizing chlorophyll fluorescence and pigment assays. A preliminary analysis of the data indicates that depending on the tree's geographic origin there are different responses to the treatments as indicated by the relative efficiencies of photochemical electron flow in photosystem II. Regardless of geographic origin there was a decrease in photosynthetic pigments in the treatment groups.

Corrosion Effects of Carbon-Steel on the Durability of Well Emplacements at the Nevada Test Site

Patricia C. Hankenson
Texas Christian University
Nuclear Chemistry Division

ABSTRACT

At the Nevada Test Site, Area 25, the USW H-5 well carbon-steel access tubing exhibited severe corrosion for the short down-hole time that it was in place. A baseline groundwater chemical composition from previous water analyses of the H-5, J-12, and J-13 wells was created. Samples taken in 1994 were analyzed for the various major, minor and trace elements using the ICP-MS and ICP-ES methods. The Cl- content was analyzed using the IC method. The results from these tests were included in this baseline. The carbon steel access tubing was analyzed by SEM to determine its content and what elements of its content might have caused it to be susceptible to corrosion. This data was also added to the baseline to determine any mixing effects that might have occurred between the water and the access tubing elements. The corrosion products were analyzed by X-ray diffraction. The conclusions made from all of these observations point toward a cause for the corrosion, any polluting effects in the groundwater, and a way to avoid this type of corrosion in the future.

Evaluating the Use of an ISDN line to Deliver Interactive Video Educational Experiences to Students

David Michaels
New Jersey Institute of Technology
Computations Division

ABSTRACT

We will use the 128 kilobit/sec ISDN connection from the Lawrence Livermore National Laboratory to the Livermore High School Math Learning Center to provide students there with interactive multimedia educational experiences. These experiences may consist of tutorials, exercises and interactive puzzles to teach students' course material. We will determine if it is possible to store the multimedia files at LLNL and deliver them to the student machines via FTP as they are needed. An evaluation of the effect of the ISDN data rate is a substantial component of our research and suggestions on how to best use the ISDN line in this capacity will be given.

Separation of a DNA Oligomer Bound by the Carcinogen 2-Amino-1-methyl-6-phenylimidazo {4,5-*b*}pyridine using Capillary Electrophoresis

Truc Ngoc Nguyen
California Polytechnic State University
Department of Biology and Biotechnology

ABSTRACT

2-amino-1-methyl-6-phenylimidazo{4.5-b}pyridine (PhIP) is a mutagenic and carcinogenic substance found in meat cooked (especially grilled) at high temperatures. PhIP is known to bind DNA covalently through the C-8 position of guanine, yet little is known about the identity of other PhIP-DNA complexes, or what conformation the PhIP molecule assumes upon binding DNA. We therefore applied the technique of capillary electrophoresis (CE) to separate, purify, and characterize nucleotides and oligonucleotides bound by PhIP molecules.

PhIP adduct to the oligodeoxynucleotide 5' dCCTACGCATCC 3' was synthesized in modest yields, with 5% of the oligomer containing one PhIP adduct at the central guanine. The UV spectrum of this carcinogen modified DNA oligomer showed 2 major PhIP aDduct species with absorbance wavelength maxima of 346 and 380 nm. Oligonucleotides bound with PhIP were easily separated from unbound oligonucleotides by electrophoresing through coated capillaries at high voltages (10-20 kV). The electropherogram from the CE experiments revealed at least two PhIP adducts. Based on these electropherograms, we were able to assign adduct molar absorbance at 355 nm of 17,000 $M^{-1}cm^{-1}$ and 19,000 $M^{-1}cm^{-1}$ for the slower and faster migrating PhIP adducts, respectively.

Development of a Method for Detecting Aneuploid Mouse Sperm by Simultaneous Three Probe Fluorescence *In situ* Hybridization

Shannon O'Hogan
University of Notre Dame
Biology and Biotechnology Research Program

ABSTRACT

Aneuploidy in male germ cells can cause serious complications during development and after birth such as spontaneous abortions, birth defects and infertility. Efficient animal models are necessary to investigate the mechanism and induction of aneuploidies. Previously, detecting chromosomal domains and aneuploidy frequencies by fluorescence *in situ* hybridization (FISH) was carried out on testicular cell preparations and only late-step spermatids were investigated. It is difficult to distinguish late-step spermatids in the testicular prep, which includes all different stages of spermatogenic cells from stem cells to late-step spermatids. However, all the sperm in the epididymis have completed meiosis II and contain a haploid number of chromosomes creating a homogenous population of cells. We present a method to detect chromosomal domains and aneuploidy on murine epididymal sperm cells using FISH with DNA probes specific for chromosome 8, X and Y simultaneously. Epididymal sperm were scored on a Rb(2.8)_ mouse which carries a Robertsonia chromosome containing chromosome 2 and 8. Mice heterozygous for this translocation are known to produce elevated frequencies of aneuploid gametes. In initial experiments the sperm bearing fluorescence phenotype X8 and Y8 are each 49.9% as predicted. The efficiency of this method is further evident by the low percent of sperm that did not hybridize (~4%). Research is in progress to apply this method to sperm of Robertsonian and normal mice to validate this method.

Human Iron-Sulfur Protein Gene Mapped to Chromosome 19

Len Alexander Pennacchio
Sonoma State University
Biology and Biotechnology Research Program

ABSTRACT

The principal goal of our laboratory is to discover new genes on Human Chromosome 19. The Rieske Iron-Sulfur Protein participates in the electron transport mechanisms necessary for cellular respiration. An oligonucleotide probe made from the Rieske-cDNA sequence hybridized to DNA from somatic cell hybrids containing only Chromosome 19. This finding strongly suggests that Chromosome 19 is the location of the gene encoding the Rieske Iron-Sulfur Protein. Finding a piece of DNA from Chromosome 19 containing the sequence of the Rieske gene would unambiguously assign its absolute location in the human genome. We were able to isolate a cosmid clone by hybridization, containing only Chromosome 19 DNA, that was homologous to the Rieske cDNA. By developing new techniques to sequence cosmids directly, the cosmid we isolated was sequenced and confirmed to be homologous to the Rieske cDNA. Additionally, flourescent *in situ* hybridization mapped this cosmid to location 19q12 of the human genome.

Production of Hydrogen from Municipal Solid Waste

Robert S. Rogers, III
Rutgers University
Chemistry & Materials Science Division

ABSTRACT

As fossil fuel reserves run lower and lower, and as their continued widespread use leads toward numerous environmental problems, the need for clean and sustainable energy alternatives becomes ever clearer. Hydrogen fuel holds promise as such an energy source, as it burns cleanly and can be extracted from a number of renewable materials such as municipal solid waste (MSW), which is considered to be largely renewable because of its high content of paper and biomass-derived products. A computer model is being developed using Aspen Plus ™ flowsheeting software to simulate a process which produces hydrogen gas from MSW; the model will later be used in studying the economics of this process and is based on an actual Texaco coal gasification plant design. This paper gives an overview of the complete MSW gasification process and describes in detail the way in which MSW is modeled by the computer as a process material, and how the gasifier unit itself is modeled, which is responsible for the simulation of the MSW being heated under pressure and reacting to form a mixture of gases which include hydrogen.

Analysis of the Acoustic Spectral Signature of Prosthetic Heart Valves in Patients Experiencing Atrial Fibrillation

David D. Scott
University of Kansas
Heart Valve Research Team

ABSTRACT

Throughout an average human life span the heart beats some three billion times never stopping to rest except for a fraction of a second between beats. This most important muscle often operates flawlessly, however, in some cases a dysfunction can prove life threatening. Prosthetic heart valves have increased the life span of many patients with life threatening heart conditions. These valves have proven extremely reliable adding years to what would have been weeks to a patient's life. Prosthetic valves, like the heart however, can suffer from this constant work load. A small number of valves have experienced structural fractures of the outlet strut due to fatigue. To study this problem a non-intrusive method to classify valves has been developed. By extracting from an acoustic signal the opening sounds which directly contain information from the outlet strut and then developing features which are supplied to an adaptive classification scheme (neural network) the condition of the valve can be determined.

The opening sound extraction process has proved to be a classification problem itself. Due to the uniqueness of each heart and the occasional irregularity of the acoustic pattern it is often questionable as to the integrity of a given signal (beat), especially one occurring during an irregular beat pattern. A common cause of these irregular patterns is a condition known as atrial fibrillation, a prevalent arrhythmia among patients with prosthetic heart valves.

Atrial fibrillation is suspected when the ECG shows no obvious P-waves[1,2]. The atria do not contract and relax correctly to help contribute to ventricular filling during a normal cardiac cycle[1]. Sometimes this leads to irregular patterns in the acoustic data. This study compares normal beat patterns to irregular patterns of the same heart. By analyzing the spectral content of the beats it can be determined whether or not these irregular patterns can contribute to the classification of a heart valve or if they should be avoided. The results have shown that the opening sounds which occur during irregular beat patterns contain the same spectral information as the openings which occur during a normal beat pattern of the same heart. Therefore, these beats can be used for classification without concern for the integrity of their spectral pattern.

CAFE: Computer Aided Fabric Evaluation

James E. Sims
Jackson State Unviersity
Engineering Research Division

ABSTRACT

With the intent of automating the inspection of fabrics for defects, the Engineering Research Division in conjunction with the textile industry has initiated the CAFE project. The project's objective is predicated on the development, implementation and testing of an algorithm for the inspection of color printed fabrics. We attempt to take advantage of the wide ranging applications possible with Computer Vision in order to achieve this. The first job of the algorithm is to teach the computer the 'correct' printed patterns by using a defect-free repeat from the pattern. Once this is learned the computer, using the 'correct' repeat as the reference, tests the remaining repeats in the pattern. There are two different ways to go about doing the first job and with this paper we will describe both methods.

Chromium Removal from Groundwater by Ion Exchange Resins

Panagiotis Skiadas
University of Florida
Environmental Restoration Division

ABSTRACT

The groundwater at several monitoring wells at LLNL has been found to exceed Surface Water Discharge Limits for Cr(VI). Ion exchange resins have been selected for its removal. A research study is underway to determine which commercial resin is preferred for LLNL's groundwater - based on chromate absorbance capacity, regeneration efficiency, and pH stabilization - and to select a sequestering agent to be used for the elimination of scaling at the treatment facilities. The chemistry of ion exchange resins is explained, and instrumentation and procedures are described. Comparison of the different resins tested lead us to the selection of the most effective one to be used in the treatment facilities.

Genetic Programming Using SISAL Parallel Programming Language

Sheila Tejada
University of California, Los Angeles
ISCR

Genetic programming is based upon the principles of genetic algorithms. It is a method to generate solutions to problems while not having to explicitly program them. A genetic algorithm is a technique to evolve good solutions by breeding a population of randomly produced solutions using operators, such as crossover and mutation. Breeding is governed by the Darwinian principle of the survival of the fittest. Genetic programming utilizes these characteristics of the genetic algorithm in order to evolve better programs. This procedure being inherently parallel translates well into a SISAL application. SISAL is a parallel functional programming language developed at Lawrence Livermore National Laboratory.

Beamlet Diagnostics

Mitch Theys
Purdue University
Inertial Confinement Fusion

ABSTRACT

Beamlet was designed and is currently being built as a proof of design for the National Ignition Facility, or NIF. NIF will be composed of approximately two hundred of these 'Beamlets.' The overall goal of NIF is to provide an efficient means to produce fusion energy. The Beamlet diagnostics are proof that the laser meets the design criteria which have been requested. Using the knowledge acquired from Beamlet we are better able to forecast the expense and work required for NIF. Tasks that have been completed and will be discussed include: design and construction of diagnostics, calibration of diagnostics and data collection/manipulation.

Nonthermal Plasma Reactors for Treatment of NOx and Other Hazardous Gas Emissions

Debbie S. Thomas
University of Illinois at Urbana-Champaign
Defense Sciences Engineering Division

ABSTRACT

The 1998 Low Emissions Standards for all automobiles passed by the United States government has prompted a great deal of interest in reducing the amount of pollutants released into the air. Of particular interest is the reduction of NOx produced by diesel exhaust. Analysis of the results from varying configurations of nonthermal plasma processors are studied and compared to determine which methods are most efficient.

Measuring Software Module Cohesion: Increasing Maintainability

John M. Tutton
California State University, Sacramento
Computer Science and Engineering

ABSTRACT

We examine the functional cohesion of software modules using a data slice abstraction. Our analysis identifies the data tokens that lie on more than one slice as the "glue" that binds separate components together. Cohesion is measured in terms of the relative number of *glue tokens*, tokens that lie on more than one data slice, and *super-glue tokens*, tokens that lie on all data slices in a procedure, and the *adhesiveness* of the tokens. Our goal is to create an automated software metric tool which will give a functional cohesion rating to any C language source code module.

Isotope Labeled ImmunoAssay for Environmental Chemical Detection

Marilyn M. Velez
Universidad Metropolitana (UMET), Puerto Rico
Biology and Biotechnology Research Program

ABSTRACT

Atrazine is one of the most heavily used agricultural pesticides in North America and has been identified as a major groundwater contaminant in the U.S. Research provides evidence that under certain conditions atrazine and some of its derivatives may prove carcinogenic and mutagenic. Immunoassays are one of the most powerful of all analytical immunochemical techniques. They employ a wide range of methods to detect and quantitate antigens or antibodies, and to study the structure of antigens. With the appropriate assay, they can be remarkably quick and easy, yielding information that would be difficult to determine by other techniques. The development of the appropriate assay, however, requires clean and precise separation of antigens bound to antibodies from those that remain free. Sensitive assays depend on quantification of these bound antigens at very low levels. We are making direct and competitive immunoassays with atrazine and its antibodies using accelerator mass spectrometry (AMS) in order to obtain a sensitive immunoassay for atrazine in environmental samples.

Reliability of the Nerve Conduction Monitor in Repeated Measures of Median and Ulnar Nerve Latencies

Iris A. Washington
Grambling State University
Health Services

ABSTRACT

According to the Bureau of Labor Statistics, carpal tunnel syndrome (CTS), one of the most rapidly growing work-related injuries, cost businesses approximately $10-15 billion dollars in medical costs each year (1992). Because conservative therapy can be implemented and CTS is more reversible in its early stages, early detection will not only save industry unnecessary health care costs, but also prevent employees from experiencing debilitating pain and unnecessary surgery. In response to the growing number of cases of CTS, many companies have introduced screening tools to detect early stages of carpal tunnel syndrome. Neurotron Medical (New Jersey) has designed a portable nerve conduction monitor (Nervepace S-200) which measures motor and sensory nerve latencies. In this study, we determined the reliability of the Nervepace Monitor in measuring ulnar and median nerve latencies during repeated testing. The slowing of these latencies is one diagnostic indicator of carpal tunnel syndrome. The testing was performed on 28 normal subjects between the ages of 20 and 35 who had no prior symptoms of CTS. They were tested at the same time each day for three consecutive days. Nerve latencies between different ethnic groups and genders were compared. Results show that there was no significant daily variation of the median motor and ulnar sensory latencies or the median sensory latencies. No significant differences of latencies was observed among ethnic groups; however, a significant difference of latencies between male and female subjects was observed ($p < 0.05$).

Contamination Analysis Unit (CAU)

Heidi K. Weber
Rochester Institute of Technology
Environmental Protection Department
Waste Minimization Division

ABSTRACT

Presently, time, labor, and chemicals are being wasted in industry due to a lack of convenient measuring instrumentation for cleaning processes. Industries, such as Aircraft Construction and Printed Circuit Board Assembly, are over cleaning products to ensure an absolutely clean surface needed for individual purposes. The Contamination Analysis Unit (CAU) addresses the need for a portable instrument to be on site for immediate analysis of such surfaces. The CAU is a portable mass spectrometer which analyzes the surface it is placed on to instantaneously determine whether the surface is sufficiently cleaned. Therefore, this development will minimize waste in the three areas previously mentioned.

The Effect of Increased Levels of Carbon Dioxide on Chlorophyll Fluorescence and Photosynthetic Pigments in *Pinus ponderosa**

David J. Anschel

State University of New York at Buffalo

Lawrence Livermore National Laboratory
Livermore, California 94550

August 12, 1994

Prepared in partial fulfillment of the requirements of the Science and Engineering Research Semester under the direction of James L. Houpis, Research Mentor, in the Lawrence Livermore National Laboratory.

*This research was supported in part by an appointment to the U.S. Department of Energy Science and Engineering Research Semester (hereinafter called SERS) program administered by LLNL under Contract W-7405-Eng-48 with Lawrence Livermore National Laboratory.

Abstract

Levels of atmospheric carbon dioxide have been increasing at an unprecedented rate in modern times. In response to this situation, we have initiated a long-term study of a forest species' response to elevated carbon dioxide levels. We have set up a facility for subjecting *P. ponderosa* to ambient, ambient + 175 $\mu l\ l^{-1}$, and ambient + 350 $\mu l\ l^{-1}$ CO_2. This report specifically concentrates on the effects of elevated CO_2 on the photosynthetic system, as indicated by chlorophyll fluorescence and pigment assays. We tested for intraspecific variability by selecting nine different families of trees from five different geographic areas of California. There are differential responses to carbon dioxide treatments which appear to be dependent upon the tree's genotype, as indicated by the relative efficiencies of photochemical electron flow in photosystem II (Fv/Fm). During the same testing period Fv/Fm varied by as much as 21.1% relative to ambient in the treated groups. Total chlorophyll, chlorophyll *a* and carotenoid values all showed statistically significant ($p \leq 0.05$) drops in the treatment groups regardless of genotype. Chlorophyll *a* at one time showed the most dramatic drop of 3 mg/m2 in the + 350 $\mu l\ l^{-1}$ CO_2 group versus the ambient. Findings for both photosynthetic pigments and chlorophyll fluorescence vary somewhat over the course of several months.

Introduction

Levels of atmospheric CO_2 have been gradually increasing in modern times. It has been estimated that prior to the industrial revolution, atmospheric CO_2 levels were between 260 and 290 $\mu l\ l^{-1}$. Measurements taken in 1980 show an almost 16% increase to 335 to 340 $\mu l\ l^{-1}$. It has been projected that CO_2 levels could increase to 600 $\mu l\ l^{-1}$ by the middle of the next century (Bacastow and Keeling 1973, Bolin et al. 1986, Clark et al. 1982).

Since CO_2 plays a major role in photosynthesis, these increasing levels of CO_2 may have an effect on plants. The majority of studies investigating the effect of elevated CO_2 have involved annular species, such as agricultural or floral crop plants. Of those few studies researching longer lived species, many of the studies were short-term. It is the goal of the present study to explore the effects of elevated CO_2 levels in a long term study of the forest species *Pinus ponderosa*.

Specifically, this report focuses on the effect of increased CO_2 on two aspects of the photosynthetic system. The first part of our study will utilize chlorophyll fluorescence to analyze the effects of CO_2 on photosynthesis. It has been shown that changes in chlorophyll fluorescence emission during the induction of photosynthesis are closely related to the rate of CO_2 assimilation (Greaves et. al. 1992). It was even suggested as early as 1874 by N.J.C. Muller that there is an inverse relationship between chlorophyll fluorescence and CO_2 assimilation (Lichtenthaler 1992). Additionally, Lichtenthaler and Rinderle (1988) have written that the reciprocal relationship between *in vivo* chlorophyll fluorescence and photosynthetic activity can be used to detect stress effects on green plants and to study the potential photosynthetic activity of leaves. Other researchers such as Schmidt et. al. (1990) have also stated that chlorophyll fluorescence has been useful in studying the effects of environmental stresses such as temperature, air pollution and water stress. The main fluorescence parameter which we will be examining is the ratio of the variable fluorescence to the maximal fluorescence (Fv/Fm), which indicates the relative photochemical efficiency of photosystem II (Greaves et. al. 1992).

Since these electron transfers use pigment molecules, we will also assay the levels of different pigments found in the needles. Krause and Weis (1991) have claimed that fluorerscence at Fo (non-vairiable fluorescence) is an emission by antenna chlorophyll *a* molecules. So then chlorophyll *a* levels might directly influence chlorophyll fluorescence. Fv/Fm would be influenced since Fv is a function of Fo. Changes in pigmentation alone have been used as an indication of air pollution induced stress (Houpis et al. 1988). We will look at changes in pigmentation levels as an indication of stress or possibly as an evolutionary response to increased CO_2.

Materials and Methods

The study was performed at Lawrence Livermore National Laboratory (Livermore, CA) utilizing outdoor CO_2 exposure facilities. All plants were grown in 3m x 3m open-top chambers (Allen et al 1992).

There were 18 chambers containing *P. ponderosa* seedlings, with three CO_2 treatments. Six chambers exposed seedlings to ambient levels of CO_2, six exposed seedlings to 1.5 times the ambient concentration of CO_2 (+ 175 $\mu l\ l^{-1}$ CO_2) and the final chambers housed plants exposed to twice the atmospheric level of CO_2 (+ 350 $\mu l\ l^{-1}$ CO_2). All chambers were arranged in a complete randomized experimental design. All trees were grown in the chambers for 10 months prior to data collection and were approximately four-year old seedlings.

To analyze intraspecific variability, we included seedling source (family) as an additional treatment, using a split-plot experimental design. We included nine different families in this experiment. There were four sets of half siblings, obtained from El Dorado National Forest (family 3087, 3088 and 3399). The other five plants were from open-pollinated sources and were obtained from different geographic regions: Mendocino California (OP5), Sierra (eastern) California (OP6), San Bernandino California (OP7), Santa Clara California (OP8) and El Dorado County California (OP9).

For each of the two assays, nine trees from each chamber and control plot were studied, for a total of 189 trees per sampling. Each of the nine trees sampled were of a different genotype. The fascicles which were used for study were taken from last year's growth. Measurements were taken periodically from January to July 1994.

For the first assay we used a CF-1000 Chlorophyll Fluorescence Measurement System (Version 2.00 Morgan Scientific, Inc., Andover MA) described elsewhere (Greaves et al. 1992), which measures fluorescence at 690 nm. The cuvettes used to dark adapt the needles, were each applied to one fascicle 45 minutes prior to measurement. Settings on the CF-1000 were : light level = 1000 $\mu mole/m^2\ s^1$ and sample time = 50 s. The CF-1000 automatically calculates the non-variable fluorescence (F_o), the maximal fluorescence (F_m), the variable fluorescence (F_v), the photochemical efficiency of photosystem II (PSII) (Fv/Fm), the half rise time from F_0 - F_m ($t_{1/2}$), the terminal fluorescence value (F_t) and the fluorescence quenching capacity (F_q) of the sample being studied.

The second assay was used to study needle pigmentation. Foliar samples were collected for analysis of chlorophyll *a* and *b* content, and carotenoids. One fascicle from each plant was collected and measured for leaf area. After removing the bundle sheath, the needles were cut with a scalpel or scissors into approximately 1 cm fragments, and then immersed in N,N-dimethyl formamide (DMF). The samples were kept in the dark at 4 °C during a 21 day pigment extraction period.. Following extraction, the absorbance of the extract was measured spectrophotometrically at wavelengths of 440 nm, 644 nm and 662 nm using an ultraviolet diode array spectrophotometer (Hewlett Packard HP8452A). The total content of chlorophyll *a*, chlorophyll *b* and carotenoids was calculated based on absorbance coefficients of Lichtenthaler and Welburn (1983). Pigment concentrations were expressed on a leaf area basis.

Height measurements were taken to the nearest half centimeter with either a tape measure or meter stick. Diameter was measured with a vernier caliper to the nearest 1/10th of a millimeter.

Results

Growth

Stem diameters differences in family growth measurements during the January measurements (figure 1) were statistically significant ($p \leq 0.05$). Additionally there was a trend of increased stem diameter growth with increased CO_2 treatment. Height measurements in January tended to show a large increase at +175 ppm CO_2, while growth relative to ambient trees was minimal or negative at + 350 ppm CO_2 (figure 2). If we look at changes in the stem volume, we can see some intraspecific variability and in both elevated CO_2 goups there was a significant increase over ambient in at least six of the nine families (figure 3).

July stem diameter measurements showed similar results to those seen in January, although there was less variability and in most cases the increases were more dramatic (figure 1). Stem height changes in July were in most cases similar to those seen in January, but there was more of trend of increased height relative to ambient trees of the same family (figure 2). Stem volume growth in July also showed less intraspecific variability, but more of a general trend of increase than that seen in January (figure 3).

Chlorophyll fluorescence

Our February chlorophyll fluorescence results showed a family specific response to the different CO_2 treatments, as indicated by the relative efficiencies of photochemical transfer in photosystem II (Fv/Fm) (figure 4). April results showed a variable family specific response independent of CO_2 treatment, while the June measurements were similar to those seen in February, although not as dramatic (figures 5 and 6 respectively). Certain trends were visible throughout, however, such as the obvious negative effect on family OP6 (a seedling source from the eastern Sierra Nevada). Increasing CO_2 resulted in a decrease in Fv/Fm in all sources of seedlings in February (Fv/Fm mean ratios of 0.74, 0.69 and 0.66 for ambient, ambient + 175 and ambient + 350 respectively) and eight of the nine families in June. The variability in percent change in Fv/Fm (comparing ambient to ambient + 350) ranged from -2.1% to -23.2% in February, 3.1% to -12.5% in June. The source of *P. ponderosa* that had the best growth performance throughout the length of the study (family 3399), also had a minimal reduction in quantum yield (maintained Fv/Fm) in the presence of elevated CO_2. Growth measurements of the better growth performers corresponded the best to chlorophyll fluorescence during the February measurement period.

Photosynthetic pigments

Chlorophylls: February results showed a significant CO_2 interaction with regard to total chlorophyll content and chlorophyll *a* (figures 7 and 8). We saw a statistically significant difference between ambient and the elevated CO_2 treatment groups, but no difference amongst the treatment groups for either total chlorophyll or chlorophyll *a* levels. In April

we saw that only chlorophyll *a* had a similar atatistically significant difference (figure 8). Additionally chlorophyll *a* levels are higher within all three groups in April versus February (12.5 mg/m2 -15.4 mg/m2 vs. 11.9 mg/m2 - 13.5 mg/m2 respectively). In June there was no significant difference in chlorophyll. Chlorophyll *b* levels and the Chlorophyll *a/b* ratio showed no significant differences between ambient and treatment groups at any of the three measuring periods.

Carotenoids: February carotenoid levels followed the pattern of the corresponding chlorophyll measurements with a statistically significant ($p \leq 0.05$) decrease in the treatment groups relative to ambient. The April and June carotenoid levels showed a significant decrease only in the ambient + 350 μversus the ambient group (figure 9).

Discussion

The Fv/Fm ratio showed the most intraspecific variability with regard to CO_2 treatment during the February measuring period. We also saw the most intraspecific CO_2 interaction in the January stem diameter measurements. As is pointed out above, very often in the treatment groups greater growth corresponds to less of a decrease in Fv/Fm compared to ambient. At the same time almost all of the treated groups (regardless of Fv/Fm) showed a consistent increase in growth compared to ambient.

The increased growth might be explained by the fact that more carbon is readily available to the plants, so more is taken up and utilized for new tissue growth. It is then possible that the poor growth performers are not adapted to handle this increase in carbon availability. These responded to elevated CO_2 through less efficient photosynthesis, thereby emitting more fluorescence. Although the seedlings still have a slight increase in growth compared to seedlings grown at ambient CO_2 concentration. It is interesting to note that one of the least adapted families is that of OP6 from the eastern Sierra Nevada, where air pollution (and presumably CO_2 levels) are lower than in other areas of California. This family has then not developed the carbon uptake physiology that would make it better adapted to higher CO_2 levels or polluted environments. Another recent study on cotton leaves (Betsche, 1994) has also found that the long-term response of leaves to atmospheric CO_2 enrichment was variable.

With regard to photosynthetic pigments, instead of an intraspecific reaction to the CO_2 treatments, we saw that the pigments of all trees were affected approximately equally by the treatments. This may lead us to conclude that it is not the pigment reduction which is responsible for the intraspecific reduction in photosystem II efficiency (Fv/Fm). This is supported by the findings of Hagg and coworkers (1992), who observed a drop in chlorophyll and carotenoid content to be unrelated to chlorophyll fluorescence, in spruce needles.

One possible explanation for the observed trend in pigmentation is that the reduction in pigment levels might not be a sign that the seedlings are stressed, but that an adaptive alteration in their physiology has occurred (Houpis et al. 1988). This would mean that the plants are actually functioning more efficiently now (although the chlorophyll fluorescence data does not support this). Apparently there is a reduction in light harvesting pigments, but an increase in light usage efficiency. It is also possible that the seedlings are being stressed, as Houpis et al. (1988) also found that at ambient + 300 ppm CO_2 treatment there actually was a decrease in growth. Perhaps as the present study continues, we will see a decrease in growth in certain families at the highest CO_2 treatment. Houpis et. al. (1988) also found some indication of intraspecific variety relating to pigment concentration which we have not yet observed at present.

Betsche (1994) mentions several ways in which high concentrations of CO_2 could cause stress to a plant: Oversized starch granules (which have been observed in trees from the present study), formed in response to elevated CO_2 levels could hinder gas diffusion or cause physical membrane damage. High CO_2 concentrations may induce low inorganic phosphate concentrations which can limit chloroplast ATP synthase. Alternatively the treatments could induce feedback-inhibition and photosynthetic decline because of

imbalance between CO_2 fixation and assimilate utilization. Future work from our study will include investigations to see which if any of these effects are occurring.

Upon examination of the data, for both chlorophyll fluorescence and pigmentation, the CO_2 specific variation observed is less in the summer than it was in the winter. There are at least three possible explanations for this observation. One possibility is that the trees are adapting favorably to the increased CO_2. At first the trees were not able to cope with the increased CO_2, but as time went on perhaps some adaptive mechanism developed. A second possibility is that there is a seasonal effect relating to temperature, length of day or intensity of light. A third consideration is that 1993 needles (which were used for the present study) are under less physiological stress or active than current year needles.

Modern fluorescence measuring devices such as the CF-1000 have resolved some problems of older techniques, such as Lichtenthaler's (1988) mention of the difficulty determining the exact height of Fo (the non-variable fluorescence) on the tracings of an oscilloscope or transient recorder. Future work may, however, include using other fluorescence measurement systems. One drawback to the CF-1000 detection system is the fact that it can only detect fluorescence at 690 nm. According to one source (Lichtenthaler and Rinderle 1988) higher chlorophyll content will shift the fluorescence maximum above 690 nm and lower chlorophyll content will shift it below 690 nm. Also the ratio F_{690}/F_{730} (Lichtenthaler et. al. 1990) or F_{690}/F_{735} (Hagg et. al. 1992) has been useful as an indicator of the *in vivo* chlorophyll content of leaves and needles. This assay could be very useful for the present study so that we have another way of verifying our pigment findings and correlating them to chlorophyll fluorescence.

Although the Fv/Fm value can be very useful, it is also limiting in that, the fluorescence rise signal only covers the first 100 to 500 msec of the induction curve, which represents only the initial photochemistry of the photosystem II and offers no information on the functioning of the whole process of photosynthesis (Lichtenthaler and Rinderle 1988). Although it is more time consuming we may in the future increase the sample time to as much as three minutes. This will allow us to determine the fluorescence-decrease ratio (R_{fd} value = ratio of the fluorescence decrease fd (Fq) to the steady state fluorescence fs (Ft)). Called the vitality index, this ratio can be very useful as an indicator of the potential photosynthetic capacity of needles when stomata are open. When stomata are closed R_{fd}-values indicate whether the internal photosynthetic apparatus is still functional or disturbed (Lichtenthaler and Rinderle 1988, Hagg et. al. 1992). The R_{fd} value would be a good way for us to ascertain if there is damage to the photosynthetic apparatus and if changes in photosynthetic pigment levels are changing the potential photosynthetic capacity of the needles.

By studying chlorophyll fluorescence and the photosynthetic pigment levels of *P. ponderosa* under treatment with eleveated levels of atmospheric CO_2 we have gained some insight into the long-term effects of this gas (which is rapidly accumulating in our environment) upon a dominant forest species. Through further work of this nature at Lawrence Livermore National Laboratory and similar facilities we hope to be able to gain a greater understanding of plant physiology while learning how atmospheric conditions affect flora.

References

Allen, L.H. Jr., Drake, B.G., Rogers, H.H., Shinn, J.H.. (1992) Field techniques for exposure of plants and ecosystems to elevated CO_2 and other trace gases. In: FACE: free-air CO_2 enrichment for plant research in the field, pp. 85-119, Hendrey, G.R., ed. CRC Press, Boca Raton, FL

Bacastow, R., Keeling, C.D. (1973) Atmospheric carbon dioxide and radiocarbon in the natural carbon cycle. II Changes from AD 1700 to 2070 as deduced from a geochemical model. In: Carbon and the Biosphere, pp. 86-134, Woodwell, G., Pecan, E., ed. USAEC, Washington, D.C.

Bolin, B., (1986) How much CO_2 will remain in the atmosphere? The carbon cycle and projections for the future. In: The greenhouse effect climatic change and ecosystems, pp. 98-99,144, Bolin, B., Doos, B.R., Jager, J., Warrick, R.A., ed. John Wiley & Sons, Chinchester, UK

Betsche, T. (1994) Atmospheric CO_2 enrichment: kinetics of chlorophyll *a* fluorescence and photosynthetic CO_2 uptake in individual, attached cotton leaves. Environmental and Experimental Botany **34**, 75-86

Clark, W.C., Cook, K.H., Marland, G., Weinburg, A.M., Rotty, R.M., Bell, P.R., Allison, L.J., Cooper, C.L. (1982) The carbondioxide question: perspectives for 1982. In: Carbon Dioxide Review: 1982. pp. 3-44, Clark, W.C., ed. Oxford University Press, New York

Greaves, J.A. (1992) Measurement of chlorophyll fluorescence kinetics in photosynthesis research with a new portable microprocessor and computer operated instrument. In: CF-1000 chlorophyll fluorescence measurement system instruction manual version 2.00, pp. 43-62, Morgan Scientific, Inc., Andover, MA

Hagg, C., Stober, F., Lichtenthaler, H.K. (1992) Pigmentcontent, chlorophyll fluorescence and photosynthetic activity of spruce clones under normal and limited mineral nutrition. Photosynthetica **27**, 401-411

Houpis, J.L.J., Surano, K.A., Cowles, S., Shinn, J.H. (1988) Chlorophyll and carotenoid concentrations in two varieties of *Pinus ponderosa* subjected to long-term elevated carbon dioxide. Tree Physiology **4**, 187-193

Houpis, J.L.J., Pushnik, J.S., Loefffler, T., Anschel, D.J., Anderson, P.D., Demaree, R. (1994) Intraspecific variability in the growth response of *Pinus ponderosa* to elevated carbon dioxide. Air Pollution Workshop, Ithaca, NY

Krause, G.H., Weis, E. (1991) Chlorophyll fluorescence: the basics. Annual Rev Plant Physiology **42**, 313-49

Lichtenthaler, H.K. (1992) The Kautsky effect: 60 years of chlorophyll fluorescence induction kinetics. Photosynthetica **27**, 45-54

Lichtenthaler, H.K., Hak, R., Rinderle, U. (1990) The chlorophyll fluorescence ratio F690/F730 in leaves of different chlorophyll content. Photosynthesis Research **25**, 295-298

Lichtenthaler, H.K., Rinderle, U. (1988) The role of chlorophyll fluorescencein the detection of stress conditions in plants. CRC Critical Reviews in Analytical Chemistry **19**, sup1, S29-S85

Lichtenthaler, H.K., Wellburn, A.R. (1983) Determinations of total carotenoids and chlorophylls a and b of leaf extracts in different solvents. *In* Abstracts of the 6th International Congress on Photosynthesis, Brussels, p 415

Ogren, E. (1988) Photoinhibition of photosynthesis in willow leaves under field conditions. Planta **175**, 229-236

Rogers, H.H., Runion, G.B., Krupa, S.V. (1994) Plant responses to atmospheric CO_2 enrichment with emphasis on roots and the rhizosphere. Environmental Pollution **83**, 155-189

Schmidt, W., Neubauer, C., Kolbowski, J., Schreiber, U., Urbach, W. (1990) Comparison of effects of air pollutants (SO_2, O_3, NO_2) on intact leaves by measaurements of chlorophyll fluorescence and P_{700} absorbance changes. Photosynthesis Research **25**, 241-248

Walker, D.A., Sivak, M.N., Prinsley, R.T., Cheesbrough, J.K. (1983) Simultaneous measurement of oscillations in oxygen evolution and chlorophyll *a* fluorescence in leaf pieces. Plant Physiology **73**, 542-549

Figure 1: Stem diameter measurements of treated *P. ponderosa* taken in Winter and Summer 1994.

Figure 2: Stem height measurements of treated *P. pondreosa* taken in Winter and Summer 1994.

Figure 3: Stem volume of treated *P. ponderosa* calculated from diameter and height.

Figure 4: Chlorophyll fluorescence (Fv/Fm) from Winter 1994, showing a high level intraspecific variabilty.

Figure 5: Chlorophyll fluorescence (Fv/Fm) from Spring 1994, showing a a variable family specific response independent of CO_2 treatment.

Figure 6: Chlorophyll fluorescence (Fv/Fm) from Summer 1994, showing a moderate amount of intraspecific variability.

Figure 7: Total chlorophyll levels averaged over all nine families. Bars with different letters above them are statistically significant ($p \leq 0.05$)

Figure 8: Chlorophyll *a* levels averaged over all nine families. Bars with different letters above them are statistically significant ($p \leq 0.05$)

Figure 9: Total carotenoid levels averaged over all nine families. Bars with different letters above them are statistically significant ($p \leq 0.05$)

Stem Diameter

January 1994

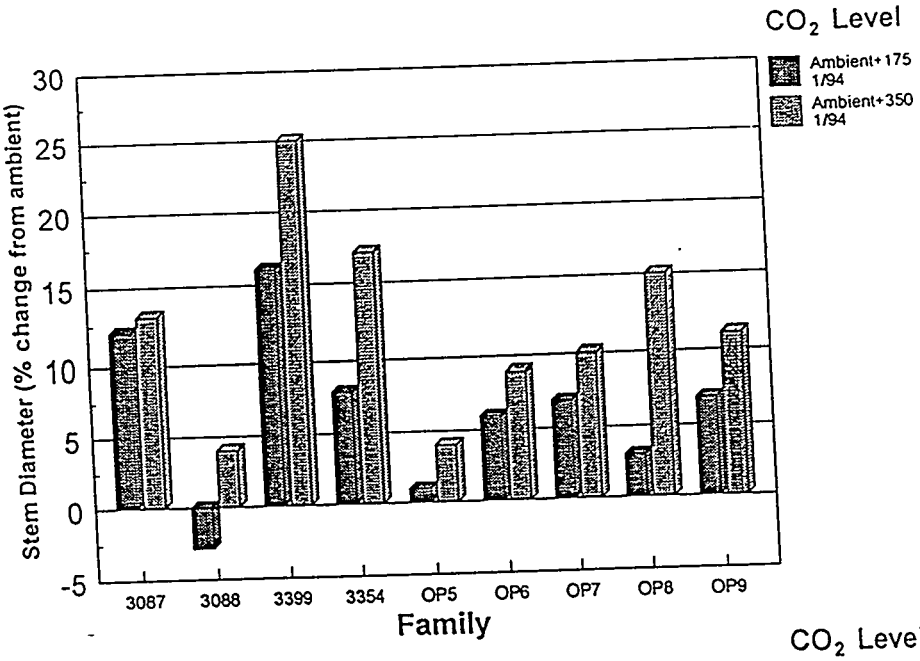

July 1994

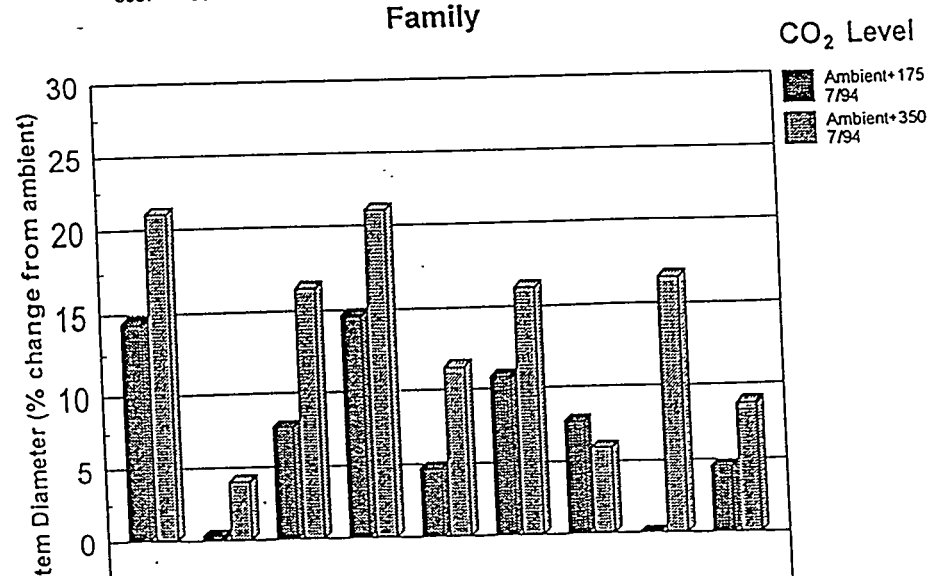

Stem Height

January 1994

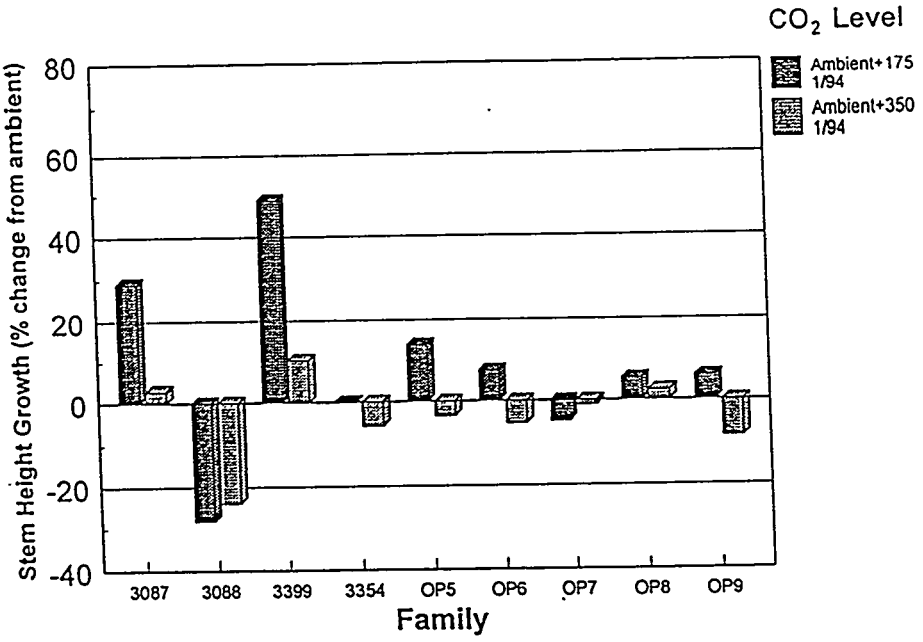

July 1994

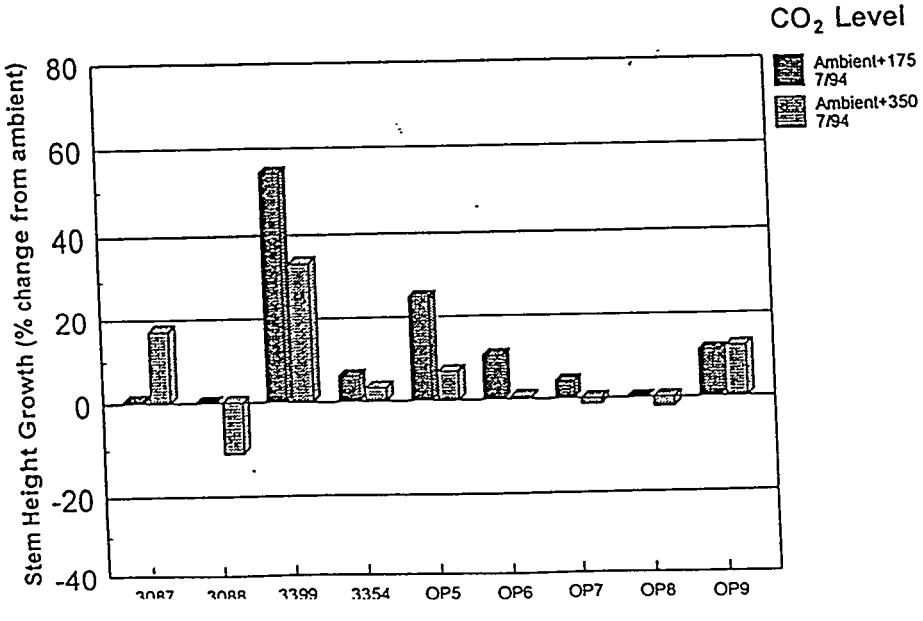

Stem Volume

January 1994

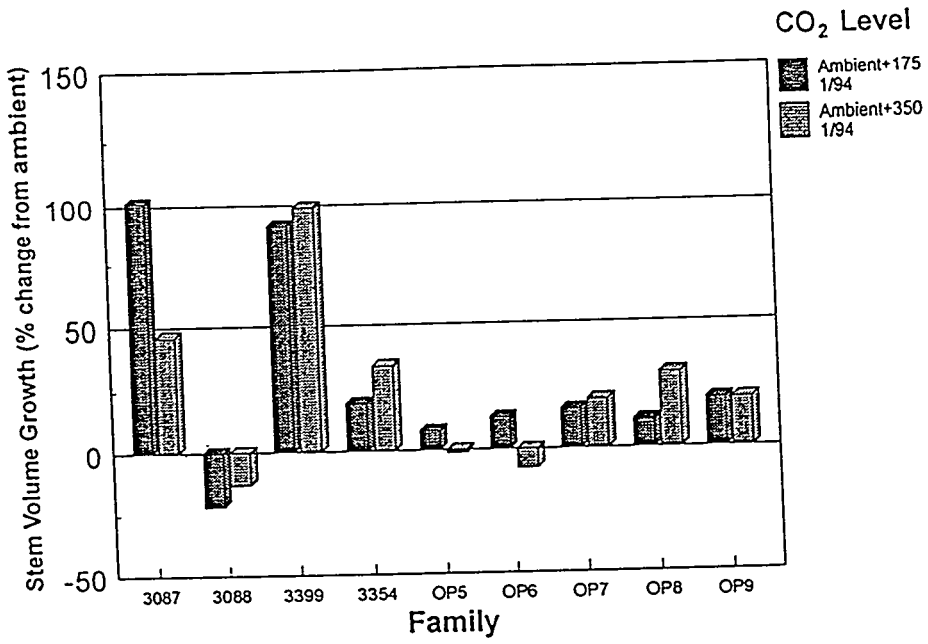

July 1994

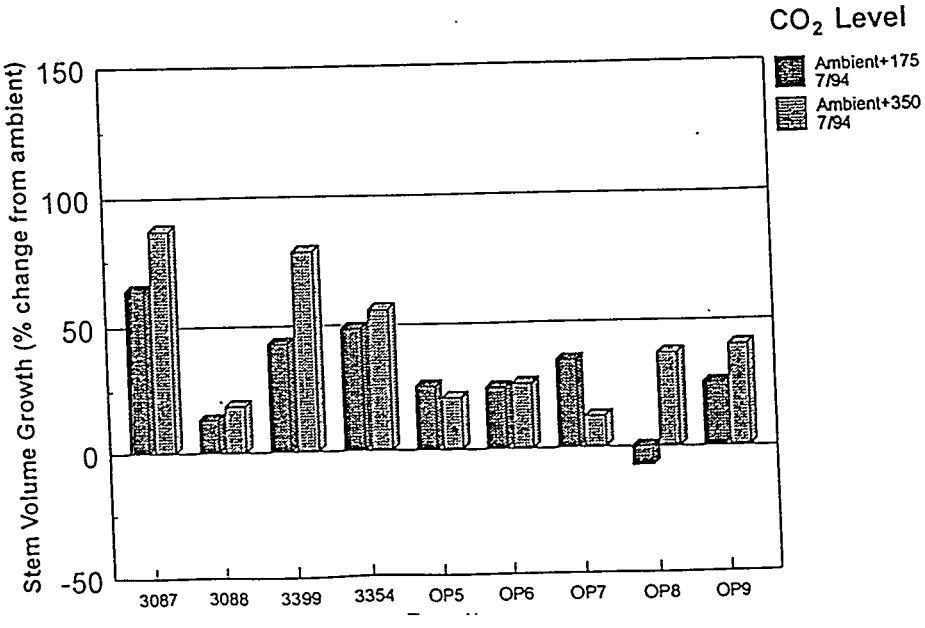

4

Chlorophyll Fluorescence - Fv/Fm

February 1994

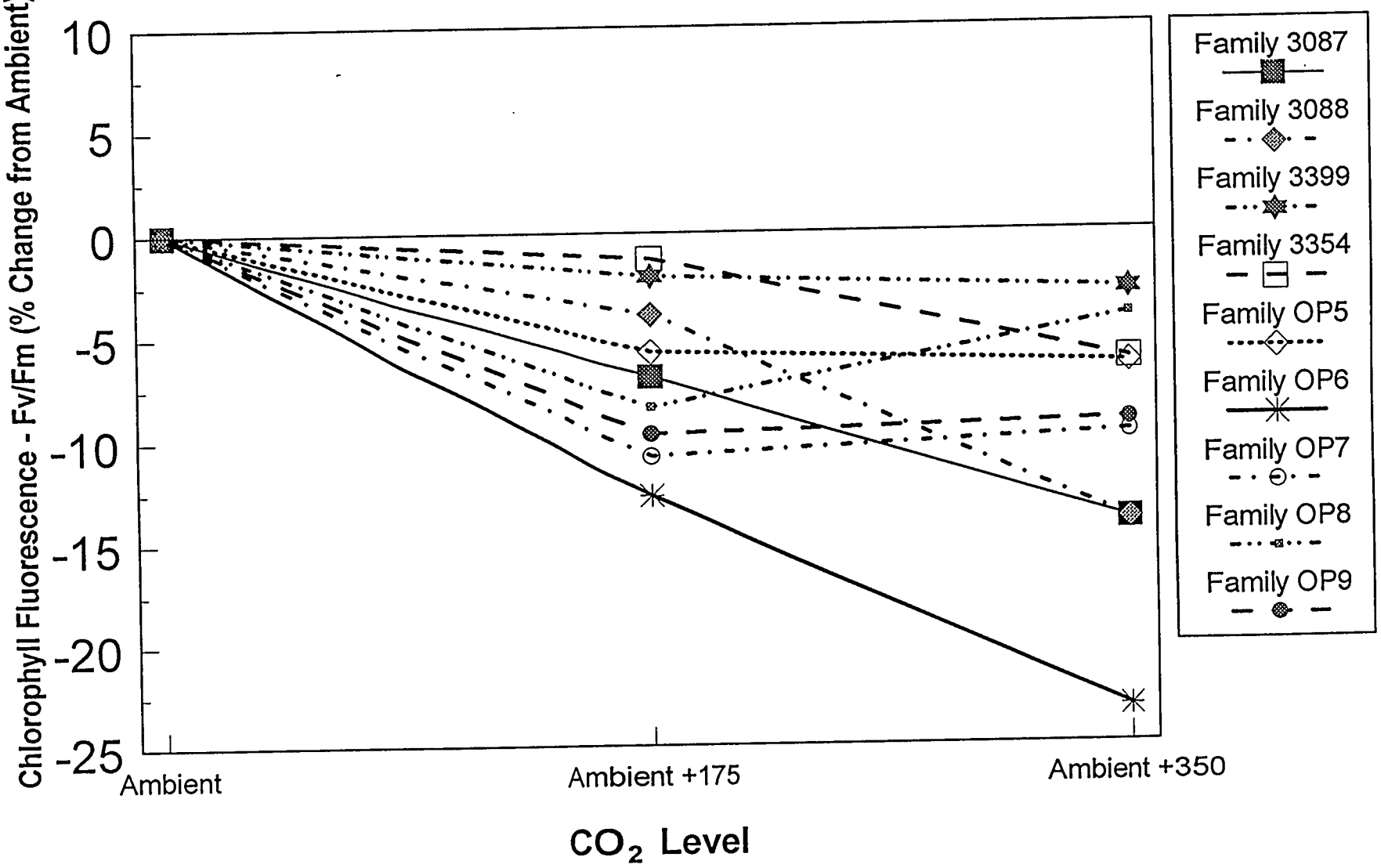

Chlorophyll Fluorescence - Fv/Fm

April 1994

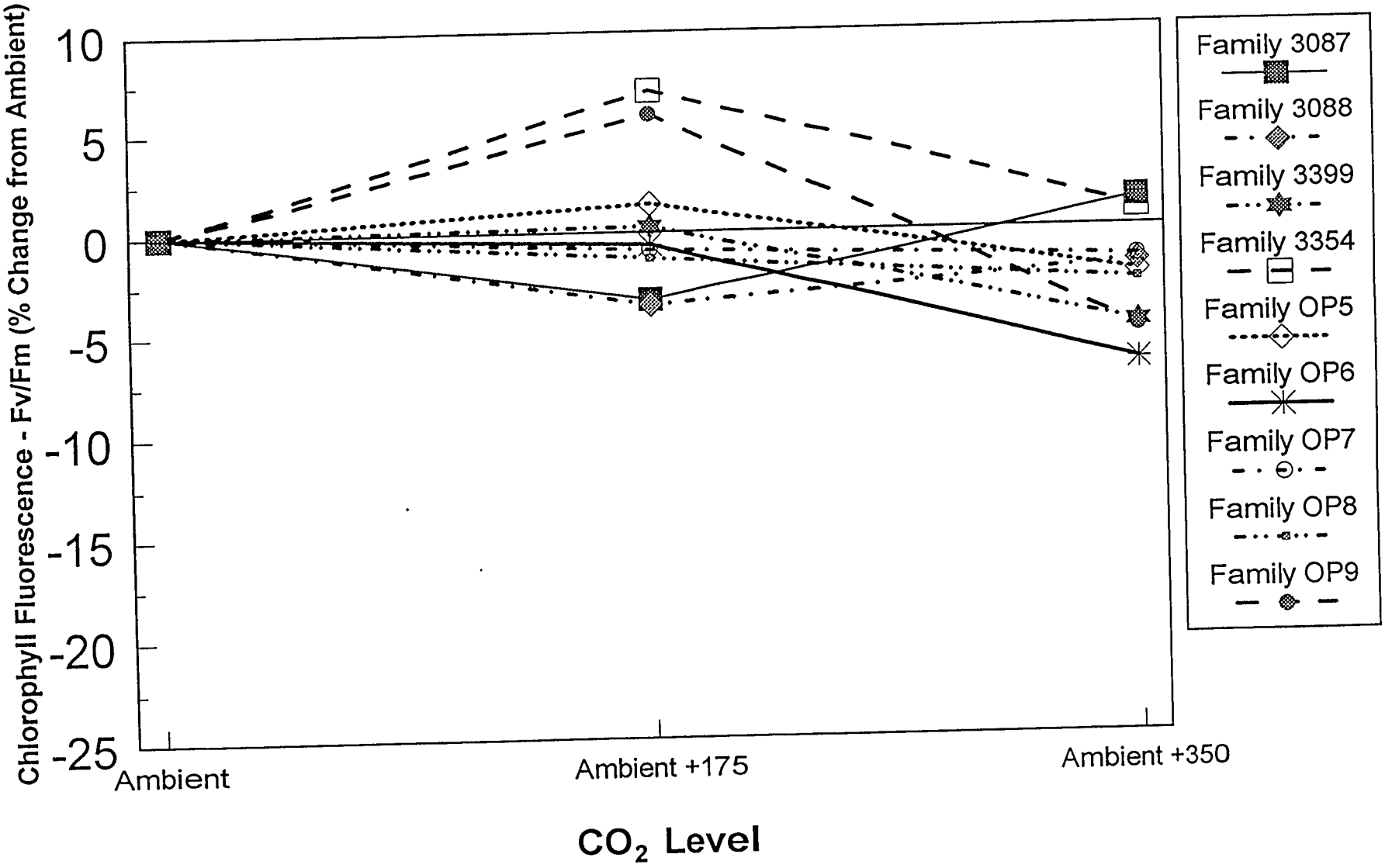

Chlorophyll Fluorescence - Fv/Fm

June 1994

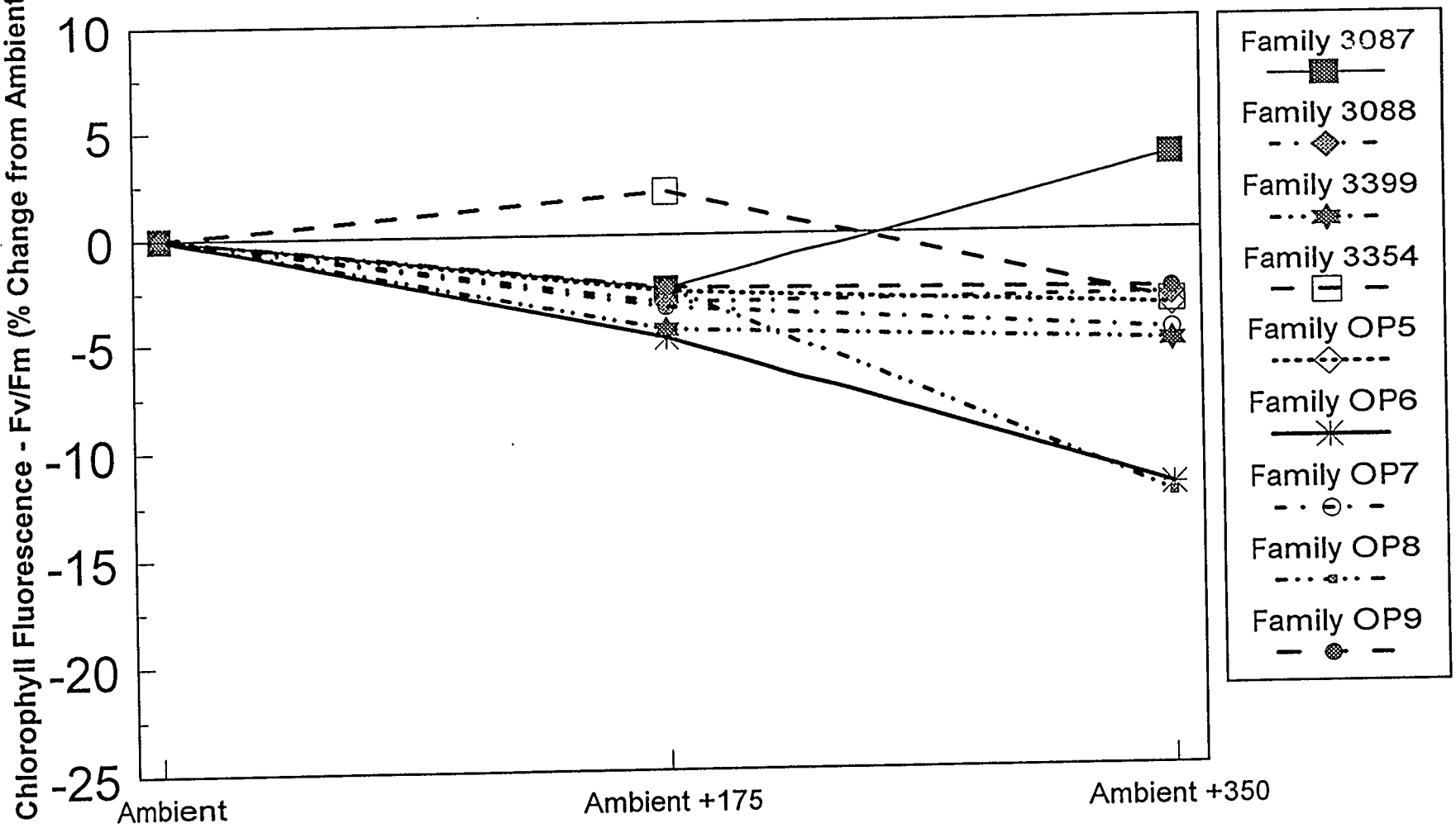

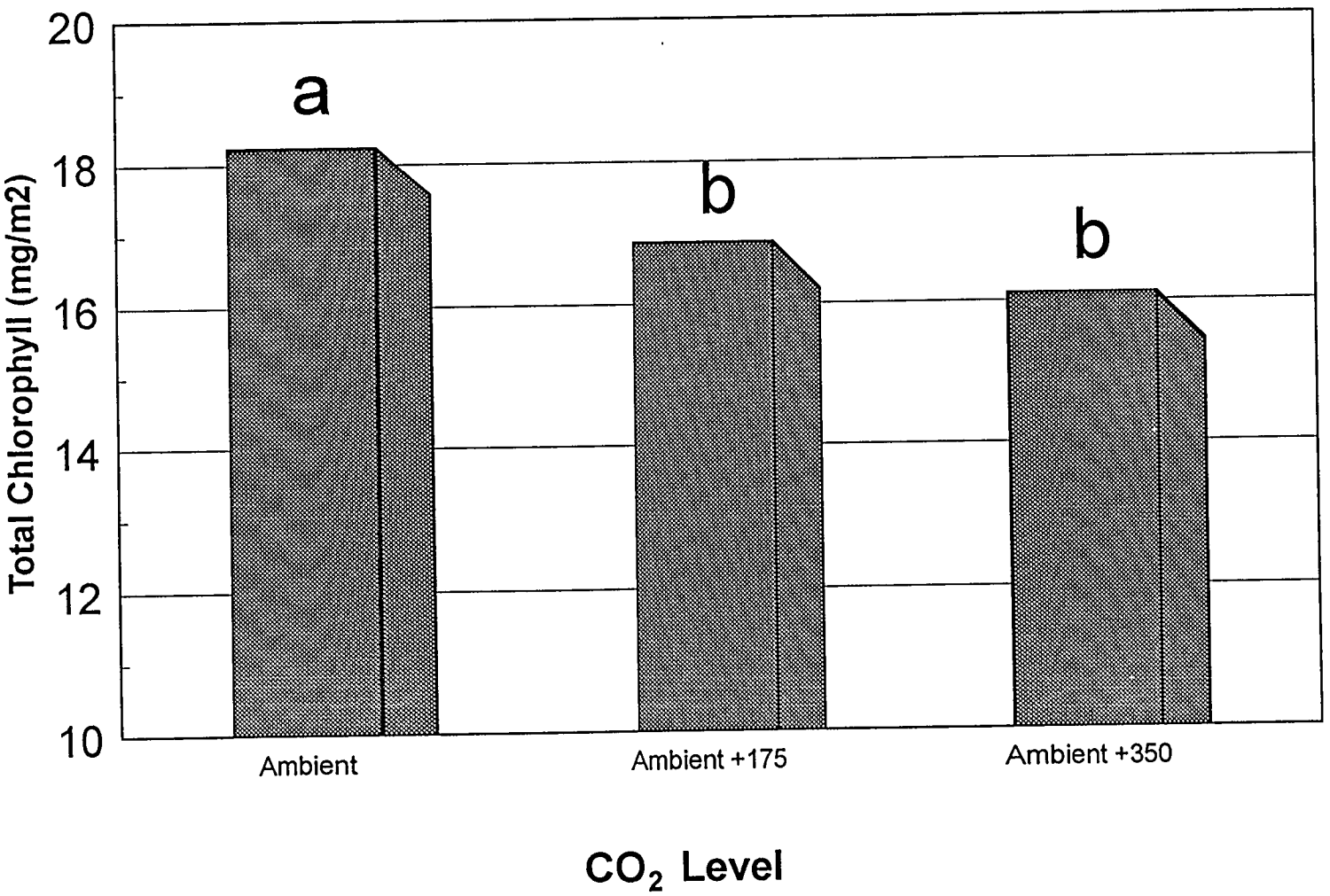
February 1994
Total Chlorophyll (mg/m2)
20
18
16
14
12
10
a
b
b
Ambient
Ambient +175
Ambient +350
CO2 Level

Chlorophyll *a*

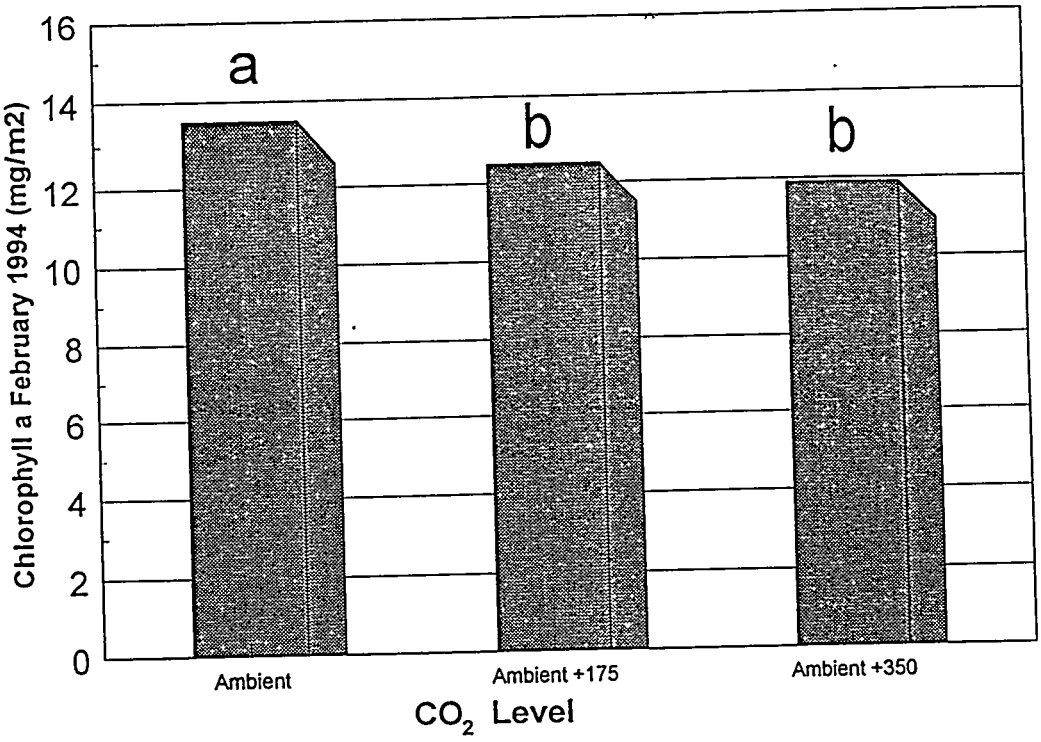

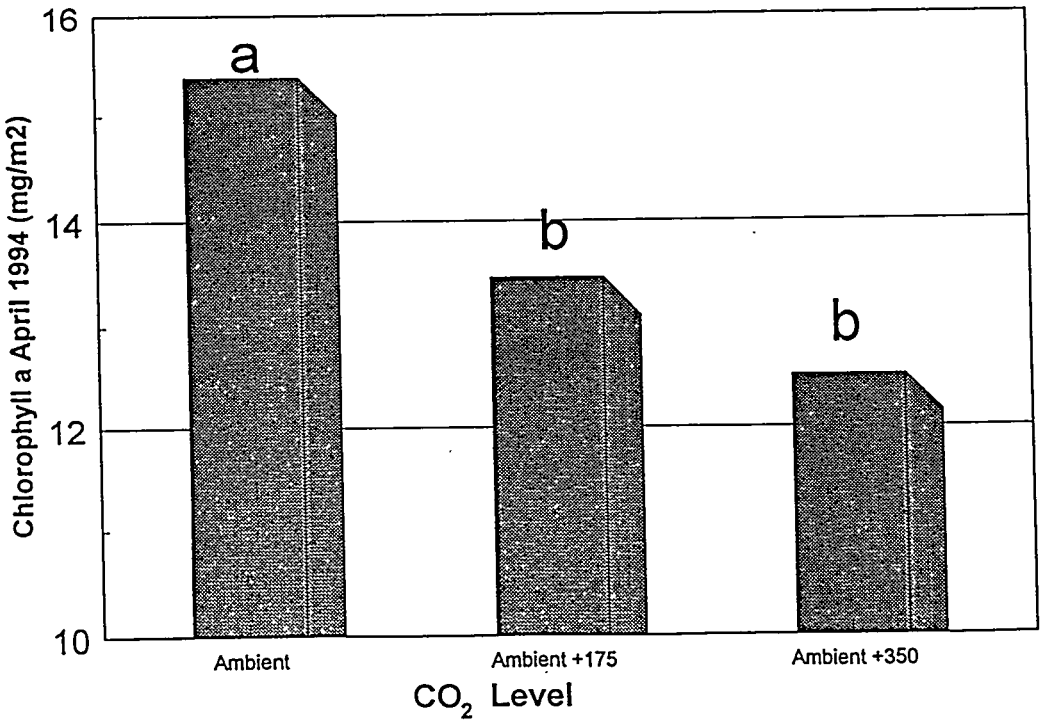

Carotenoids

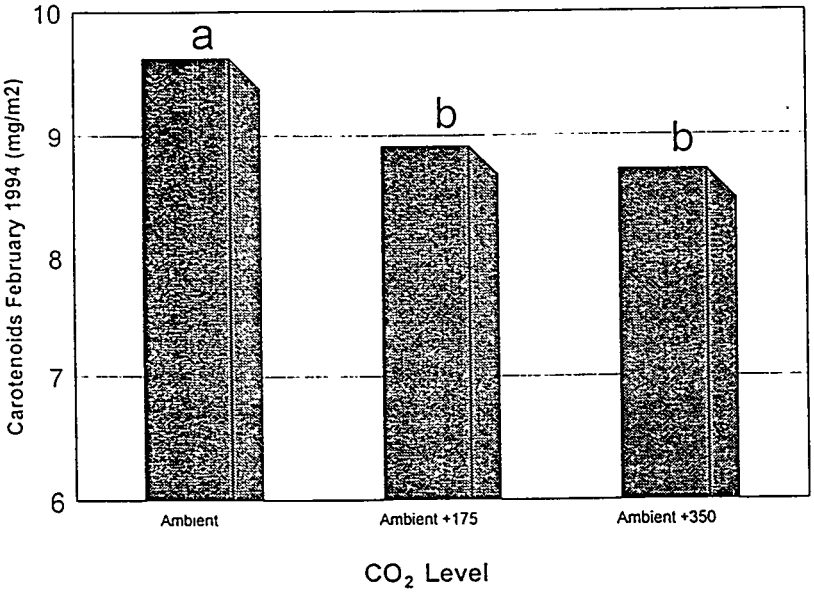

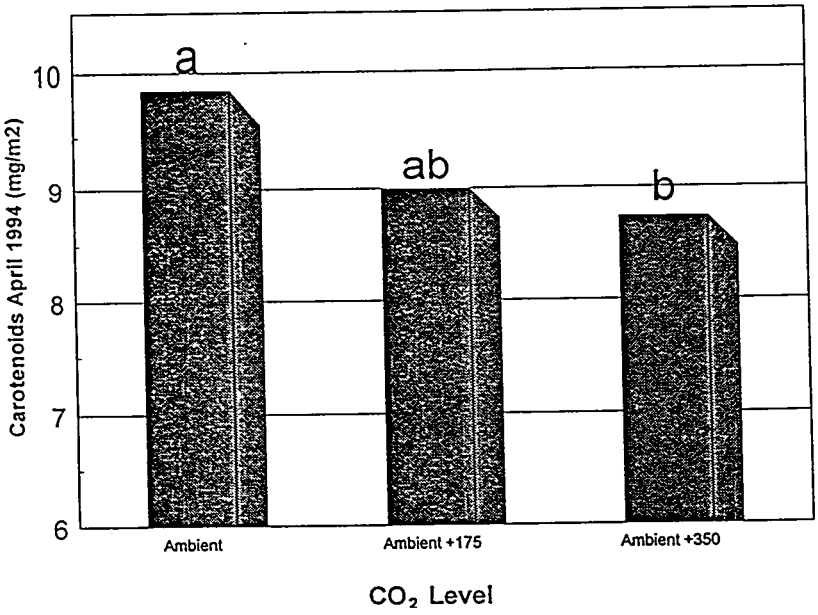

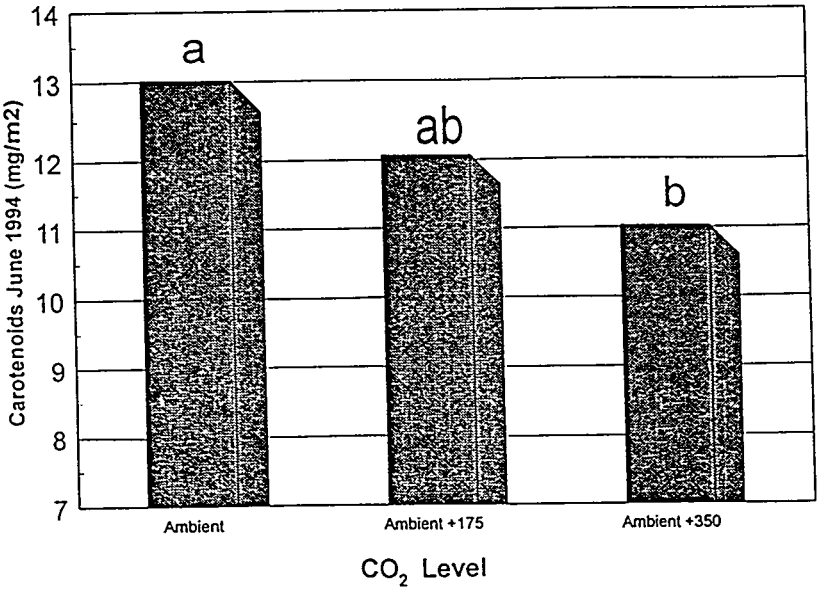

Evaluating the ISDN Line to Deliver Interactive Multimedia Experiences

David K. Michaels
New Jersey Institute of Technology
michael1@nes.nersc.gov

Lawrence Livermore National Laboratory
Livermore, CA 94550

11 March 1994

Abstract

We will use the 128 kilobit/sec ISDN connection from the Lawrence Livermore National Laboratory to the Livermore High School Math Learning Center to provide students there with interactive multimedia educational experiences. These experiences may consist of tutorials, exercises, and interactive puzzles to teach students' course material. We will determine if it is possible to store the multimedia files at LLNL and deliver them to the student machines via FTP as they are needed. An evaluation of the effect of the ISDN data rate is a substantial component of our research and suggestions on how to best use the ISDN line in this capacity will be given.

Prepared in partial fulfillment of the requirements of the Science and Engineering Research Semester under the direction of Jerry Owens, Research Mentor, in the Lawrence Livermore National Laboratory.

This research was supported in part by an appointment to the US. Department of Energy Science and Engineering Research Semester (hereinafter called SERS) program administered by LLNL under Contract W-7405-Eng-48 with Lawrence Livermore National Laboratory.

1 Introduction

1.1 Project Concepts

We believe multimedia experiences on computer may be used as an effective tool to complement traditional classroom education. These multimedia experiences can be developed by students to be used by other students. We started our work in the Math Learning Center at Livermore High School where certain students volunteered their time to create our first set of on-line educational experiences.

1.2 Several Types of Educational Experiences

We have selected three major categories of educational experiences that students may create. Tutorials introduce new topics over the computer primarily by using videotaped classroom sequences. They also may include audio-only portions and animation's created on the computer itself. Tutorials also include the capability to play videos that answer frequently asked questions. Another type of experience is interactive problems for the students to solve on-line to test their understanding and practice concepts. A benefit of allowing the students to work their problems on the computer is that mistakes can be corrected immediately by presenting a video explaining why the selected answer was incorrect. Finally, interactive games or puzzles and can reinforce concepts taught in the tutorials and help aid recall by allowing the students to practice using their new material in a more interesting way.

1.3 Advantages of Students Creating Tutorials

Allowing the students to create the educational experiences has the benefit of teaching them how to use the multimedia capabilities of modern personal computers. Also students tend to create presentations that are able to hold other student's interest well. Teachers may function as consultants to assist students' efforts and suggest topic and content for the experiences.

2 Advantages of On-line Education

On-line experiences supplement regular classroom instruction and provide several advantages when used this way. Advanced students can proceed ahead at their own pace by using the computer-based tutorials to introduce new topics ahead of the class. Average students can practice on-line and get instant feedback about their mistakes. This feedback may include automatically playing an appropriate tutorial which explains the concept that the student misunderstood. Below average students may ask the computer for more detailed tutorials about the specific items which they do not understand and can practice those concepts until they master them.

3 ISDN

Many schools will soon have inexpensive access to the Internet via ISDN lines. We hope to use this technology to create a centralized database of educational experiences that will be created by the volunteer efforts of students across the country and worldwide. Schools can run our software to connect to this database and provide the educational experiences as they are needed without requiring large amounts of storage on the school's computers. We will attempt to determine how the ISDN line may be used in this capacity and discuss the performance we achieve.

4 Results - ISDN Performance

The times for delivery of multimedia video files over the ISDN line from the Lawrence Livermore National Laboratory to the Math Learning Center at Livermore High School are given below. The 3 files used for this test were a short (4 second) congratulations file to be played when the student gets a problem right, a moderate (53 second) answer to a commonly asked student question, and a long (2 1/2 minute) video lecture.

File length	Average time to transfer
Short(350K)	45 seconds
Moderate(2M)	7 minutes 15 seconds
Long(12M)	23 minutes 30 seconds

Our measurements were made on three consecutive weekdays at various times of day. The files were transferred using FTP and the complete transfer time was recorded. The times listed represent the average of 6 attempts to transfer each file, rounded to the nearest 15 second increment. The files included audio and were compressed with Microsoft Video 1(TM) compression. No special compression hardware was used. The connection was made via Ethernet with two CombiNet boxes providing the Ethernet-ISDN interface. Our ISDN line has a rated bandwidth of 64kbit/sec on each of its two channels which may be used simultaneously.

5 New Tutorial

In order to determine what steps are involved in creating a tutorial and the time necessary to do so we proceeded to build a new tutorial. The tutorial includes video lessons and video answers to common questions which are played when the students click on the appropriate question. At key points in the lecture captions appear to emphasize important information. The program also includes a feedback mechanism where students can enter questions they would like to see answered in future versions of the tutorial. This feedback is stored on disk and may be accessed by the teacher or other authors of the tutorial. There are also sample problems provided for students to view and interactive problems for students to solve. This tutorial took about a month to build and the steps involved are within the reach of high school student's ability and the school's budget.

6 Conclusion

From the performance data obtained in section 4, we have concluded that the ISDN line is insufficient to deliver multimedia video experiences in real time. The excessive delay would lose student interest and severely limit the length of files that can be used to ineffectively short lengths.

We suggest that if this type of educational project is to be distributed over the Internet, the entire package associated with each lesson be transferred overnight before the class in which it will be used.

7 Future Work

7.1 Distribution of our work over Mosaic

Mosaic provides a user-friendly way to access files over the Internet and invoke a program that can present the type of information contained within that file. This may be a valuable tool to deliver our work. We hope to create a special program that will present our tutorial, and distribute this program for people to add to their copy of Mosaic. This would then allow students to download tutorials over Mosaic and automatically run them.

7.2 Audio-only presentations in real time over ISDN

Having concluded that the ISDN line data rate is not sufficient to deliver video experiences in real time, we intend to look at the possibility of delivering audio-only presentations. We will attempt to determine the utility of such presentations and ability of ISDN to deliver them in real time.

8 Acknowledgments

We wish to thank Nancy Owens for her help in developing our first on-line tutorial. Also thanks to Al Ofiesh for his suggestions and time spent being recorded for our classroom lecture segments. Thanks also go to the Livermore Valley Joint Unified School District for providing the hardware used to carry out this research and the Department of Energy for funding this project under the Science and Engineering Research Semester program.

Truc Ngoc Nguyen

California Polytechnic State University,
San Luis Obispo

Lawrence Livermore National Laboratory
Livermore, California 94550

May 13, 1994

Prepared in partial fulfillment of the requirements of the Science and Engineering Research Semester under the direction of Glenn A. Marsch, Research Mentor, at Lawrence Livermore National Laboratory.

*This research was supported in part by an appointment to the U.S. Department of Energy Science and Engineering Research Semester (hereinafter called SERS) program administered by LLNL under Contract W-7405-Eng-48 with Lawrence Livermore National Laboratory.

Separation of a chemically modified DNA oligomer bound by the carcinogen 2-Amino-1-methy-6-phenylimidazo[4,5-*b*]pyridine using capillary gel electrophoresis

Truc Ngoc Nguyen
Biology and Biotechnology Research Program, L-452
Lawrence Livermore National Laboratory

I. Abstract

We have optimized the reaction conditions under which unactivated metabolite of the food borne carcinogen 2-amino-1-methyl-6-phenylimidazo[4,5-*b*]pyridine (PhIP) is covalently bound to the oligodeoxynucleotide d(CCTACGCATCC). Capillary electrophoresis (CE) was used to separate and characterize this DNA oligomer bound by PhIP. We observed 2 major and several minor PhIP adduct species. The 2 major adducts had different absorbance maxima; the major adduct eluates with faster and slower mobilities had absorbance maxima of 360 and 340 nm, respectively. One of the two major PhIP adduct species was resolvable but the peak was broad. Using detection at 260 nm, the other major PhIP adduct with fastest electrophoretic mobility was not resolvable, but coelute with the huge broad unmodified DNA oligomer peak. However, at higher wavelengths (>320 nm) where DNA does not absorb, electropherograms generated by detection at these higher wavelengths showed very heterogeneous binding by PhIP to the DNA oligomer with no interfering absorbance by the DNA.

II. Introduction

2-Amino-1-methyl-6-phenylimidazo[4,5-*b*]pyridine (PhIP) is a mutagenic and carcinogenic substance found in meat cooked at high

temperatures (about 200-300 ^{o}C) (1). Radiocarbon-labeled phenylalanine and creatine showed incorporation of these molecules into PhIP (2). Compared to other aminoimidazoazaarenes (AIAs) found in high-protein-content food, PhIP is formed in the highest concentration (70 ug/kg of fried ground beef). In the Ames/*Salmonella* assay using strain TA 1538, PhIP was moderately mutagenic, inducing 60,000 revertants/ug (3).

In vivo studies showed that PhIP metabolizes to *N*-hydroxy-PhIP by the cytochromes P450. Through further metabolism by acetylation or sulfation, the ultimate metabolites that bind DNA, *N*-acetoxy or *N*-sulfonyl-PhIP are formed (4). Evidence from ^{32}P-postlabelling, NMR and mass spectrometry revealed that the covalent binding of *N*-acetoxy-PhIP occurred at the C8 position of the base guanine as the major adduct(5). In addition, HPLC, postlabelling, and fluorescence spectroscopy (done here at the Lawrence Livermore Lab) suggested that *N*-acetoxy-PhIP binds to other positions on the guanine to form DNA-PhIP adducts as well.

Using capillary electrophoresis (CE), an analytical technique of very high resolution, we separated DNA oligomer-PhIP adducts in order to later characterize and to determine their structure. Our aim was to better understand the mutagenic and carcinogenic effects of different DNA-PhIP adduct conformers. In general, capillary zone electrophoresis separates molecules on the basis of their electrical charges, but by using gel-filled capillaries with a rigid acrylamide, cellulose or agarose matrix, the mass and shape of the analyte also influences the separation efficiency. In the case of this capillary gel electrophoresis (CGE) protocol,

this matrix acts as a sieving medium through which the analytes move. For highly resolved separations, it is important to optimize running conditions. Factors to consider include: buffer concentration, ionic strength, and pH; injection volume; running voltage; capillary temperature; and capillary length. In order to obtain high sample stacking in the sample zone, the conductivity of the sample zone and buffer must not be very different to reduce ~~effects of~~ band-broadening effects.

III. Materials and Methods

Activation of *N*-hydroxy-PhIP to *N*-acetoxy-PhIP

N-hydroxy-PhIP was dissolved in DMSO to an 18.6 mM concentration. 250 uL (1120 ug) of this solution was obtained for the activation. *N*-hydroxy-PhIP was activated to *N*-acetoxy-PhIP by adding a 2.3 fold molar excess of glacial acetic acid followed by four additions of 2.8 times molar excess acetic anhydride in 2.5 minute intervals. The activation was done at room temperature while continuously purging with $N_2(g)$. After completion of the reaction, the *N*-acetoxy-PhIP was saved on dry ice until needed for the binding step. A few uL of the activated *N*-hydroxy-PhIP was retained for HPLC to make sure the *N*-hydroxy-PhIP was fully activated.

Covalent modification of the DNA oligomer

The covalent binding of PhIP to single-stranded oligonucleotides was accomplished by modifying the protocol of Cosman et al (7). The oligodeoxynucleotide 5' dCCTACGCATCC 3' was suspended in two 1

mL aliquots of 20 mM sodium phosphate, 0.1 M NaCl, 0.1 mM EDTA and 1.5% triethylamine for a 79 uM strand (0.86 mM bases) concentration to be used in two reactions. The activated *N*-hydroxy-PhIP was added 5 times in 30 minute intervals yielding final molar ratios of 2 or 11 PhIP molecules per oligomer strand, depending on the concentration of *N*-acetoxy PhIP added to the DNA oligomer solution. After addition of the last aliquot of the activated *N*-hydroxy-PhIP, the reaction mixture was left at 4 °C overnight for complete reaction.

Purification of the modified DNA oligomer

To purify the DNA oligomer-PhIP adducts, the sample mixtures were extracted with equal volumes of a pure 1-butanol five times. During the reaction a red precipitate was formed, probably a bis-azo by-product from the decomposition of *N*-acetoxy-PhIP. This was removed by pelleting the precipitate and drawing off the supernatant. After the butanol extraction, the adduct samples were de-salted by Sep-Pak C18 cartridges and the DNA oligomer and adducts were eluted off the column with a two 60:40 methanol/water (v/v) washes. UV/VIS absorbance spectra of the Sep-Pak washes (e.g. the pass-through and water wash stages) were measured to evaluate the amount of DNA oligomer that might not have remained absorbed to the C18 matrix up to the MeOH/water eluting stage. The oligomer-containing methanol-water washes were dried down on a Savant speed-vac concentrator.

UV absorbance spectra of the solutions were measured with a UV2101-PC UV/VIS Spectrophotometer (Norwalk, CT).

Oligodeoxynucleotide analytes were separated and analyzed by capillary electrophoresis (Bio-Focus instrument from Bio-Rad, Hercules, CA) using either coated capillaries from Bio-Rad, or gel-filled capillaries purchased from Beckman (eCAP ss DNA kit, Beckman, Fullerton, CA).

Separations using the 51 cm * 50 um i.d. gel-filled capillary were done using TBE buffer (0.1 M Tris[hydroxymethyl]aminomethane (pH 8.1), 0.25 M boric acid, 7 M urea) as the running buffer. Samples were injected electrokinetically for up to 40 seconds at 15.5 kV. Analytes were also separated by capillary zone electrophoresis (CZE), using non-gel filled coated capillaries to eliminate electroosmotic flow.

IV. Results

Characterization of PhIP-DNA oligomer adducts formed *in vitro*

We observed maximum peaks at 357.20 nm and 344.60 nm with absorbancies of 0.631 and 0.389, respectively, for the 2 PhIP/1 strand and 1 PhIP/1 base binding, respectively (Figure 1).

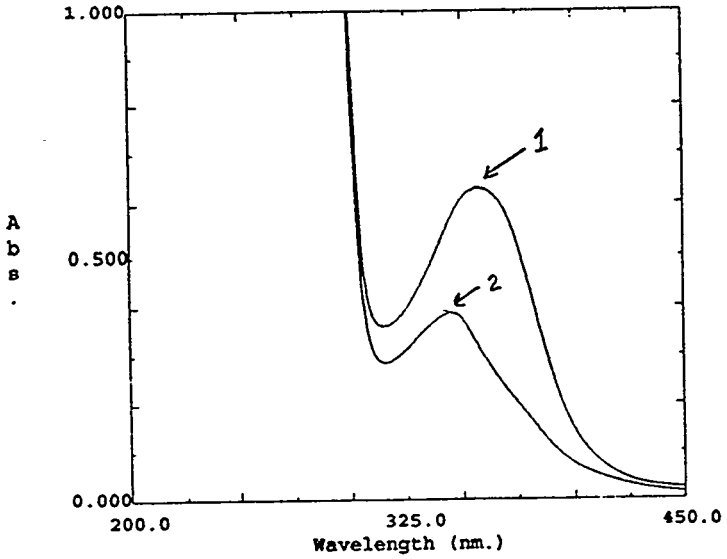

Figure I. UV absorbance of DNA oligomer-PhIP adduct sample. Upper spectrum (1): 2 PhIP/1 strand binding, lower spectrum (2): 1 PhIP/1 base binding. The maximum absorbancies were at 357.20 and 344.60 nm for Peaks 1 and 2, respectively.

The absorbacne maxima of the resulting adduct were dependent on the concentration of PhIP added to the single-stranded DNA oligomer. This suggests that different types of adducts were formed in varying amounts depending on the level of concentrations of PhIP used. The C8 position of guanine is the preferred site of binding of PhIP (8); however, in saturating the DNA oligomer with PhIP, covalent binding may occur elsewhere on the guanine. This blue shift of the absorbance peak has been observed in previous reactions resulting from reacting PhIP at high concentrations with oligodeoxynucleotides. Binding of *N*-acetoxy-PhIP to calf thymus DNA at low PhIP/ base-pair ratios showed UV absorbance spectra with a maximum at 355 nm, suggesting that the adducts formed in the 2 PhIP/1 strand reaction are similar to adducts formed in DNAs.

Separation of DNA oligomer-PhIP adducts by capillary gel electrophoresis

Using capillary gel electrophoresis, we were able to separate PhIP modified DNA oligomers from unmodified oligomers. Two distinct peaks corresponding to DNA oligomer-PhIP adducts were observed-one coeluting with the unmodified oligomer at 36.97 and 38.22 min; and slower-migrating species at 37.86 and 39.32 min. for the lower and higher concentration of PhIP to DNA oligomer (Figure 2A and B), respectively. The electropherograms showing the entire spectrum between 230-362 nm (4 nm intervals) (Figure 3A and B) reveal

clearly an adduct species coeluting with the DNA oligomer peak. Because DNA does not absorb beyond 300 nm, scanning in the higher wavelength region allows the detection of the adduct species that co-migrate with the unmodified DNA oligomer. The scanned spectra show evidence of perhaps two other adduct species between the faster (peak A) and slower (peak B) migrating peaks. Also, there seems to be adduct species of less electrophoretic mobility beyond the slower major migrating peak which still absorb to low energies. Injection of more samples are required in order to better identify these peaks.

Taking a slice of the spectrum where the two major adduct species migrate, we observed an interesting difference in the absorbance spectra of the two species for both reactions (Figure 4A and B). The adduct species that coelutes with the unmodified oligomer (Peak A) has a maximum absorbancy at about 360 nm; whereas, the slower-migrating major adduct (Peak B) has an absorbance maximum of about 340 nm. These data correlates with fluorescence studies (done by Glenn Marsch, unpublished data) on DNA-PhIP adducts.

Comparing the two reactions-the 2 PhIP/1 DNA oligomer strand and the 11 PhIP/1 strand, differences in the distribution of adduct types are recognizable (Figure 3A and B). When *N*-acetoxy-PhIP is added to solutions of single-stranded DNA oligomer at lower concentrations, the adduct represented by peak A is the predominant species. But at high PhIP to oligomer base ratios, the adducts represented by peaks A and B form with approximately the same efficiency.

V. Discussion

The high resolution separations obtained by capillary gel electrophoresis enabled the separation of several DNA oligomer-PhIP adduct species. In addition, we were able to generate high yields of adducts-1 PhIP bound per 2 DNA oligomer strands and 1 PhIP bound per 3 DNA oligomer strands for the 2 PhIP/1 strand and 11 PhIP/1 strand reaction. Two adduct species, in particular, were easily identifiable-the adduct that comigrates with the broad, unmodified DNA oligomer, and another major adduct of slower mobility. The faster-migrating adduct, because it is produced in high yields from high or low PhIP/ base molar ratios, is likely the major adduct bound at the preferred C8 site of guanine. No advantage was conferred by using more *N*-acetoxy-PhIP in the adduction; if anything, more adduct was obtained by using lower N-acetoxy-PhIP to oligomer base ratios. This finding will be a major factor in future work. Future work will involve further optimization of CE separations in order to obtain better separations for easier fraction collecting.

This initial work sets the stage for the structural determination of PhIP-DNA covalent complexes. Pure samples are of utmost importance in obtaining accurate structural data from NMR, mass spectrometry, and X-ray crystallography.

Bibliography

(1) Felton, James S., Knize, M. G., Shen, N. H., Andresen, B. D., Bjeldanes, L. F. and Hatch, F. T. (1986) Identification of the Mutagens in Cooked Beef. *Environmental Health Perspectives* **67,** 17-24.

(2) Felton, J. S. and Knize, M. G. (1990) Heterocyclic-Amine Mutagens/Carcinogens in Foods. *Handbook of Experimental Pharmacology* **94/I**, 471-502.

(3) Felton, J. S. , Knize, M. G., Shen, N. H., Andresen, B. D., Bjeldanes, L. F. and Hatch, F. T. (1986) Identification of the Mutagens in Cooked Beef. *Environmental Health Perspectives* **67**, 17-24.

(4) Buonarati, M. H. and Felton, J. S. (1990) Activation of 2-amino-1-methyl-6-phenylimidazo[4,5-b]pyridine (PhIP) to mutagenic metabolites. *Carcinogenesis* **11:7**, 1133-1138.

(5) Frandsen, H., Grivas, S., Andersson, R., Dragsted, L., and Larsen, J. C. (1992) Reaction of the N^2-acetoxy derivative of 2-amino-1-methyl-6-phenylimidazo[4,5-*b*]pyridine (PhIP) with 2--deoxyguanosine and DNA. Synthesis and identification of N^2-(2'-deoxyguanosin-8-yl)-PhIP. *Carcinogenesis* **13:4**, 629-635.

(6) Engelhardt, H., Beck, W., Kohr, J., and Schmitt, T. (1993) Capillary Electrophoresis: Methods and Scope. *Angewandte Chemie* **32:5**, 629-766.

(7) Cosman, M., Ibanez, V., Geacintov, N. E., and Harvey, R. G. (1990) Preparation and isolation of adducts in high yield derived from the binding of two benzo[*a*[pyrene-7,8-dihydroxy-9,10-oxide stereoisomers to the oligonucleotide d(ATATGTATA). *Carcinogenesis* **11:9**, 1667-1672.

(8) Lin, D., Kaderlik, K. R., Turesky, R. J., Miller, D. W., Lay, J. O., and Kadlubar, F. F. (1992) Identification of *N*-(Deoxyguanosin-8-yl)-2-amino-1-methyl-6-phenylimidaxo[4,5-*b*]pyridine as the Major Adduct Formed by the Food-Borne Carcinogen, 2-Amino-1-methyl-6-phenylimidazo[4,5-*b*]pyridine, with DNA. *Chem. Res. Toxicol.* **5**, 691-697.

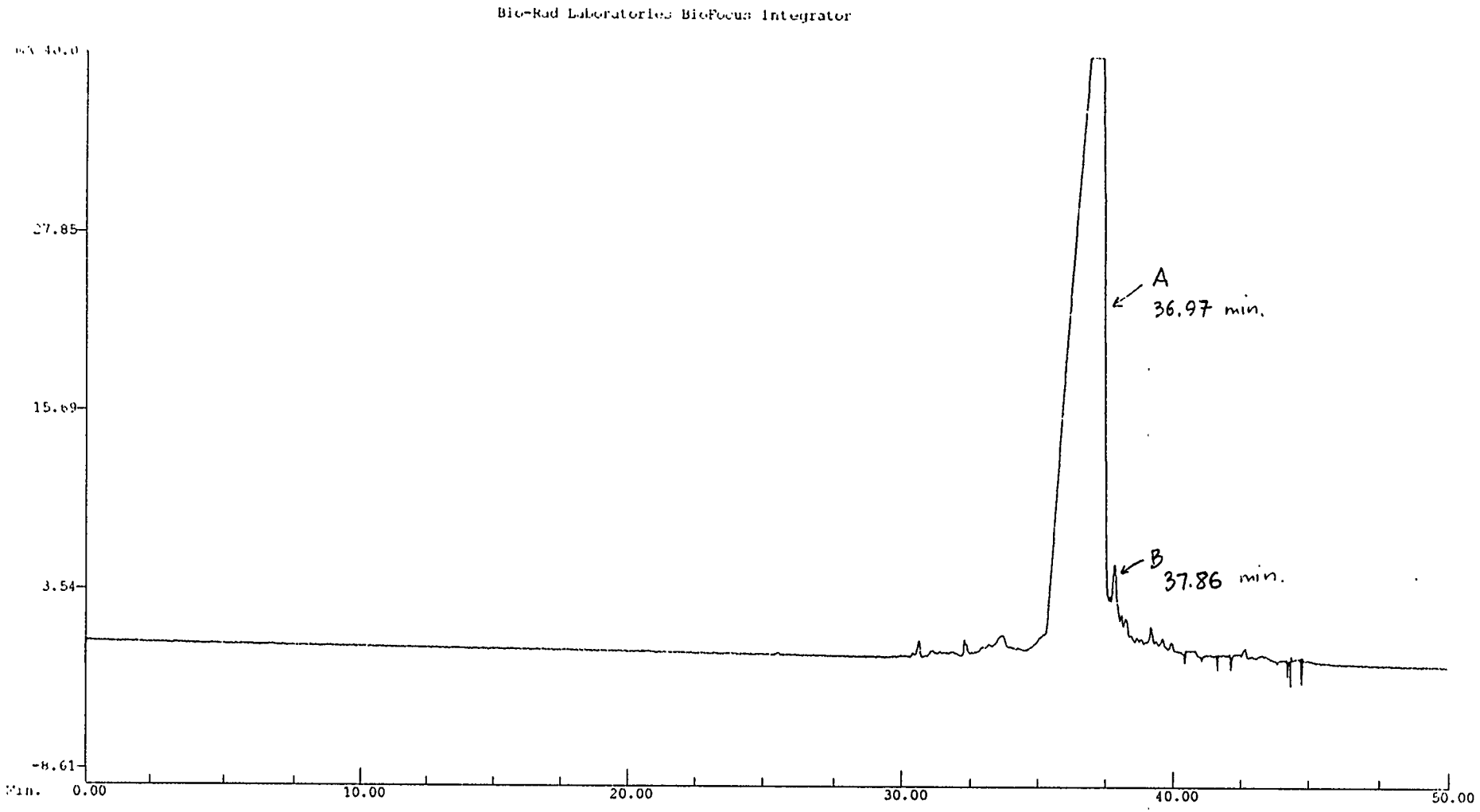

PEN	AXIS	TYPE	NAME	DATE	INSTANCE	DATA FILE
	1	METHOD	GFSAM	05-11-94	013	CHAN_1.ACQ

Running conditions

Sample: DNA oligomer; PhIP/later CZE Method GEL-FILLSAM
Capillary: 51 cm x 50 um , ID: 11445, Coated, Setpoint Temp(C): 20
Inlet: TRIS-BORATE tris borate urea
Outlet: TRIS-BORATE tris borate urea
Injection: 15.50 kV, 50 sec
Run: 15.50 kV, Polarity: - to +
Wavelength(nm): Scan 230-365, 2nm step
Carousel Setpoint Temp(C): 5
Wed May 11 13:02:04 1994 File name: C:\CE3000\CZE\GFSAM013.BFF

Figure 2A. Separation of DNA oligomer-PhIP adducts in the 2 PhIP / 1 strand molar binding ratio

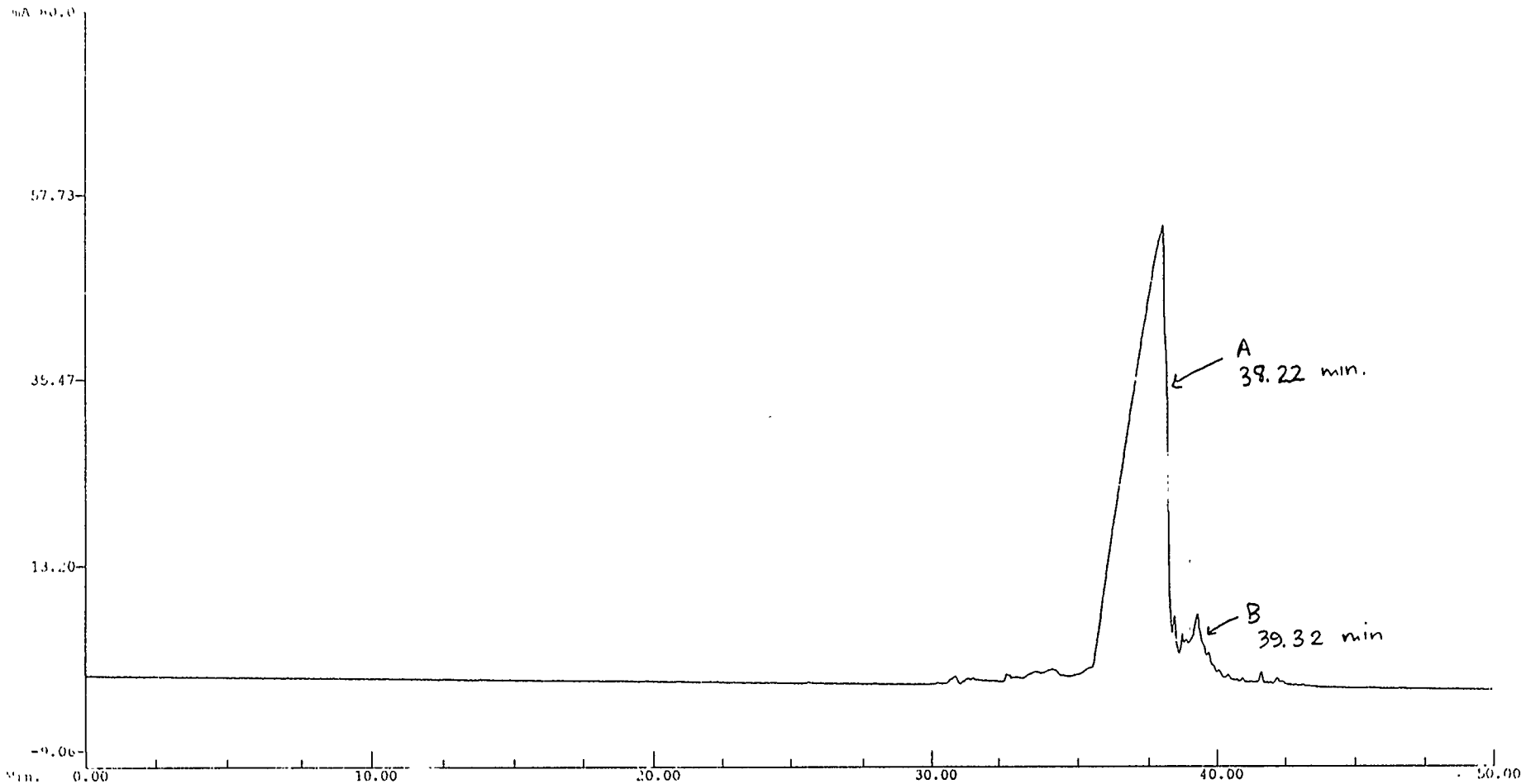

PEN	AXIS	TYPE	NAME	DATE	INSTANCE	DATA FILE
———	1	METHOD	GFSAM	05-11-94	014	CHAN_1.ACQ

Running conditions

Sample: DNA oligomer; 1PhIP/1base CZE Method GEL-FILL2SAM
Capillary: 51 cm x 50 um , ID: 11445, Coated, Setpoint Temp(C): 20
Inlet: TRIS-BORATE tris borate urea
Outlet: TRIS-BORATE tris borate urea
Injection: 15.50 kV, 50 sec
Run: 15.50 kV, Polarity: - to +
WaveLength(nm): Scan 230-365, 2nm step
Carousel Setpoint Temp(C): 5
Wed May 11 15:07:32 1994 File name: C:\CE3000\CZE\GFSAM014.BFF

Figure 2B - Separation of DNA oligomer - PhIP adducts in the 1PhIP / 1 base molar binding ratio.

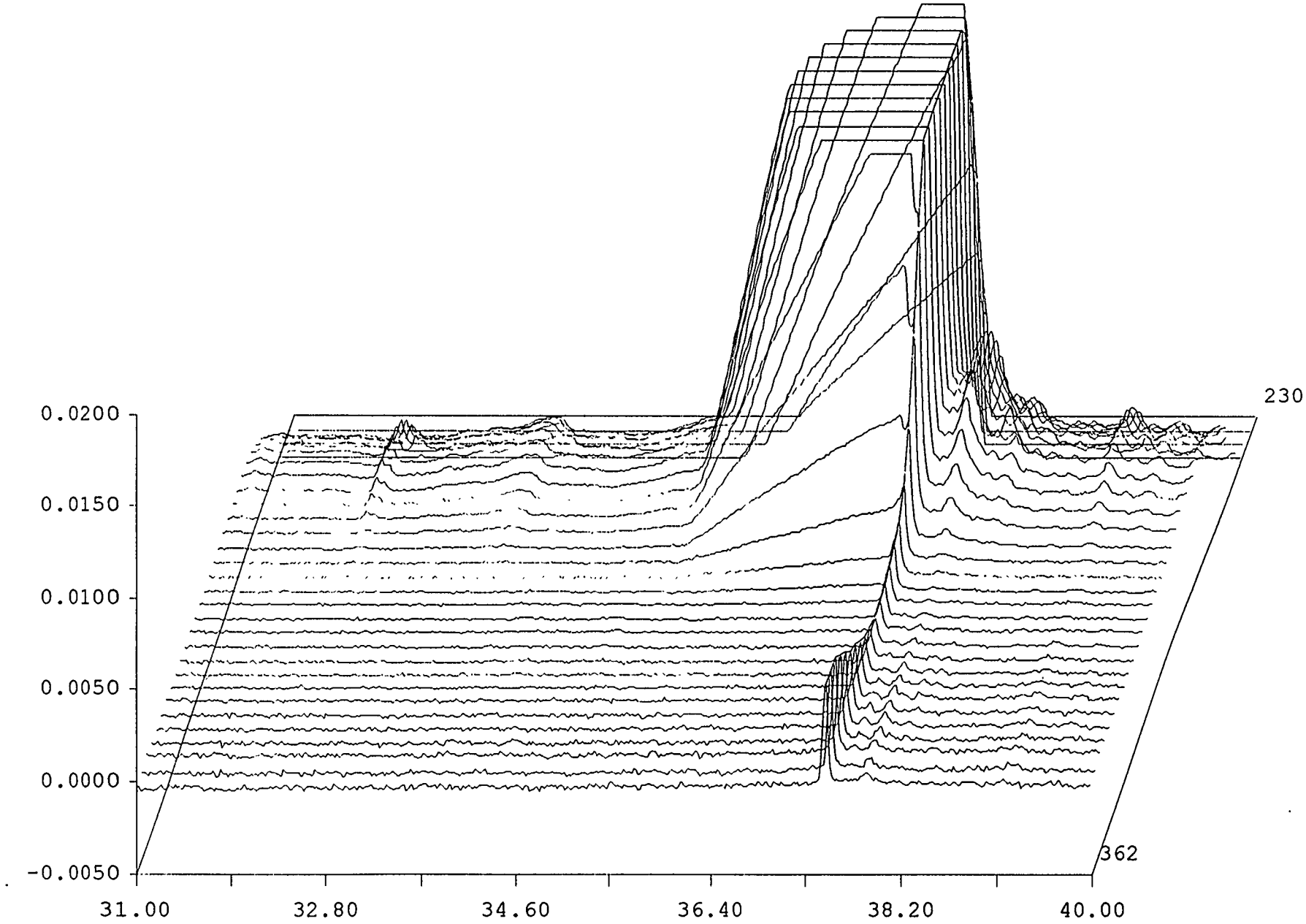

Figure 3A. Spectrum.

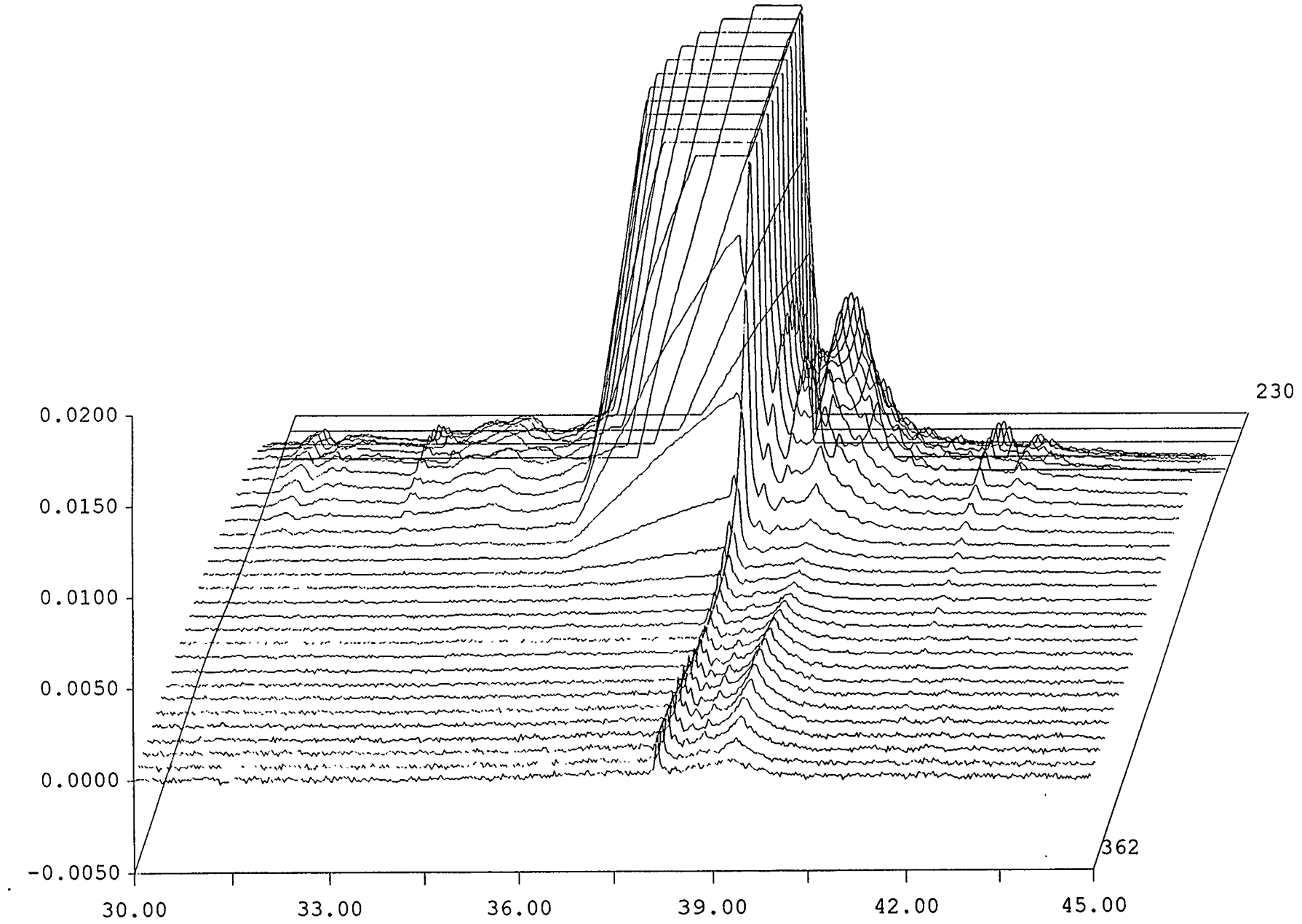

Figure 3B. Spectrum
running conditions same as in Fig 2B

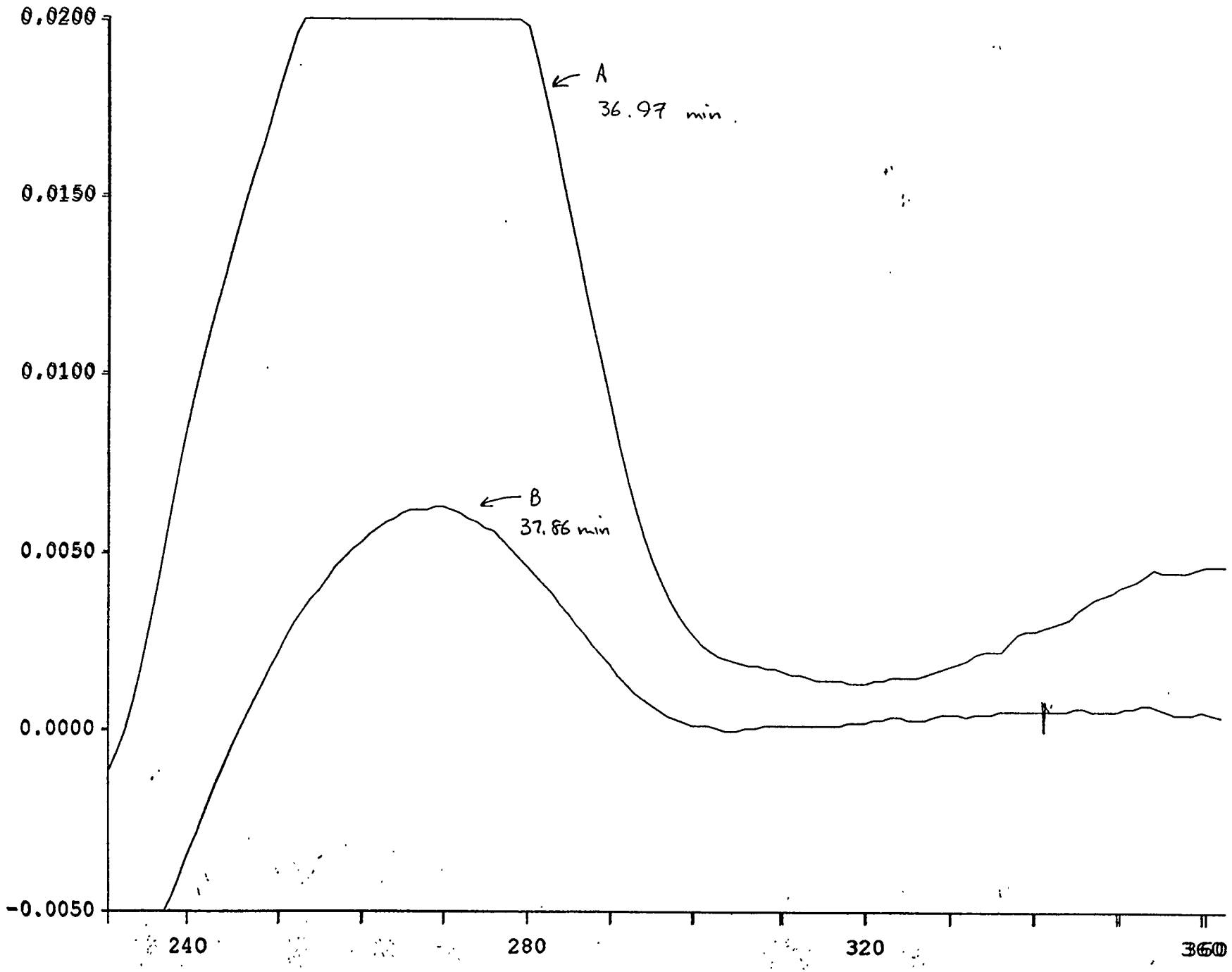
0.0200
0.0150
0.0100
0.0050
0.0000
-0.0050
A
36.97 min
B
37.86 min
240
280
320
360

Figure 4A

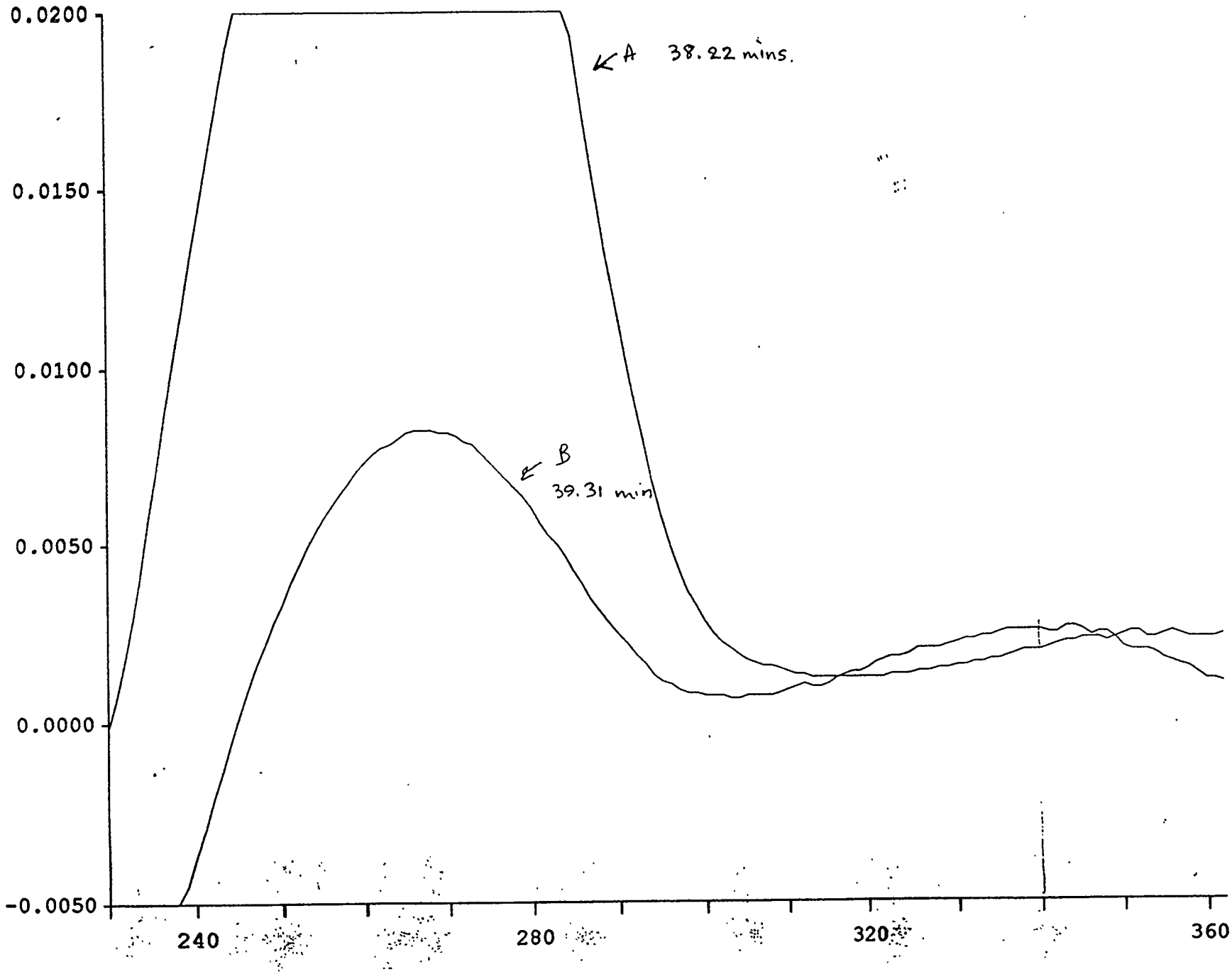
0.0200
0.0150
0.0100
0.0050
0.0000
-0.0050
A 38.22 mins.
B
39.31 min
240
280
320
360

Figura 4B.

IDENTIFICATION OF THE GENOMIC LOCUS FOR HUMAN RIESKE Fe-S PROTEIN GENE ON CHROMOSOME 19q12*

Len Alexander Pennacchio

Sonoma State University

Human Genome Center
Biology and Biotechnology Research Program
Lawrence Livermore National Laboratory
Livermore, California 94550

Spring 1994

Prepared in partial fulfillment of the requirements of the Science and Engineering Research Semester under the direction of Greg Lennon Ph.D., Research Mentor, in the Lawrence Livermore National Laboratory.

* This research was supported in part by an appointment to the U.S. Department of Energy Science and Engineering Research Semester (hereinafter called SERS) program administered by LLNL under Contract W-7405-Eng-48 with Lawrence Livermore National Laboratory.

Identification of the genomic locus for the human Rieske Fe-S Protein gene on Chromosome 19q12.

Len Alexander Pennacchio

Abstract:

We have identified the chromosomal location of the human Rieske Iron-Sulfur Protein (UQCRFS1) gene. Mapping by hybridization to a panel of monochromosomal hybrid cell lines indicated that the gene was either on chromosome 19 or 22. By screening a human chromosome 19 specific genomic cosmid library with an oligonucleotide probe made from the published Rieske cDNA sequence, we identified a corresponding cosmid. Portions of this cosmid were sequenced directly. The exon, exon:intron junction, and flanking sequences verified that this cosmid contains the genomic locus. Fluorescent *in situ* hybridization (FISH) was performed to localize this cosmid to chromosome band 19q12.

INTRODUCTION

Iron-Sulfur proteins have long been known to be key enzymes in the electron transport pathway. The ubiquinol cytochrome c reductase UQCRFS1 (as it is officially designated), otherwise known as the Rieske Iron-Sulfur protein, is a key subunit of the cytochrome bc_1 complex in the mitochondria (1,2,3). Involved in electron transport and photosynthesis, the Rieske Iron-Sulfur protein is important in redox reactions in these organelles (2). Within the mitochondria, the Rieske Fe-S protein catalyzes the transfer of electrons from cytochrome b_{566} to cytochrome c_1 (Figure 1). Although this protein is used primarily in chloroplasts and mitochondria, the Rieske gene itself is located in the nuclear genome in eukaryotes (4,5). After being transcribed, this protein's message is translated on cytoplasmic ribosomes and transported through the mitochondrial membrane to the mitochondrial cytochrome bc_1 complex (4,5). Brandt *et. al* (6). have proposed that after a single post-translational modification this protein inserts into the cytochrome bc_1 complex.

Recently, others have suggested that this protein may be implicated in various mitochondrial myopathies (7). For one type of myopathy, Schapira *et. al.* (8) suggest that a defect limiting the protein's ability to transverse the mitochondrial membrane may underlie these myopathies. These mitochondrial myopathy patients, in which the disease is inherited as an autosomal recessive, may thus have mutant Iron-Sulfur protein leader sequences preventing entry into the mitochondria. In 1988, Capaldi *et. al.* (9) found tissue specific differences between heart and liver cytochrome *c* oxidase, providing the first model for isoenzyme forms of the respiratory chain complexes. Furthermore, they refered to numerous other mitochondrial myopathies where defects are present in only one to a few tissues. In order to provide data to complement genetic linkage studies, as well as to provide a genomic source for mutation scanning within patients with various mitochondrial myopathies, we have isolated, mapped and characterized the genomic Rieske locus.

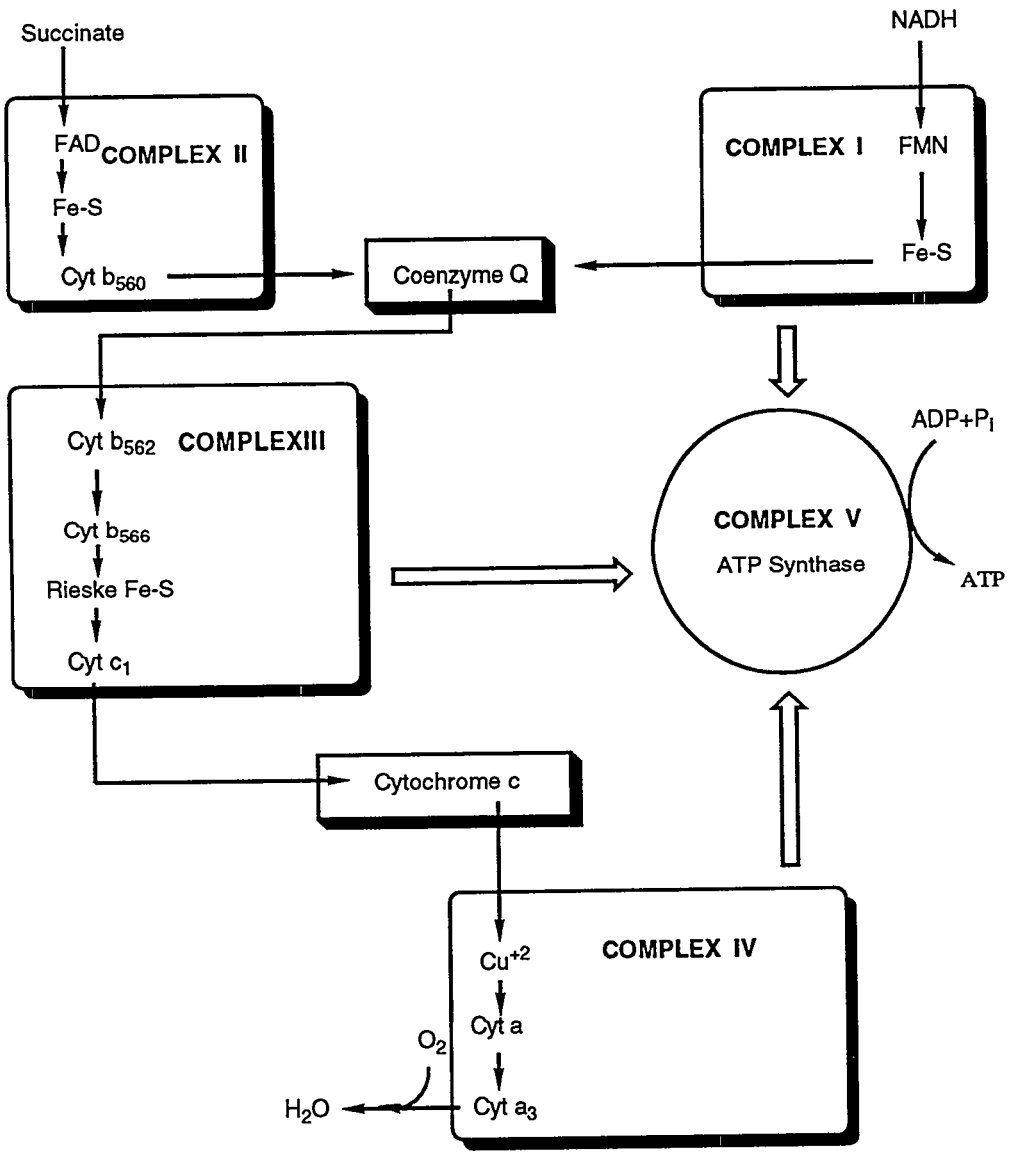

Figure 1: Biochemical pathway for electron transfer within the mitochondria.
Note the position of the Rieske Fe-S protein in the energy generation process.

RESULTS

A partial cDNA clone known as hm02g01, originally sequenced as part of an EST sequencing project (10), was mapped by Southern hybridization to DNAs prepared from human monochromosomal mouse somatic cells (11) and indicated that the corresponding locus was on either chromosome 19 or 22 (Figure 2). This partial cDNA fragment corresponds to bases 748-887 of the published Rieske cDNA sequence (12). In order to characterize the chromosome 19 cognate, a probe made from the hm02g01 PCR product was hybridized to the LLNL chromosome 19-specific arrayed cosmid library. Two clones were identified as hybridization positives : f22979 and f17252. Cosmid clone f17252 was verified by PCR to contain hm02g01 sequences. By Southern hybridization to an EcoRI restriction digestion of this cosmid, a 4.8 kb fragment was identified that was hm02g01 positive, and overlapping it, a 1.3 kb Pst I fragment. As expected, the EcoRI digested human 19 monochromosomal mouse somatic cell hybrid Southern also resulted in a 4.8kb positive fragment (Figure 2). The 4.8kb EcoRI cosmid fragment was unsuccessfully subclone but an overlapping 1.3kb EcoRI/PstI fragment was subcloned, yielding sequence data from base 567 through the 3' end of this gene. All other sequence was obtained by direct sequencing of cosmid f17252.

The sequence (Figure 3) derived from the coding region matched that of the published cDNA sequence, but a single intron is present between bases 214-215 (as numbered in Figure 3). Sequence was also obtained from regions flanking the published cDNA sequence (Figure 3).

In order to fine-map cosmid 17252 on chromosome 19, fluorescence in situ hybridization (FISH) was performed using the cosmid as probe. Hybridizations observed from ten metaphase nuclei were scored. All 20 chromatids were localized to band 19q12 (Figure 4), and no grains were observed over other chromosomes (including in particular chromosome 22.)

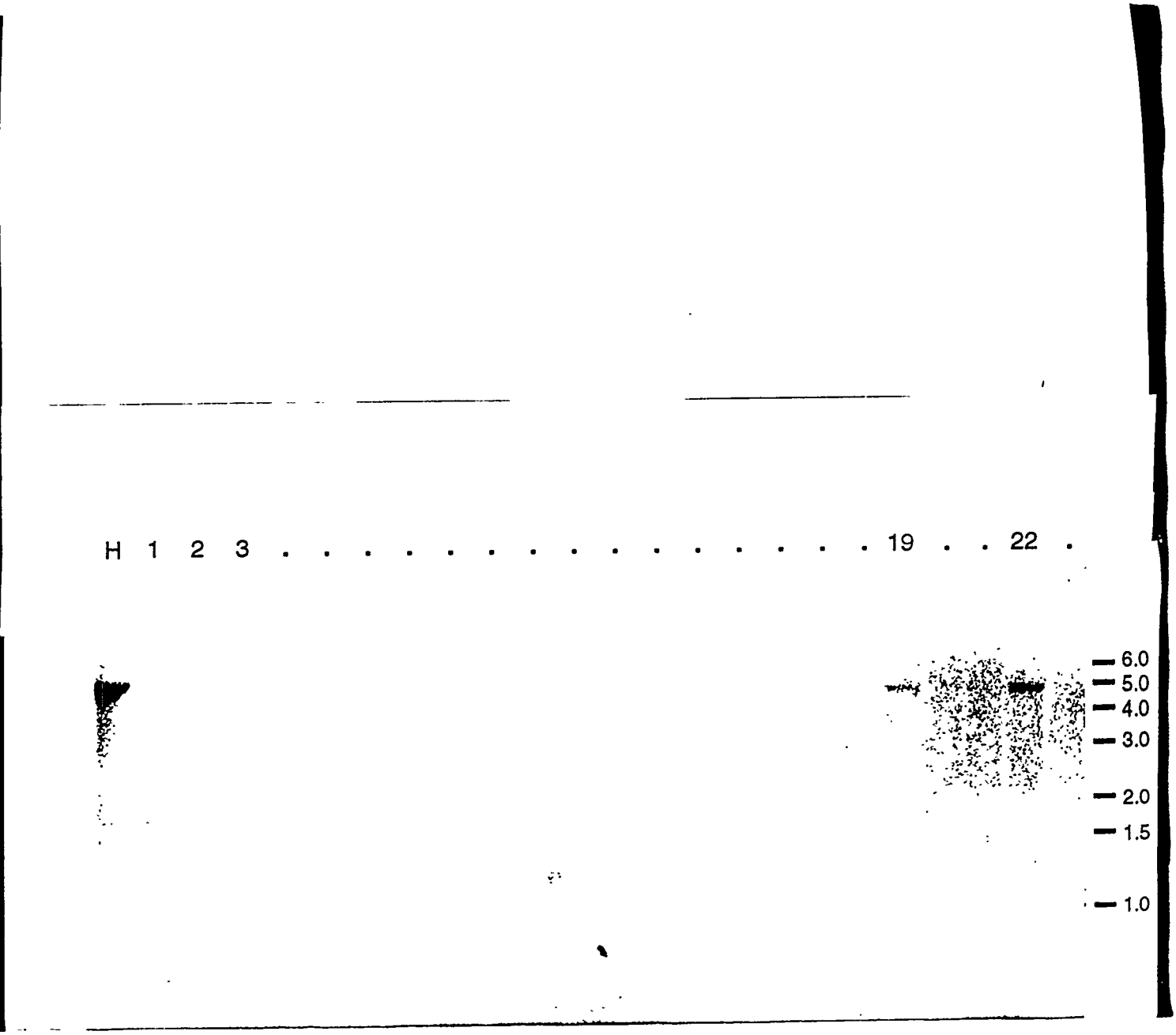

Figure 2: Human monochromosomal mouse hybrid Southern panel for the hmO2go1 probe. Note that the 4.8kb positive EcoRI fragment is the same size as the Rieske positive fragment in cosmid f17252.

```
 CCTCTCCAGGTTTGCCCCGCCCTGCAGGACTGCAGAATTTCCTTTCCGGCGGCGCGCT
GTCGTCACGCGTCCCGCGCCTCCTCGCGCCTGCACCGTGGTTGGAAGGTCGTCCCCTGT
GACCGGTTGGGCGGTTGGAGCGGCTGTCGCC ATG TTG TCG GTA GCA GCC CGC
                                 M   L   S   V   A   A   R

TCG GGC CCG TTC GCG CCC GTC CTG TCG GCC ACG TCC CGC GGG GTG
 S   G   P   F   A   P   V   L   S   A   T   S   R   G   V

GCG GGC GCG CTG CGG CCC TTG GTG CAG GCC ACG GTG CCC GCC ACC
 A   G   A   L   R   P   L   V   Q   A   T   V   P   A   T

CCG GAG CAG CCT GTG TTG GAC CTG AAG CGG CCC TTC CTC AGC CGG
 P   E   Q   P   V   L   D   L   K   R   P   F   L   S   R

GAG TCG CTG AGC GGC CAG GCC GTG CGC CGG CCT TTG GTC GCC TCC
 E   S   L   S   G   Q   A   V   R   R   P   L   V   A   S

GTG GGC CTC AAT G[gtgagccggggcgagggccg..()..gtgtttttttaacctt
 V   G   L   N

ctgtttgtcttgcag] TC CCT GCT TCT GTT TGT TAT TCC CAC ACA GAC
                   V   P   A   S   V   C   Y   S   H   T   D

ATC AAG GTG CCT GAC TTC TCT GAA TAC CGC CGC CTT GAA GTT TTA
 I   K   V   P   D   F   S   E   Y   R   R   L   E   V   L

GAT AGT ACG AAG TCT TCA AGA GAA AGC AGC GAG GCT AGG AAA GGT
 D   S   T   K   S   S   R   E   S   S   E   A   R   K   G

TTC TCC TAT TTG GTA ACT GGA GTA ACT ACT GTG GGT GTC GCA TAT
 F   S   Y   L   V   T   G   V   T   T   V   G   V   A   Y

GCT GCC AAG AAT GCC GTC ACC CAG TTC GTT TCC AGC ATG AGT GCT
 A   A   K   N   A   V   T   Q   F   V   S   S   M   S   A

TCT GCT GAT GTG TTG GCC CTG GCG AAA ATC GAA ATC AAG TTA TCC
 S   A   D   V   L   A   L   A   K   I   E   I   K   L   S

GAT ATT CCA GAA GGC AAG AAC ATG GCT TTC AAA TGG AGA GGC AAA
 D   I   P   E   G   K   N   M   A   F   K   W   R   G   K

CCC CTG TTT GTG CGT CAT AGA ACC CAG AAG GAA ATT GAG CAG GAA
 P   L   F   V   R   H   R   T   Q   K   E   I   E   Q   E

GCT GCA GTT GAA TTA TCA CAG TTG AGG GAC CCA CAG CAT GAT CTA
 A   A   V   E   L   S   Q   L   R   D   P   Q   H   D   L

GAT CGA GTA AAG AAA CCT GAA TGG GTT ATC CTG ATA GGT GTT TGC
 D   R   V   K   K   P   E   W   V   I   L   I   G   V   C

ACT CAT CTT GGC TGT GTA CCC ATT GCA AAT GCA GGA GAT TTT GGT
 T   H   L   G   C   V   P   I   A   N   A   G   D   F   G

GGT TAT TAC TGC CCT TGC CAT GGG TCA CAC TAT GAT GCA TCT GGC
 G   Y   Y   C   P   C   H   G   S   H   Y   D   A   S   G

AGG ATC AGA TTG GGT CCT GCT CCT CTC AAC CTT GAA GTC CCC ACG
 R   I   R   L   G   P   A   P   L   N   L   E   V   P   T

TAT GAG TTC ACC AGT GAC GAT ATG GTG ATT GTT GGT TAAGAGACTTG
 Y   E   F   T   S   D   D   M   V   I   V   G   *

GACTCAAGTCATAGGCTTCTTTCAGTCTTTATGTCACCTCAGGAGACTTATTTGAGAGG
AAGCCTTCTGTACTTGAAGTTGATTTGAAATATGTAAGAATTGATGATGTATTTGCAAA
CATTAATGTGAAATAAATTGAATTTAATGTTGAATACTTTCAGGCATTCACTTAATAAA
GACACTGTTAAGCACTGTTATGCTCAGTCATACACGCGAAAGGTACAATGTCTTTTAGC
TAATTCTAATTAAAAATTACAGACTGGTGTACAAGATACTTGTGAAATCTGTAACTGAC
TTTATTTTCTTGCCCTATATTTGGTTCCCGCTTTGCGTCAGGGACGCAGGTTCTGCACG
GGCATTGGTGGGATGAAGTCAAATTAACGGG
```

Figure 3. Human Chromosome 19 genomic sequence for the Rieske Fe-S protein gene. Underlined regions indicate transcribed but untranslated regions. Lowercase sequence notes the intron. Bold letters are the intron consensus acceptor and donor sequence.

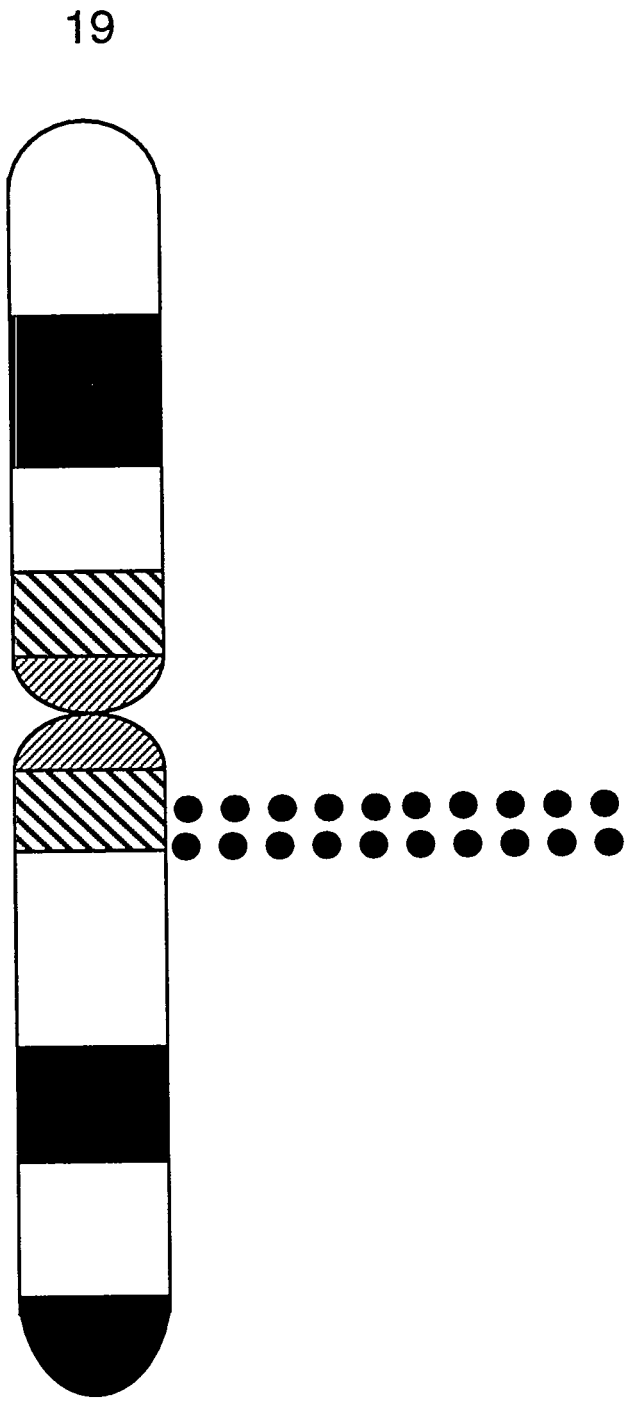

Figure 4: Idiograms of G banded chromosome 19 showing the location of cosmid clone f17252. The fluorescent signals were seen on both chromatids for 20 metaphase chromosome spreads of peripheral blood lymphocytes of a normal donor. Fluorescent bands were produced by incubation of the slides before analysis in DAPI followed by actinomycin. No hybridization signals were seen on other chromosomes.

DISCUSSION

After originally determining through mouse somatic cell hybrid experiments that regions of chromosomes 19 and 22 were homologous to the Rieske cDNA, we became interested in the nature of the chromosome 19 Rieske-homologous locus. The initial question focused on whether the chromosome 19 locus represented a pseudogene, as many of the other nuclear-encoded respiratory chain genes have been found to have pseudogene copies dispersed on various chromosomes (13, 14). The isolation of a chromosome 19 cosmid containing the Rieske locus allowed us to determine that the chromosome 19 locus is likely to be the one from which the Rieske mRNA is transcribed, and is unlikely to be a pseudogene. Four types of data support this conclusion. First, the exonic genomic sequence is identical to that of the cDNA. Second, genomic sequence 5' to the cDNA sequence has characteristics of a promoter (GC-rich, with potential transcription factor binding sites as indicated in Figure 3), and lacks repeated elements. It does not have an obvious TATAA or CCAAT box, and therefore resembles promoters observed from other housekeeping genes. Third, an intron was found within the chromosome 19 genomic Rieske sequence (Figure 3). At the exon:intron boundaries, acceptor and donor intron consensus sequences are present. This intron may therefore indicate that the Rieske protein is composed of two domains. Fourth, genomic sequence found 3' to the site of polyadenylation did not consist of a run of A's or other identifiable repeated elements, and therefore appears to represent unique sequence (Figure 3). Although the nature of the chromosome 22 Rieske-homologous locus remains unknown, it may represent a pseudogene of the gene on chromosome 19. We can not rule out the possibility that the DNA prepared from the chromosome 22 somatic cell hybrid was contaminated with chromosome 19 DNA, although this seems unlikely based on the strength of the signal seen in Figure 2. Indeed, hybridization signals derived from the use of cDNA probes may in fact be stronger to highly conserved processed pseudogene loci than to the intron-containing, and thus interrupted, transcribed loci. It is also unlikely that a duplication involving a large segment of DNA has occured, since in the

FISH experiment using the entire cosmid signal was only observed over cytogenetic band 19q12 and not over chromosome 22.

While this localization confirms that this gene is encoded within the nuclear genome, making it the third gene (after COX6B and COX7A1) involved in a mitochondrial respiratory chain complex to be mapped to chromosome 19, it does not appear that either these or other similiar genes are clustered in one region of the genome. The two chromosome 19 COX genes map to different locations (COX6B to 19q13.1 (15); COX7A1 to 19p13.1 (16, 17, pers. comm.), and the two other ubiquinol cytochrome c reductases known (UQCRC1 and UQCRC2) map to chromosomes 3 and 16, respectively (17, 18).

The localization of the Rieske locus to chromosome 19q12 and the characterization of the genomic structure of the gene may now encourage further efforts at identifying the specific mutations associated with associated mitochondrial myopathies.

MATERIALS AND METHODS

Oligonucleotide synthesis

Based on the published Rieske cDNA sequence (12), the following oligonucleotides were synthesized by the phosphoramidite method on an ABI DNA Synthesizer.

A (F4) CTG AGC GGC CAG GCC GTG CGC C

B (R2) GGA ATA ACA AAC AGA AGC AGG G

C (hm02go1F1) ACG TAT GAG TTC ACC AGT GAC G

D(hm02go1 R1) GGC TTC CAC TCA AAT AAG TCT CC

E(RmidR2) CCC ATT CAG GTT TCT TTA CTC G

F(R4) CTG AGC GGC CAG GCC GTG CGC C

G(RnonCF1) CGG TTG GAG CGG CTG TCG

H(R8) CAG CGC GCC CGC CAC CCC GCG GGT

Somatic cell mapping

Human monochromosomal somatic cell southern hybridizations were done by Fukushima *et. al.* as described previously. (11) The DNA Database of Japan (DDBJ) accession number for clone hm02g01 is D11847.

Cosmid Screening and Subcloning

Polymerase Chain Reaction (PCR) was performed on flow sorted human chromosome 19 DNA with primers hm02g01F1 and hm02g01R1. The cycling conditions were as follows: 94 10", 55 30", 72 20" (Perkin Elmer 9600). The product was separated on a 1.5% agarose gel, and visualized by Ethidium Bromide staining. The band of interest was excised and eluted by placing at 55 degrees in 100ul of TE. This DNA was then labeled by assymetric PCR using primer hmogo1 R1 and [α-P^{32}]dCTP. This probe was used to screen a chromosome 19 specific cosmid library. Filters were washed at low stringency (2XSSC, 1%SDS) twice for 30 minutes at 65 degrees. Next, filters were washing twice in a high stringency wash (.2XSSC,1%SDS). Signals were visualized using a Molecular Dynamics PhosphorImager. A clone positive for the probe was EcoR1 digested, analyzed by electrophoresis on a .8% agarose gel, Southern blotted, and hybridized to the same assymetrical PCR probe as used above. A positive 4.8kb fragment was further digested with Pst1, analyzed on a 1% agarose gel, Southern blotted and rehybridized with the same assymetrical PCR probe. The resulting positive 1.3 kb fragment was cloned into pKS^- cut with EcoR1/Pst1. Positive clones were identified by Grunstein-Hogness colony screening methods as described in Sambrook *et al.* (19)

Sequencing

This clone was sequenced using a flourescent dye terminator kit (SequiTherm^{TM}, ABI) and 25 cyles of PCR. Other regions of this gene were sequenced by direct Dye Terminator sequencing of EcoR1 cut cosmid. For each sequencing reaction 2.5ug of cosmid f17252 was used as template.

Fluorescence *in situ* Hybridization (FISH)

A cosmid probe was hybridized to metaphase chromosomes. The slide preparation and hybridization conditions used in the procedure was as described previously (20). A total of 10 cells were scored.

ACKNOWLEDGEMENTS

This work was performed under the auspices of the U.S. Department of Energy by Lawrence Livermore National Laboratory under contract no. W-7405-Eng-48. I was a participant of the Department of Energy Science & Engineering Semester (SERS) program. I wish to thank Dr. Barb Trask for FISH advice, the Sequencing Laboratory of Dr. A. Carrano and J. Lamerdin for technical assistance, Drs. K. Okubo and K. Matsubara for their support of this work, and Arash Salemi, Anne Bergmann, Greg Lennon, Kimberly Lieuallen, Jackie Perry, Jason Martin and Christa Prange.

REFERENCES

1. Rieske, J.S. (1967) In Estabrook RW, Pullman ME (ed). Methods in Enzymology-Oxidation and phosphorylation. Academic Press, New York. **10**, 239-245.
2. Rieske, J.S. (1976) Biochem. Biophys. Acta **456**, 195-247.
3. Trumpower, B.L., Edwards, C.A. (1979) The Journal of Biological Chemistry **254**, 8697-8706.
4. Glick,B.S., Beasley, E.M., Schatz, G. (1992) Trends in Biochemical Science **17**, 453-459.
5. Hartl, F.U., Neupert, W. (1990) Science **247**, 930-937.
6. Brandt, U., Yu, L., Yu, C.A., Trumpower, B.L. (1993) The Journal of Biological Chemistry **268**, 8387-8390.
7. Slipetz, D.M. Aprille, J.R., Goodyer, P.R., Rozen, R. (1991) American Journal of Human Genetics **48**, 502-510.
8. Schapira ,A.H.V., Cooper, J.M., Morgan-Hughes, J.A., Landon, D.N. Clark, J.B. (1990) The New England Journal of Medicine **323**, 37-42.
9. Yanamura, W., Yhang, Y.Z., Takamiya, S., Capaldi, R.A. (1988) Biochemistry **27**, 4909-4914.
10. Okubu, K., Hori, N., Matoba, R., Niyama, T., Fukushima, A., Kojima, Y., Matsubara, K. (1992) Nature Genetics **2**, 173-178.
11. Fuskushima, A., Okubo, K., Sugino, H., Hori, N., Matoba, R., Niyama, T., Murakawa, K., Yoshii, J., Yokoyama, M., Matsubara, K. (1994) Genomics **21**, 1-11.
12. Nishikimi, M, Hosokawa, Y., Toda, H., Suzuki, H, Ozawa, T. (1990) Biochemistry International **20**, 155-160.
13. Vanin, E.F. (1985) Annual Review in Genetics. **19**, 253-272.
14. Seelan,R.S., Padmanaban, G. (1988) Gene **67**, 125-130.
15. Taanman, J.W., van der Veen, A.Y., Schrage, C., de Vries, H., Buys, C.H.C.M. (1991) Human Genetics **87**, 325-327.
16. Arnaudo, E., Hirano, M., Seelan, R.S., Milatovich, A., Hsieh, C.L., Fabrizi, G.M., Grossman, L.I., Francke, U., Schon, E.A. (1992) Gene **119**, 299-305.
17. Hoffman, G.G., Lee, S., Christiano, A.M., Chung-Honet, L.C., Katchman, S., Uittos, J., Greenspan, D.S. (1993) The Journal of Biological Chemistry **268**, 21113-21119.
18. Duncan, A.M.V., Ozawa, T., Suzuki, H., Rozen, R. (1993) Genomics **18**, 455-456.
19. Maniatis, T., Fritsch, E.F. and Sambrook, J. (1982) Molecular Cloning: A Laboratory Manual. Cold Spring Harbor.
20. Trask, B.F. (1990) In Functional Organization of the Nucleus- A Laboratory Guide, Methods in Cell Biology **35**, (eds). Hamkalo, B.A. and Eglin, S.C.R. (Academic Press, San Diego), 3-35.

My research at Lawrence Livermore National Laboratory concentrated on the application of sol-gel and photoresist thin films(on the order of 100-300nm) by a new coating process called meniscus coating. I worked under Jerry Britten, a chemical engineer matrixed into the lasers program and Ian Thomas, a chemist matrixed into the lasers program. Before describing my work, I will first describe the reasoning behind meniscus coating and then its coating process.

Coupled with the construction of Inertial Confinement Fusion(ICF) lasers, such as *Beamlett*, is the need for large, dielectric, laser-damage resistant, multilayer reflectors for high power laser applications(Britten, 1993). Until recently, such reflectors were manufactured using electron-beam evaporation technology; now, however, sol-gel processing techniques have vindicated the prospect of making these mirrors at a substantially lower cost. In 1989, Ian Thomas, produced damage resistant alumina/silica sol-gel multilayer quarter-wave interference mirrors which met ICF requirements-laser damage threshold (40J/cm^2 at 10ns) and reflection (>99%). Interference mirrors are made by alternatively applying reflective and anti-reflective sol-gel coatings to a glass substrate. The thickness of the coatings are varied according to the desired interference effects, either constructive or destructive interferences.

The feasible and low-cost application of these thin films on large substrates justifies meniscus coating or laminar flow coating. Spin coating large(50cm in length) square substrates proved non-feasible and thickness nonuniformities due to non-Newtonian rheology also posed problems. Dip coating required large amounts of suspensions which were susceptible to gelation. The possibility of contamination between sol suspensions was another problem. The above complications lead to the construction of a large scale meniscus coater.

The meniscus coater works by producing a thin liquid film over the flattened top of a long tubular metal applicator. The thin liquid film is created by pumping suspension out of a long slit in the top of the metal applicator. The applicator moves under the substrate such that the film comes in contact with the substrate surface. As the applicator is moved relative to the substrate it leaves behind a very thin coating on the substrate. The excess suspension is collected in a trough located beneath the applicator tube, filtered, and then recirculated.

The majority of my research dealt with characterizing these coatings through interferometry, although I did spend a sufficient amount of time with the calibration of film thickness and the maintenance of the meniscus coater. In dealing with the measurement of thin films I used three instruments: a spectrophotometer, an ellispometer, and a Dektak. The spectrophotometer measures transmission or reflection wavelength. I used the spectrophotometer, on a daily basis, to plot percent transmission versus wavelength. From these graphs I was able to

calculate the thickness of the coating using the formula:

$$nd=\lambda/4$$

where **n** is the theoretical index of the coating, **d** is the thickness of the coating, and the greek letter lambda is the wavelength of the first harmonic. I seldom used the ellipsometer, which measures index and coating thickness, and the Dektak, which utilizes a contact sytlus to measure optical thickness through surface step. From the above instruments, I was interested in determining the refractive index and, more often, the thickness of the coating.

Thin film thickness varies both with applicator speed and the dissolved/suspended solid concentration in the suspension. I focused more on the applicator speed as a method of varying coating thickness. The curvature of the meniscus determines the initial liquid film height. The reason I mention initial liquid film height is because initially the coating is entrained as a liquid coating, but during drying there is much evaporation causing the final film height to be thinner. One would expect the film to be thinner for faster applicator speeds or larger curvatures, but the exact opposite is true, the faster the applicator speed the thicker the films. Much of my time was spent calibrating film thickness by adjustment of applicator speed on the meniscus coater.

The characterization of the films and the calibration of film thickness were fairly straightforward, however, my mentor and I did spend valuable time correcting complications with the coatings that were visible to the naked eye such as edge effects and dust contaminates. Edge effects are created when suspension accumulates along the edges and then creeps back onto the coating. These edge effects were more prominent along the edges parallel to the applicator tube, particularly the back edge where the applicator leaves the substrate. A knife edge, which contacts the back edge of the substrate, was supposed to compensate for these edge effects, but they were still present in our coatings. We first reasoned that the edge effects were present because the knife was not fully contacting the glass substrate, thus allowing suspension to creep back onto the substrate instead of the knife edge. Therefore, we increased the air pressure of the pneumatically controlled knife edge so that we could actually hear the edge contacting the substrate. This turned out to correct the problem. A more involved problem with edge effects was coating round glass substrates. To compensate for such edge effects, we glued a square extension onto the round substrate so that all the suspension would creep back onto the glued piece. This idea worked very well.

Another problem encountered during coating was dust contaminates. Ideally, it would be appropriate to meniscus coat in a clean room, but since we were not afforded such luxuries we had to compromise. In dealing with dust we tried to keep the

inside of the meniscus coater as dust free as possible and this included building dust lids. Although the lids did keep dust out, they could not be closed during coating because they would cause random airflow currents in the coater. This in turn would create visual drying bands on the coatings and it was therefore necessary to keep the lids up during coating. We tried to decrease the airflow currents inside the coater by placing a mesh underneath the substrates during drying, but still, drying bands were present. We decided that it would be best if we left at least one lid up during coating; this in fact allowed for the least amount of dust contaminates on the coatings.

Although the scope of my work at Livermore involved characterizing the coatings and correcting any problems encountered during the coating process, my main objective was to create a multilayer mirror. Near the end of my stay at Livermore I was approaching this goal, but due to problems with the chemistry of the sol-gels and the breakdown of the meniscus coater I was unable to create a mirror. Thus, the only drawback of my research at Lawrence Livermore National Laboratory was the lack of time. My research was very interesting and my mentor provided me with a HP workstation so I was able to learn the basics of UNIX. My research at Lawrence Livermore was a valuable compliment to my education. I was able to break away from the books and see the laboratory side of engineering.

Hydrogen Production by Gasification of Municipal Solid Waste

Robert Rogers

Rutgers University

Lawrence Livermore National Laboratory
Livermore, California 94550

May 20, 1994

Prepared in partial fulfillment of the requirements of the Science and Engineering Research Semester under the direction of Charles Thorseness, Research Mentor, in the Lawrence Livermore National Laboratory.

*This research was supported in part by an appointment to the US Department of Energy Science and Engineering Research Semester (hereinafter called SERS) program administered by LLNL under Contract W-7405-Eng-48 with Lawrence Livermore National Laboratory.

Abstract

Abstract As fossil fuel reserves run lower and lower, and as their continued widespread use leads toward numerous environmental problems, the need for clean and sustainable energy alternatives becomes ever clearer. Hydrogen fuel holds promise as such an energy source, as it burns cleanly and can be extracted from a number of renewable materials such as municipal solid waste (MSW), which is considered to be largely renewable because of its high content of paper and biomass-derived products. A computer model is being developed using Aspen Plus™ flowsheeting software to simulate a process which produces hydrogen gas from MSW; the model will later be used in studying the economics of this process and is based on an actual Texaco coal gasification plant design. This paper gives an overview of the complete MSW gasification process, and describes in detail the way in which MSW is modeled by the computer as a process material, and how the gasifier unit itself is modeled, which is responsible for the simulation of the MSW being heated under pressure and reacting to form a mixture of gases which include hydrogen.

Introduction - MSW gasification

The municipal solid waste (MSW) gasification to hydrogen process follows the following scheme:

Preprocessing: The raw MSW is fed into the preprocessing section of the plant, where the MSW is shredded into appropriate-sized pieces. It then is mixed with water and heated anaerobically until the material begins to break down, forming a black gooey substance that is fluid-like enough to be a pumpable material. Some CO_2 formation takes place during this step, and efforts are made to remove it so that the gasifier can avoid the needless energy burden of having to heat it.

Gasification: The pretreated MSW/water slurry is fed into the gasifier with oxygen. The materials enter through the top of the gasifier and react as they fall down the length of its height. Reactants provide all the heat needed for gasification, as some of the feed undergoes combustion.

Quench: The bottom half of the gasification unit acts as a quench unit. Water is sprayed in under high pressure from spray jets on the walls and is contacted with the hot gas, thereby cooling the product stream and slowing reaction kinetics to prevent complete conversion to CO_2 and H_2O. The dirty water collects at the bottom of the unit in a pool, which collects the ash (now in liquid state) from the gas stream. An outlet liquid stream removes both dirty water and ash together, leaving a clean and moisture-saturated gas stream to exit the unit.

Shift: The quenched gas stream comes into the shift reactors saturated with water vapor. Using catalyst technologies, one can cause the CO and H_2O to exchange an oxygen atom, leaving H_2 and CO_2 as products.

Separation: This section will probably be preceded by heat exchangers and pressurization equipment, which both cool and pressurize the gas stream, thus "squeezing" much of the water vapor out of the product gases. Pressure-Swing-Adsorption columns remove remaining water. The gas stream enters these columns under high pressure and conditions which selectively adsorb CO_2, H_2O and other impurities, allowing a purified hydrogen stream to emerge from the process. When the adsorbent has taken up as much as it can hold, the gas stream is switched to pass through another set of PSA columns to allow continuous processing. The pressure is reduced in the saturated columns, and the CO_2, H_2O, etc. desorb.

Modeling MSW

MSW has no strict chemical formula, as it is a mixture of many different materials, and has a composition that changes depending on where it comes from. However, ASPEN PLUS can only calculate chemical reactions with so called "conventional components", those that have strict chemical formulas (H_2O, for example), and whose properties are well understood and measurable.

Thus, a way to characterize the MSW was taken from the coal industry, which is supported in Aspen Plus. The coal industry uses Ultimate, Proximate, and Sulfur analyses to describe its coal samples, and the same method was applied to characterizing MSW:

Ultimate Analysis: MSW samples are characterized by their C, H, N, O, S, and Ash content, on a moisture-free weight percent basis.

Proximate Analysis: MSW samples are characterized by their Fixed Carbon, Volatile Carbon, Ash, and Moisture weight percent. The first three parameters are entered on a moisture free basis, and should together total 100%. Any moisture content native to the MSW sample itself is included here, entered as a weight percent of a wet sample. Unless better information is available, the ratio between the Fixed and Volatile Carbon contents is set 1:1.

Sulfur Analysis: The sulfur content of the MSW is split into three categories: Sulfatic, pyritic, and organic. All of these are entered as weight percents of the total dry sample. They should not add up 100%; rather, they should total the weight percent of the sulfur content entered in the Ultimate Analysis. Unless better information is available, all of the sulfur is assumed to be organic.

Figure 1:[i]

Dry MSW Ultimate Analysis

Sample*	C	H	N	Cl	S	O	Ash
MSW 1	43.67	5.65	0.24	0.00	0.11	33.45	16.88
MSW 2	37.08	5.31	0.50	0.00	0.21	26.89	30.02
MSW 3	44.40	6.01	0.70	0.47	0.19	33.24	15.00
MSW 4	49.70	5.40	0.20	0.00	0.10	39.30	5.30
MSW 5	40.09	6.20	0.55	0.31	0.56	29.73	22.57
MSW 6	47.60	6.00	1.20	0.00	0.30	32.90	12.00
MSW 7	33.90	4.60	0.70	0.00	0.40	22.40	38.00
MSW 8	45.48	5.93	0.60	0.14	0.28	34.18	13.39
MSW 9	34.89	4.66	0.80	0.13	0.13	29.43	29.96

Heat of Combustion Model

The heat of combustion of the MSW can be modeled in one of two ways: using a correlation (the Boie Correlation or other, such as the IGT Correlation) or by inputting the value manually, if it is known. To do either, one must go into the ASPEN PLUS input (*.inp) file running the simulation, and look for code similar to the following:

```
NC-PROPS {name1} ENTHALPY HCOALGEN {1 or 6} 1 1 1 / DENSITY DCOALIGT

PROP-DATA
    PROP-LIST BOIEC
    PVAL {name1} 98 499.77 45 25 27 -189
```

PROP-DATA
PROP-LIST HCOMB
PVAL {name1} {heat of combustion, in J/kg}

{name1} corresponds to the variable name assigned to the biomass or MSW material being gasified.

The sequence of numbers: 1 1 1 1 in the "NC-PROPS" line defines how the simulation handles various calculations. by changing the first of these four values, one can alter how it calculates the heat of combustion.

If the first value is set to "1", then the model uses the Boie Correlation to calculate the heat of combustion; the code below this that begins with: PROP-DATA / PROP-LIST BOIEC defines what coefficients should be used in the Boie Correlation. These values should not be changed.

If the first value is set to "6", then the model uses a user-input value for the heat of combustion of the MSW (if obtained from other sources, or if using a correlation not included in Aspen Plus, such as the modified IGT Correlation); the code below this that begins with: PROP-DATA / PROP-LIST HCOMB defines what heat of combustion will be assigned to the MSW, regardless of its Ultimate Analysis makeup.

Boie Correlation

The coal industry defines the Boie Correlation to be:

$$\Delta Hc(BTU/lb.) = a_1C + a_2H + a_3S + a_4O + a_5N + a_6$$

The value returned for the heat of combustion is on a moisture-free, but ash-containing basis. The C, H, O, etc. contents are taken from the Ultimate Analysis. When the constants which are standard for this correlation[ii] were used in calculating the heats of combustion of MSW samples, unsatisfactory results were obtained. However, when two of the constants were modified (a1 and a4), more accurate results were obtained; the modified set of constants are the ones presently included in the process model.

Standard Constants	Modified Constants
$a_1 = 151.2$	$a_1 = 98$
$a_2 = 499.77$	$a_2 = 499.77$
$a_3 = 45.0$	$a_3 = 45$
$a_4 = -47.7$	$a_4 = 25$
$a_5 = 27.0$	$a_5 = 27$
$a_6 = -189.0$	$a_6 = -189$

User Input Value

If the heat of combustion is known for a given MSW sample, its value may be input manually into the model. It must be input in units of [J/kg], on a moisture-free, ash-containing basis.

IGT Correlation

A modified version of the IGT correlation was also considered as a correlation to predict the heat of combustion of MSW. It was of the form:[iii]

$$\Delta H_c(KJ/g) = 0.341C + 1.322H - 0.12(O+N) - 0.0153Ash + 0.0686S$$

Results

What follows are sets of MSW and Biomass samples which compare predicted heats of combustion, or Higher Heating Values (HHV), obtained from the modified Boie and IGT correlations against values found in the literature.

Figure 2:

Comparison of dry MSW HHV's

Sample	HHV (MJ/kg) Literature	HHV (MJ/kg) modified Boie	% error (vs Lit)	HHV (MJ/kg) modified IGT	% error (vs Lit)
MSW 1 *	15.78	17.83	12.99	18.06	14.45
MSW 2 *	14.95	15.43	3.21	15.93	6.56
MSW 3	18.81	18.46	-1.86	18.79	-0.11
MSW 4	19.40	19.38	-0.10	19.27	-0.67
MSW 5 *	16.95	17.45	2.95	17.93	5.78
MSW 6	19.87	19.22	-3.27	19.91	0.20
MSW 7	13.13	13.56	3.27	14.32	9.06
MSW 8 *	19.16	19.47	1.62	18.98	-0.94
MSW 9 *	14.53	14.33	-1.38	13.98	-3.79

* Literature dry HHV was calculated from actual reported wet HHV
i.e. wet HHV = dry HHV (1 - moisture fraction)

Figure 3:[iv]

Comparison of dry Biomass HHV's

Sample	Literature	HHV (MJ/kg) modified Boie	% error (vs Lit)	HHV (MJ/kg) modified IGT	% error (vs Lit)
Pinot Noir Clippings	19.05	14.20	-25.46	18.46	-3.10
Black Locust	19.71	20.20	2.49	19.73	0.10
Manure - fresh	17.36	18.06	4.03	18.56	6.91
Cotton Gin Waste	16.24	16.71	2.89	15.58	-4.06
Rice Straw (weathered)	14.56	13.85	-4.88	12.27	-15.73
Tan Oak (combined)	18.93	19.89	5.07	18.80	-0.69
Brown Paper	17.92	19.65	9.65	17.60	-1.79
Waxed Cartons	27.28	25.57	-6.27	28.77	5.46
Pineapple Waste	18.47	19.76	6.98	19.00	2.87
Corn Cobbs	18.77	17.70	-5.70	18.11	-3.52

Discussion

Clearly, the data above show that no one model can be used to predict the heats of combustion for all materials. In terms of modeling MSW, the best model that was achievable was a modified form of the Boie correlation; it predicted heats of combustion for nine MSW samples, usually within a 3% error range. One of the nine cases had a glaring error of 13%, although it is not understood why this is the case, since the sample's Ultimate Analysis data did not vary greatly from any of the other samples.

A similar situation was true when predicting the heats of combustion for the random biomass samples. In this case, the most effective correlation was the modified IGT equation; it predicted within 6% error for most of the samples, but again there was one glaring case where the error was much larger.

Gasifier Model

Because MSW is a "non-conventional" (no set chemical structure) type of material, some special steps must be taken within the simulation to deal with this problem. The first step is to introduce an RYIELD reactor into the simulation; this unit performs no real chemical calculations that are indicative of what happens in real life, but rather its output is specified to set conditions which enable another ASPEN PLUS reactor, the RGIBBS reactor, to perform the actual chemical reaction simulations that occur within the gasifier. The combined energy requirements of the two reactors make up the overall heat duty for the actual gasification unit which is being simulated.

RYIELD

The MSW material enters the RYIELD reactor and is broken down into its elemental components. Based on its Ultimate Analysis data, a FORTRAN routine within the ASPEN PLUS input file calculates how many moles of elemental C, H, O, etc. make up the MSW. The RYIELD reactor then outputs a stream of material containing moles of H2O, C, H, O, N, S, Cl, and Ash; it no longer contains any single type of material which is characteristic of MSW.

RGIBBS

The RGIBBS reactor is the actual unit which performs chemical equilibrium calculations to represent the reactions which occur within the gasification unit.

Reactions Modeled

For an RGIBBS reactor, ASPEN PLUS requires that (A-M) number of chemical reactions be specified, where A is the number of different atomic species expected to leave the reactor, and M is the number of molecular species expected to leave the reactor. The chemical reactions specified do not have to represent the reactions which actually occur within the reactor, but must involve all atoms and molecules

expected to leave the reactor, and must be reactions which are linearly independent of each other. The following are the reactions which are considered by the RGIBBS reactor:

1) $H_2 + \frac{1}{2} O_2 \leftrightarrow H_2O$
2) $CO + H_2O \leftrightarrow H_2 + CO_2$ **(Water - Gas - Shift Reaction)**
3) $CH_4 + H_2O \leftrightarrow 3H_2 + CO$ **(Methanation Reaction)**
4) $COS + H_2 \leftrightarrow H_2S + CO$

The fact that all species and molecules must be accounted for leads to one major problem. That is, reactions cannot be entered into Aspen which do not occur all of the time. For instance, some MSW samples contain chlorine, and others do not. Thus, samples which contain chlorine in real life will lead to the formation of some HCl in a real life gasifier, but this cannot be taken into account in our model because not all MSW samples contain chlorine, and if the reaction representative of HCl formation were to be entered into ASPEN PLUS, the simulation would crash when it tried to perform calculations on an MSW sample which did not contain any chlorine.

One possible solution to this problem would be to include the reaction for HCl formation, and to ensure that all the Ultimate Analysis data which is entered for any MSW sample contain at least 0.0000001 wt% of chlorine. If chlorine were to be entered in this amount for a MSW sample which actually continued no chlorine, the overall outcome of the simulation would not be altered in any significant way, but the trace amount of chlorine would allow the RGIBBS reactor to perform its HCl formation calculation, thus preventing the simulation from crashing.

Temperature Approach

To adjust the output of the simulation gas composition so that it matches the output composition of a real life gasifier, one may adjust the temperatures at which the chemical equilibriums are calculated for each reaction considered. To do this, Temperature Approaches are set for the RGIBBS reactor in the ASPEN PLUS input file. A temperature approach is a temperature difference between the reactor temperature and the temperature at which equilibrium is calculated for a given reaction.

Reactor Temperature

Because the output composition of the RGIBBS unit is controlled mainly by the temperature approaches of the reactions considered, the actual temperature of the gasifier has very little effect on its output composition (i.e. the equilibrium of the water-gas-shift reaction is often computed near the same absolute temperature, because design specifications within the simulation adjust temperature approach values counter to changes in the reactor temperature, in order to obtain the correct outlet composition). Yet, it remains important for the RGIBBS gasifier run at an appropriate temperature (1400-1500C), because its temperature will effect heat duties, heat losses, energy balances, etc.

Heat Loss

The gasifier must have a heat loss associated with it. Most test runs have seen a heat loss on the order of 1-2% of the Higher Heating Value (HHV) of the raw MSW; this value is arrived at by taking into account the size (surface area) a gasifier would necessarily have to be in order to handle a given flow rate, and then calculating the heat loss through the surface area of its walls. The oxygen feed rate is adjusted so that the amount of heat which results from its reactions with other process materials is enough to total the heat loss plus the energy required to heat the process material to the reactor

temperature. In this manner, some sense of scale can be included in the simulation. The basis for the heat loss calculations is as follows:

(Gasifier geometry assumed to be cylindrical)

L = Reactor length
D = Reactor diameter
F = Volumetric flowrate of gasifier outlet
SA = Gasifier surface area
k = Thermal conductivity of reactor wall
Q = Heat loss through reactor wall
T = Gasifier internal temperature
τ = Residence time

$B = L / D$ Definition

$V = \pi \frac{D^2}{4} L = F\tau$ Reactor volume

$D^3 = 4\frac{F\tau}{\pi B}$ Substitute for L, and solve for D

$SA = \pi \frac{D^2}{4} + \pi D(DB)$

$Q = T(SA)k$ Surface area - dependant heat loss equation

Results

Figure 4:[v]

Simulation Inputs		Component	Gasifier Outlet Makeup (mol%) TEXACO pilot plant data	ASPEN Simulation
Gasifier T	1450 C	Ar	0.08	N/A
Gasifier P	4083 kPa	H2	36.14	35.37
Coal/H2O slurry flow	2235 lb/hr	CO	46.51	48.09
Coal slurry H2O %	35 % (mass)	CO2	15.36	15.23
O2 mass feedrate	1411 lb/hr	N2	2.01	0.54
		CH4	0.02	0.00
Simulation Characteristics		H2S	0.26	0.70
WGS T Approach	-415 C	COS	0.02	0.03
Heat Loss (%HHV)	4.2 %			

Figure 5:[vi]

Simulation Inputs		Component	Gasifier Outlet Makeup (mol%) TEXACO pilot plant stream	ASPEN Simulation
Gasifier T	1316 C	H2	29.80	29.79
Gasifier P	4083 kPa	CO	41.00	41.00
Coal/H2O slurry flow	62505 kg/hr	CO2	10.20	10.20
Coal slurry H2O %	33% (mass)	N2	0.80	0.95
O2 mass feedrate	35836.2 kg/hr	CH4	0.30	0.30
		H2S	1.10	1.03
Simulation Characteristics		COS	0.00	0.05
WGS T Approach	-199 C	H2O	17.10	16.65
CH4 rxn T Approach	-227 C			
Heat loss (% HHV)	5.48%			

Discussion

The simulations performed above were of the TEXACO gasifier using coal as process feed material. Simulations using MSW were not done, because of a lack of hard data from real-world needed to compare our simulation's results with.

The results indicate that the Texaco gasifier can be modeled within acceptable accuracy. The original goal of this project was to create a model of an industrial process that produces hydrogen fuel from municipal solid waste; the model would then be used to make some economic predictions about how feasible or realistic this process would be as a way to produce hydrogen as an energy source. The errors seen in comparing the simulation's data against physically measured data are quite small, usually within 1-2%; this size of error, while unacceptable from a design/engineering standpoint, should not cause a great deal of misjudgment in the conclusions drawn on the *economics* of the process, since they are dependent largely on the cost of materials which are needed as inputs to the process and the worth of the products which come out of it. The bottom-line economic conclusions from such an analysis should not vary greatly if costs based on material flows in or out of the process were to be in error by the amounts shown above.

In addition, the pilot plant input data which was given by TEXACO was incomplete. Exact material inputs, and especially gasifier temperatures were not known, though reasonable estimates for these values were obtained from data that was available. Surely this is a source of error. Future cooperation with TEXACO should provide the model with more accurate input data, which should increase the overall accuracy of the model as a whole.

It is encouraging especially to see that, while the two simulations above require different temperature approach values for their Water-Gas-Shift (WGS) reactions, the temperatures at which WGS equilibriums are calculated (Reactor Temp. + Approach Temp) are quite close together. For the simulation considered in Figure , the equilibrium temperature for the WGS reaction is 1035 C, while the corresponding temperature for the simulation considered in Figure is 1117 C. The fact that these two temperatures are within 100 C of each other, even when exact gasifier temperatures are not known, indicates some consistency across different simulation runs, which is always encouraging.

The fact that the simulations' heat losses are high (4-5% of the dry HHV) is of some concern. These heat losses were not calculated according to the method described earlier, as that method adjusts

the oxygen stream feed rate; and we did not want this to happen because the oxygen feed rates were given data. TEXACO did not supply heat loss values with its data, however, so the extents to which the simulations' heat losses are in error are not known. This heat loss is certainly too high though , since TEXACO estimates that heat losses should be less than 1% of the dry HHV, but it should be noted that the test runs were done using comparatively low flow rates through the gasifier (thousands of pounds per hour); the heat loss would be much lower with the same input conditions if only the flow rates were set at higher values (thousands of pounds per minute), which is what a full-scale industrial plant would do.

Summary

The model is still in development. However, it has been successful thus far in giving a satisfactory approximation to the MSW gasification process. As far as the contributions from this paper go, they are positive ones, but there is future work to be done. As of this writing, the gasification section is useful, but requires much "tweaking" by the user to achieve an accurate simulation. It lacks the automation to handle a wide variety of inputs without such user involvement; what is needed most importantly is an automatic way in which to set temperature approaches based on the characteristics of the material coming in and other simulation parameters. More complete data from real-world gasification runs should help this problem tremendously. The heat of combustion model is fairly sound, as it accurately predicts heats of combustion within a few percent. However, improvements can always be made.

References

[i] References for Figure 1:

MSW 1 - Refuse Sample - taken from "The New Quebec Metro Incinerator," Herve Aubin, in Resource Recovery Through Incineration - 1974 National Incineration Conference, American Society of Mechanical Engineers, p. 204

MSW 2 - St. Louis Municipal Waste - taken from "Steam Generation from Solid Wastes - the Connecticut rationale Related to the St. Louis Experience," J F Mullen, in Resource Recovery Through Incineration - 1974 National Incineration Conference, American Society of Mechanical Engineers, p. 195

MSW 3, MSW 4 - Prepared Refuse, Bark Sample - taken from "Energy Recovery from Solid Waste," W J Landman, W J Darmstadt, in Conversion of Refuse to Energy - 1st International Conference and Exhibition 1975, Montreaux, Switzerland, p. 593

MSW 5 - Iowa RDF - taken from Refuse Derived Fuels, A. Porteous, Applied Science Publishers Ltd, London, 1981, p. 63

MSW 6, MSW 7 - Municipal Solid Waste Samples - taken from Biomass Handbook, Kitani and Hall, Gordon and Breach Science Publishers, 1989, p. 881

MSW 8 - Maine RDF - "Results of Emissions and Ash Testing at a Modern Refuse-Derived Fuel Plant," F A Ferraro, AIChE Symposium Series - Resource Recovery of Municipal Solid Wastes, 265 Vol 84, pp. 36-43

MSW 9 - GE MSW - Solid Waste Management Technology Assessment, General Electric Co., New York Van Nostrand Reinhold Co., 1975

[ii] Aspen Plus Coal Models, Manual accompanying Release 8 of Aspen Plus software, Aspen Technology Inc., Cambridge, MA, 1988, p. 1

[iii] Fundamentals, Development and Scaleup of the Air-Oxygen Stratified Downdraft Gasifier, Reed, Levie, Graboski, Pacific Northwest Laboratory, DOE, prepared for Solar Energy Research Institiute, 1988, p. 7-5

[iv] Literature values taken from Biomass Handbook, Kitani and Hall, Gordon and Breach Science Publishers, 1989, pp. 880-882

[v] Pilot plant data taken from "Integration and Testing of Hot Desulfurization and Entrained-flow Gasification for Power Generation Systems - Phase I", Robin, Wu, Kassman, TEXACO Montabello Laboratory, prepared for Morgantown Energy Technology Center, 1989, pp. 77, 123, 144

[vi] Data taken from "A Prediction of Performance of Commercial Coal Gasifiers", Watkinson, Lucas, Lim, FUEL, April 1991, Vol 70, p. .522

Analysis of the Acoustic Spectral Signature of Prosthetic Heart Valves in Patients Experiencing Atrial Fibrillation

David D. Scott
Department of Energy
Science and Engineering Research Semester
Lawrence Livermore National Laboratory

H.E. Jones
University of California
Lawrence Livermore National Laboratory

P.O. Box 808, L-258
Livermore, CA 94550
Phone (510) 423-5879

Abstract

Throughout an average human life span the heart beats some three billion times never stopping to rest except for a fraction of a second between beats. This most important muscle often operates flawlessly, however, in some cases a dysfunction can prove life threatening. Prosthetic heart valves have increased the life span of many patients with life threatening heart conditions. These valves have proven extremely reliable adding years to what would have been weeks to a patient's life. Prosthetic valves, like the heart however, can suffer from this constant work load. A small number of valves have experienced structural fractures of the outlet strut due to fatigue. To study this problem a non-intrusive method to classify valves has been developed. By extracting from an acoustic signal the opening sounds which directly contain information from the outlet strut and then developing features which are supplied to an adaptive classification scheme (neural network) the condition of the valve can be determined.

The opening sound extraction process has proved to be a classification problem itself. Due to the uniqueness of each heart and the occasional irregularity of the acoustic pattern it is often questionable as to the integrity of a given signal (beat), especially one occurring during an irregular beat pattern. A common cause of these irregular patterns is a condition known as atrial fibrillation, a prevalent arrhythmia among patients with prosthetic heart valves.

Atrial fibrillation is suspected when the ECG shows no obvious P-waves[1,2]. The atria do not contract and relax correctly to help contribute to ventricular filling during a normal cardiac cycle[1]. Sometimes this leads to irregular patterns in the acoustic data. This study compares normal beat patterns to irregular patterns of the same heart. By analyzing the spectral content of the beats it can be determined whether or not these irregular patterns can contribute to the classification of a heart valve or if they should be avoided. The results have shown that the opening sounds which occur during irregular beat patterns contain the same spectral information as the openings which occur during a normal beat pattern of the same heart. Therefore, these beats can be used for classification without concern for the integrity of their spectral pattern.

I. Introduction

There have been approximately 86,000 patients worldwide who have been implanted with the Bjork-Shiley Convexo Concave (BSCC) heart valve[3]. Figure 1 illustrates the prosthetic valve and Figure 2 shows the cross section of a human heart. The valve controls the flow of blood with a disc that rotates against the

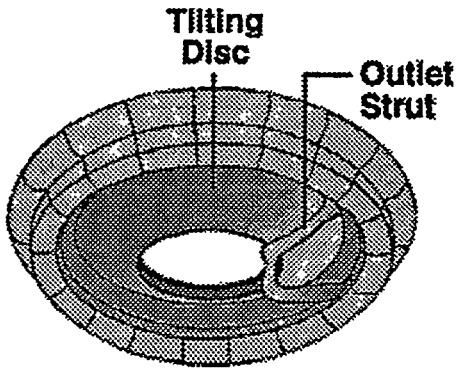

Figure 1a BSCC Valve in Closed Position

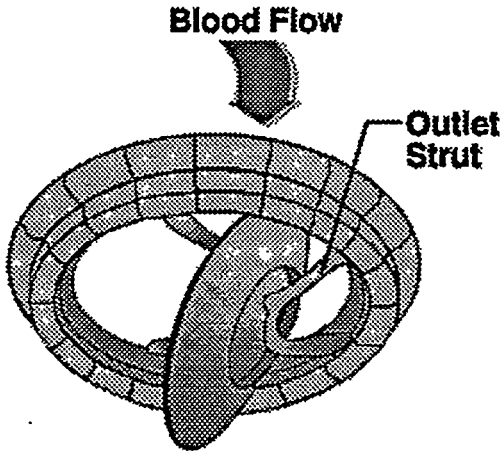

Figure 1b BSCC Valve in Open Position

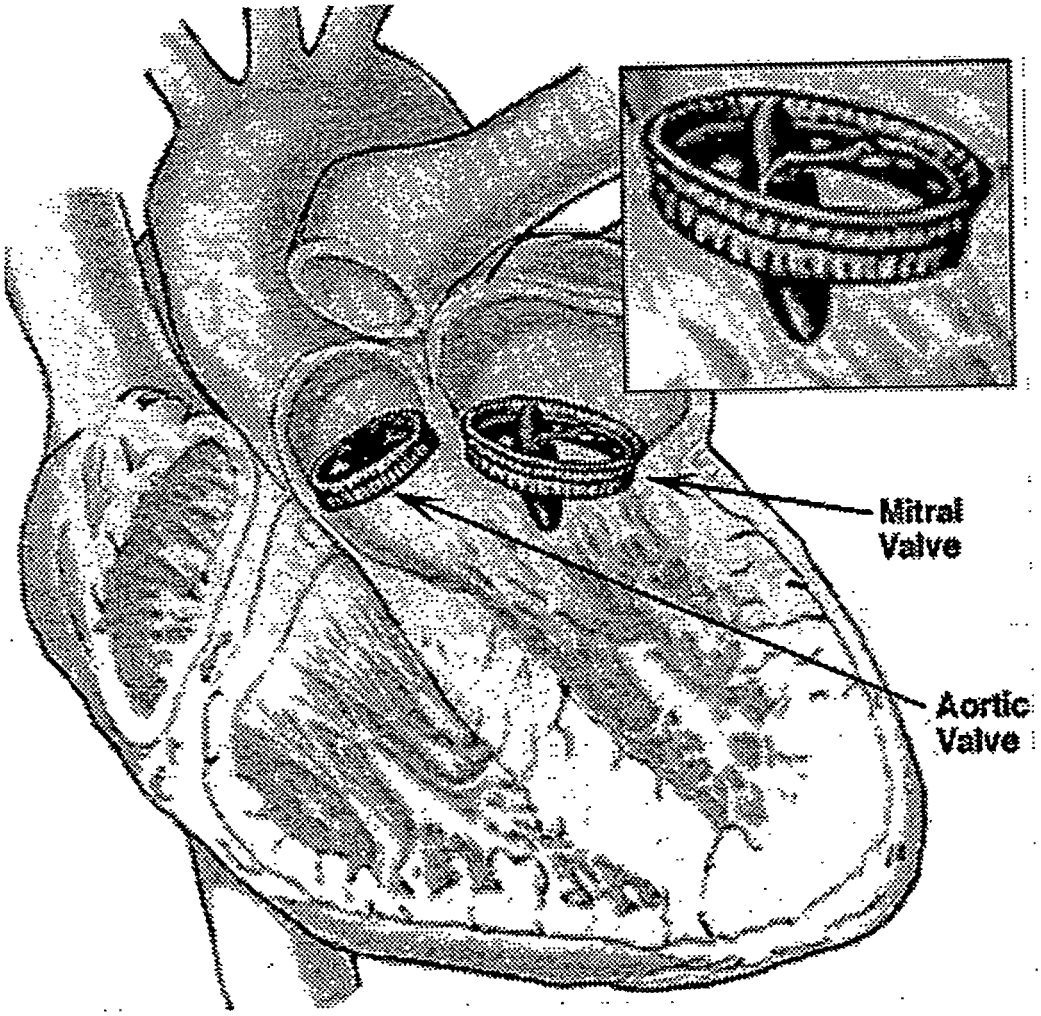

Figure 2 Cross Section of Human Heart Showing Valve Location

inlet (closed position) and outlet (open position) struts. Due to fatigue one of the legs of the outlet strut separates from the flange resulting in single leg separation (SLS). Although actuarial analysis predicts that the risk of mortality due to a fracture of both legs of the outlet strut is less than that associated with open heart surgery required to replace the BSSC valve the Shiley Heart Valve Research Center, (SHVRC) is attempting to develop technology to identify the SLS valves[4].

To classify these valves the opening sounds must be extracted and then screened to ensure the integrity of acoustic data used in the classification. The opening sounds are currently extracted using an automated routine which, based on the acoustic signal pattern, recognizes openings and closings and categorizes them as such. Next, a parametric approach is used to develop a model to estimate the power spectrum emanating from an ensemble of acceptable valve opening sounds[4]. The subsequent beats are then screened using this model. The screening is based on testing the difference between the measured and predicted acoustic signal (residual sequence) for "whiteness"[4]. Should the residual sequence test white then, theoretically, the estimated model fits the data[4]. If it tests non-white then the beat is not accepted. Each beat is processed in this manner and those that are accepted are incorporated into the spectrogram (beat power vs frequency) for the valve under examination.

During the beat extraction process it has been observed that patients who have been diagnosed with atrial fibrillation have unusual and irregular beat patterns. This irregularity in the beat pattern raises the question as to whether or not these irregular beats contain the same acoustic spectral signature as beats during a "normal" beat pattern. If these beats are different it would be desirable to avoid them during extraction so that they are not used to develop the model upon which other beats are screened. If their spectral content is not different, however, then these beats can be accepted with confidence that they are not contaminating the model and spectrogram.

In this paper we discuss the beat extraction process, the method by which a model is developed for the opening signals and finally the screening process which irregular patterns had to pass to be accepted for classification. By first developing a model based on a normal beat pattern and then screening beats that occur during an irregular acoustic pattern it can be determined whether or not the irregularity of the pattern is coupled with the spectral content of the signal.

II. Beat Extraction

To analyze the power spectrum of a desired beat it must first be extracted from the raw data. The method employed to extract the opening signals is based

upon pattern recognition of the raw data. By coalescing events into 512 sample points and eliminating closing events by an adaptive threshold to account for variations in the amplitude of the signal, the opening beats can be extracted using an automated algorithm.

The physiology of the heart and the details of electrocardiography are beyond the scope of this paper, however, a simple explanation of some of the cardiology involved is given for insight into the relationship of the acoustic and electrocardiograph (ECG) patterns with the working of a prosthetic valve. Figure 3 shows a plot of the acoustic and ECG signals of a normal beat pattern with the opening and closing sounds highlighted. Figure 4 shows a plot of the acoustic and ECG pattern of a heart with atrial fibrillation. A normal cardiac cycle is characterized in the ECG with three distinctive wave forms (see Figure 3). The P-wave corresponds to atrial depolarization. The QRS complex represents ventricular depolarization and the T-wave represents ventricular repolarization[5]. The patients in this study all had mitral valves. Notice that the peak of the R-wave corresponds to ventricular contraction and the closing of the mitral valve.

Atrial fibrillation is a common arrythmia of the heart characterized by rapid, irregular, uncoordinated depolarizations of the atria with no definite P-wave. This can be seen in Figure 4. Atrial contractions are thus uncoordinated and asynchronized. This causes the ventricular rhythm to be irregular also which results in variable lengths of time for ventricular filling. When less filling occurs there may be a lack of blood to produce a palpable pulse[5]. This results in the irregular beat pattern which is monitored acoustically. There is simply not enough blood to force the valve to open or close with enough magnitude to produce a sound.

A comparison was made between the acoustic spectral signature of normal beat patterns and the signature of irregular patterns. Software was developed to "hand select" beats in order to eliminate or avoid beats that occurred during irregular patterns. In the same way, these irregular beats were selected and the normal patterns were eliminated. The ECG was used extensively to help with the pattern recognition of closing and opening events in order not to mistake noise or a small amplitude closing event as an opening occurring during an irregular pattern.

By this method two sets of opening sounds were created; the first having only beats from a normal beat pattern, the second containing only beats from an irregular pattern. After the beats are extracted they can then be modeled using an auto-regressive model.

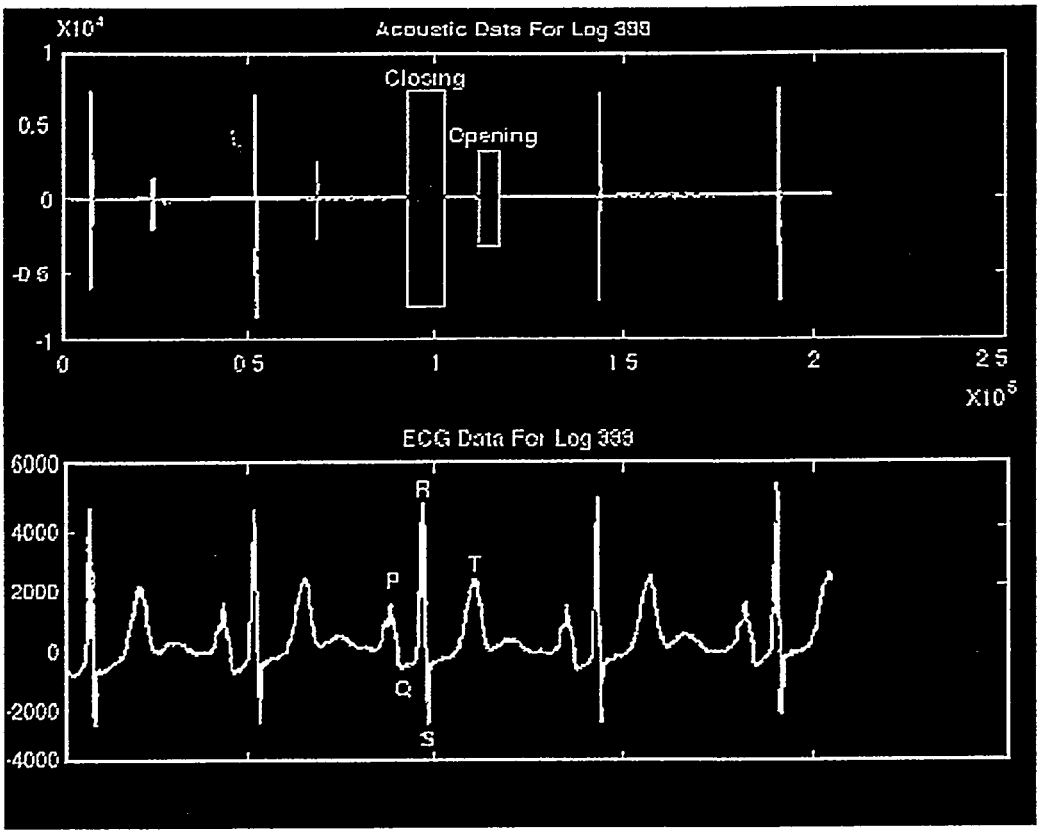

Figure 3 Acoustic and ECG Signal of Normal Heartbeat.

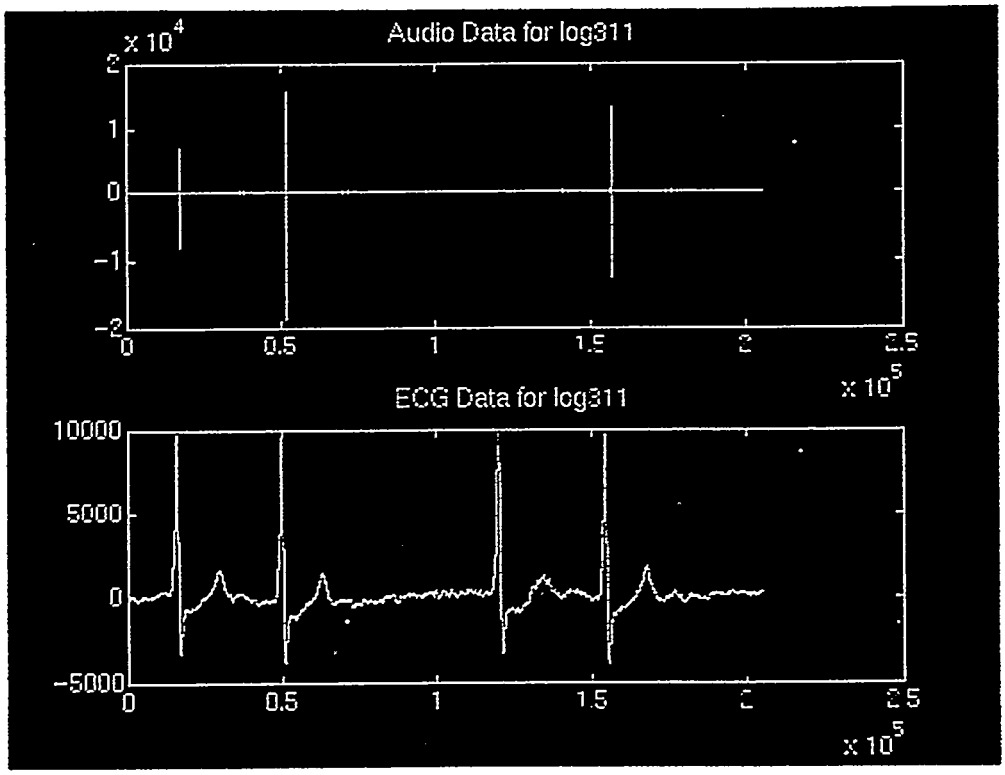

Figure 4 Acoustic and ECG Signal of Heart Experiencing Atrial Fibrillation.

III. The Autoregressive Model and Beat Monitor[4]

Once the opening sounds from each valve session have been extracted and imported into a data base, they are available for processing and classification. We have developed a *parametric approach* to estimate the power spectrum emanating from the prosthetic heart valve opening sounds during each beat cycle. This approach is based on estimating a parametric model of the beat transient signal characterized by an *autoregressive* (AR) or all-pole model which is used primarily to extract damped sinusoidal signals in noise -- a reasonable representation of the acoustical signal. The AR model is defined by the difference equation

$$y(n) = -\sum_{i=1}^{N} a_i y(n-i) + \sigma\varepsilon(n), \tag{1}$$

where $y(n)$ is the output or response (valve sound),
$\varepsilon(n)$ is the input or excitation (impulse or prediction error),
$[\{a_i\}, \sigma]$ is the set of AR model parameters.

If we apply Z-transforms to Eqn. 1, then we obtain the *transfer function* given by

$$H(z) = \frac{Y(z)}{E(z)} = \frac{\sigma}{A(z)}, \tag{2}$$

where $A(z) = 1 + a_1 z^{-1} + \cdots + a_N z^{-N}$ is the characteristic polynomial of the AR model whose roots $\{p_i\}$ are the *poles* of the system, that is,

$$A(z) = (1 - p_1 z^{-1})(1 - p_2 z^{-1}) \quad \cdots \quad (1 - p_N z^{-1}),$$

or

$$H_{AR}(z) = \frac{Y(z)}{E(z)} = \frac{\sigma}{\prod_{i=1}^{N}(1 - p_i z^{-1})}, \tag{3}$$

For the heart valve acoustic signal estimation problem, we note that the spectral content of the data is characterized by sharp resonant peaks corresponding to lightly damped sinusoids in noise. It is for this reason that we select the Nth order autoregressive model $AR(N)$ to characterize the heart sounds emanating from the prosthetic heart valve. Note that this phenomenon implies that the poles appear as complex pairs, close to the unit circle and therefore, we have

$$H_{AR}(z) = \frac{Y(z)}{E(z)} = \frac{\sigma}{\prod_{i=1}^{N/2} (1 - p_i z^{-1})(1 - p_i^* z^{-1})}, \tag{4}$$

where $\{p_i, p_i^*\}$ represent the complex resonance or pole pair appearing in the heart valve acoustic spectrum.

Since the data are noisy, the excitation $\varepsilon(n)$ of the $AR(N)$ is modeled as a zero-mean, unit variance, completely random (white) noise process whose discrete Fourier spectrum $H_{AR}(\Omega)$ must be replaced by the corresponding power spectral density[6] defined by

$$S_{AR}(\Omega) = H_{AR}(\Omega) H_{AR}^*(\Omega) = \frac{\sigma^2}{|A(\Omega)|^2}, \tag{5}$$

in order to "average out" the effect of the noise, that is, $S_{AR}(\Omega) = E\{Y(\Omega)Y^*(\Omega)\}$.

Thus, the "parametric approach" to represent the heart valve sounds essentially becomes that of estimating the parametric set defined by $\Theta_{AR} := [\{\hat{a}_i\}, \hat{\sigma}]$ from the noisy acoustic measurement data $\{y(n)\}$. Once these parameters are estimated, then the corresponding $AR(N)$ model and spectrum $\hat{S}_{AR}(\Omega)$ are constructed for <u>each</u> individual heart valve sound, creating the corresponding heart valve acoustic spectrogram (beat power versus frequency). It should also be noted that the order N of the $AR(N)$ model must be estimated.

Order estimation is accomplished using the *Akaike Information Criterion* (AIC) statistic defined by

$$AIC(N) = -2 \ln \sigma_\varepsilon^2 + 2N, \tag{6}$$

where σ_ε^2 is the prediction error variance

N is the model order.

The optimal order is

$$N = \min AIC(N), \tag{7}$$

There are a variety of parameter estimation algorithms available for this application, we choose to use the lattice algorithms[6] which essentially is obtained by performing an LD-decomposition of the Toeplitz correlation matrix R[7]

$$R = L^{-1} D L^{-T},$$

leading to the parametric solution for the vector of AR model of parameters given by

$$\underline{a} = R^{-1}\underline{r} = (L^T D^{-1} L)\underline{r}, \tag{8}$$

Theory shows[7] that the resulting elements of L are given by

$$L = \begin{bmatrix} 1 & 0 & 0 & 0 & 0 \\ a_{11} & 1 & 0 & 0 & 0 \\ a_{22} & a_{21} & 1 & 0 & 0 \\ \vdots & \vdots & \vdots & \vdots & \vdots \\ a_{NN} & a_{NN-1} & a_{NN-2} & \cdots & 1 \end{bmatrix},$$

where $a_{ii} = \kappa_i$ is the ith order reflection coefficient or lattice parameter

a_{ij} is the jth AR model coefficient of the ith order model

enabling us to not only estimate the $AR(N)$, but also all of the lower order AR models. This is quite useful in developing other related power spectral estimators.[8] Using the lattice algorithm, we estimate the required parameter set $\hat{\Theta}_k$ and the corresponding power spectrum $\hat{S}_k(\Omega)$ for the k^{th} heart valve sound and stack them to create the spectrogram. A spectrogram for opening sounds

which occurred during normal beat patterns is shown in Figure 5 and Figure 6 shows the spectrogram for beats occurring during irregular beat patterns.

Note the repeatability of each spectrum (shown in green) along with the average spectrum (in red). The corresponding spectrogram is shown in the figure as beat power versus beat number versus frequency along with the corresponding resonant peak histogram. Once the spectral estimator is designed for the *k-th* beat, the resonant frequencies must be estimated from the power spectrum $\hat{S}_k(\Omega)$. Here our approach is to estimate the peaks of the spectrum above a pre-set threshold, τ. That is, first *all* of the spectral peaks are detected from the estimated power spectrum as

$$P_k(f_j) = S_k(f_j) \qquad f_{low} < f_j < f_{high},$$

where P_k consist only of the detected spectral peaks of S_k at corresponding frequency f_j in a pre-specified frequency band $[f_{low}, f_{high}]$. From the spectrum of peaks, we estimate the corresponding resonant frequencies present in the data from its location, that is,

$$\hat{f}_j = P_k(f)\Big|_{f=f_j} > \quad \tau.$$

Thus, the output of the frequency estimator is a set of estimated frequencies $\{f_j\}$ corresponding to the resonant frequency peaks appearing in the given spectrum. Clearly, if the heart valve sounds were stationary, then only a single spectral line would appear at each frequency during each beat, but due to reasons discussed previously the acoustic data is non-stationary and therefore, we expect frequencies to "cluster" about a mean frequency, $f_m(j)$. In fact, this technique then leads to the *frequency band estimator*. Here the approach is to estimate the probability of occurrence of a set of resonant frequencies and look for clustering about various mean frequencies. We estimate this multivariate probability mass function using a histogram estimator with bin size corresponding to the frequency resolution of the processed data. This approach leads to a new set of features which will be used in the final classifier. Once the lattice parameters, spectrogram and peak frequency histogram are estimated for a given valve, they are stored in the data base and made available to the various classifiers on demand. Besides the peak histogram, the spectral power in various bands are averaged over the ensemble and used as components of feature vectors along with the reflection coefficients themselves, which have proved to be

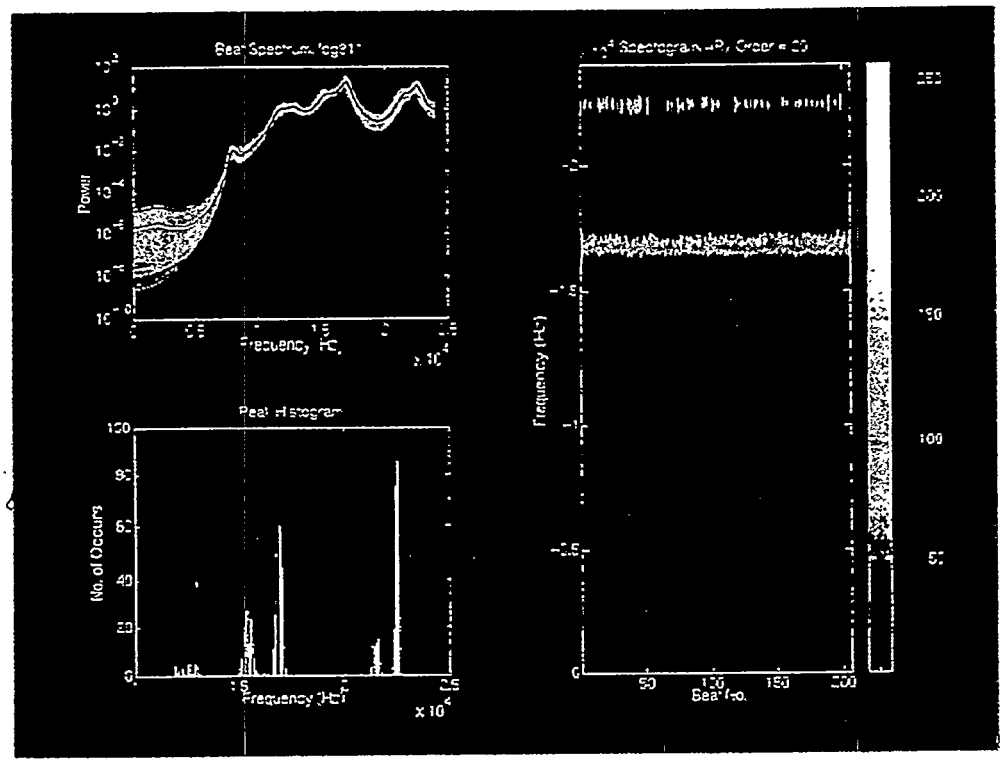

Figure 5 Power Spectrum for Normal Opening Signals, (irregular patterns rejected).

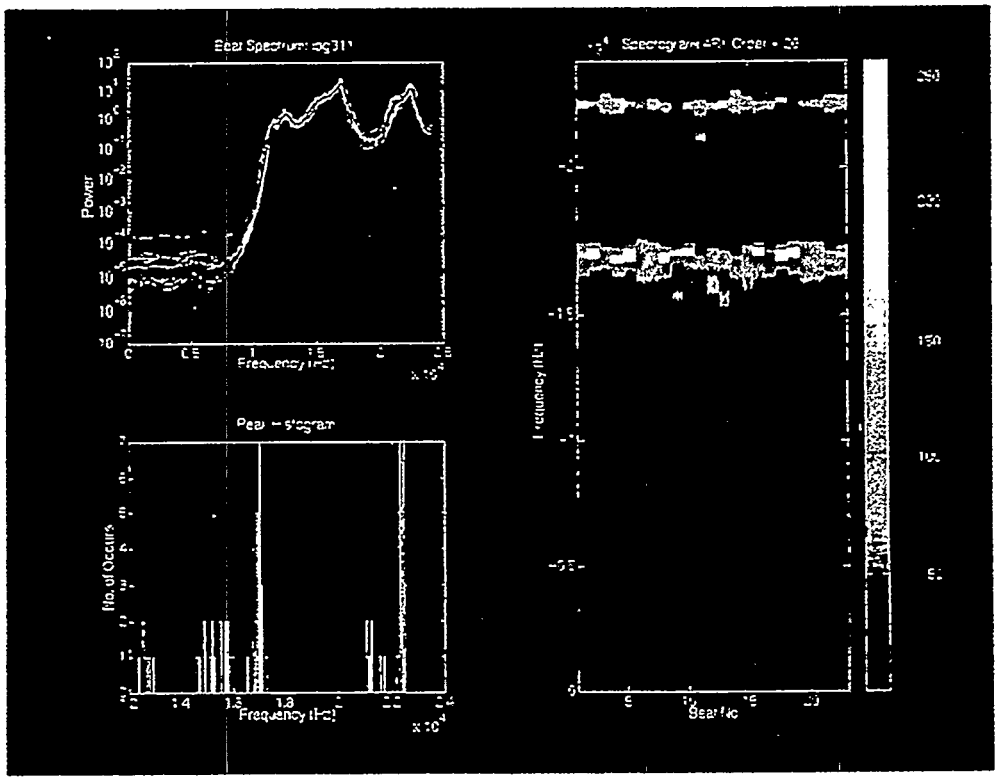

Figure 6 Power Spectrum for Signals During Irregular Beat Patterns.

reliable features for other applications.[9,10] So we see that the parametric approach offers reasonable estimates of desirable features which can ultimately be used to classify heart valve conditions. By applying this approach for beats that occur during regular beat patterns we have a basis upon which we can compare beats that occur during irregular patterns (of the same file).

IV. BEAT MONITORING [4]

Classifying the heart valve condition from the acoustic signatures requires unambiguous data, selection and extraction of the significant features, and development of a classification algorithm which identifies the valve condition with the best sensitivity and specificity. It is important to acquire noise free, uncontaminated signals in the appropriate frequency range to provide enough information to classify the signals. Poor data will significantly hamper the attempts to predict the heart valve condition because the classifiers will be based on random noise instead of signal information related to valve condition. Thus, it is essential not only to extract the opening transients, but to assure that the beats extracted have an adequate signal-to-noise ratio to provide the classifier high quality resonance information as features. We have developed a sophisticated Beat Monitor that utilizes the spectral content of acceptable opening transients to accept/reject subsequent openings which occur during irregular beat patterns or may be questionable for whatever reason. The Monitor uses the opening heart valve beat sounds to develop a parametric model and then predicts the acoustic response on a beat-to-beat basis. The algorithm, first captures an ensemble of acceptable beats (during training), estimates an "average" parametric model, and then screens subsequent beats using the model. This processor is based on testing the residual sequence, which is the difference between the measured and predicted acoustic signal, for the statistical property of "whiteness". This scheme relies on the underlying fact that if the parametric model reliably represents or "fits" the data, then the residual sequence contains no other information about valve acoustics (resonances). Therefore, the sequence should be purely random or "white". Should the residual sequence test statistically white, then theoretically the estimated model fits the data and the beat passes; however, should it test non-white, then the questionable beat does not contain the same information as the "normal" beats and it does not pass (see Refs. 11, 12, 13 for more details).

Theoretically, the heart valve Beat Monitor is implemented using the $AR(N)$ model whose parameters are estimated using the Levinson recursion[6] to

"fit" the model to pre-selected beats yielding the "inverse" or residual filter, that is,

$$H_{INV}(z) = \frac{E(z)}{Y(z)} = \frac{\sigma}{A(z)}, \tag{9}$$

or equivalently in the time domain with q^{-k}, the delay or k-step time delay operator for the ith heart sound $y_i(n)$

$$[1 - A_i(q^{-1})]\varepsilon_i(n) = \sigma_i y_i(n), \tag{10}$$

Once the valve sound is processed by the residual filter, its estimated correlation is tested for statistical whiteness using the correlation estimates

$$\hat{\rho}_{\varepsilon\varepsilon}(k) = \frac{R_{\varepsilon\varepsilon}(k)}{R_{\varepsilon\varepsilon}(0)}$$

$$R_{\varepsilon\varepsilon}(k) = E\{\varepsilon^2(n)\} \tag{11}$$

to perform the*whiteness test* given by

$$\left[\rho_{\varepsilon\varepsilon}(k) \pm \frac{1.96}{\sqrt{K}}\right] \quad , \tag{12}$$

where k is the lag variable and K is the number of samples in the signal. Here 95% of the normalized correlation samples must lie within the bounds (or equivalently 5% can exceed the bounds) for the sequence to be deemed white.

The raw data is processed beat-by-beat for the beats occuring during a regular beat pattern. First, the parametric model is designed based on these "good" beats. During the training phase of the Beat Monitor, any beat that is deemed white is also further modeled and averaged with the previous beat models to train the algorithm and produce a set of average coefficients for the given valve (patient). The coefficients for this model are then used to calculate the prediction error for the questionable beats and each beat is tested for whiteness according to Eq. 12. The results of the Whiteness Test are also shown in Figure 7. All of the questionable beats fell within 10% and all but two were within 5%. The corresponding power spectra (raw and estimated) show good

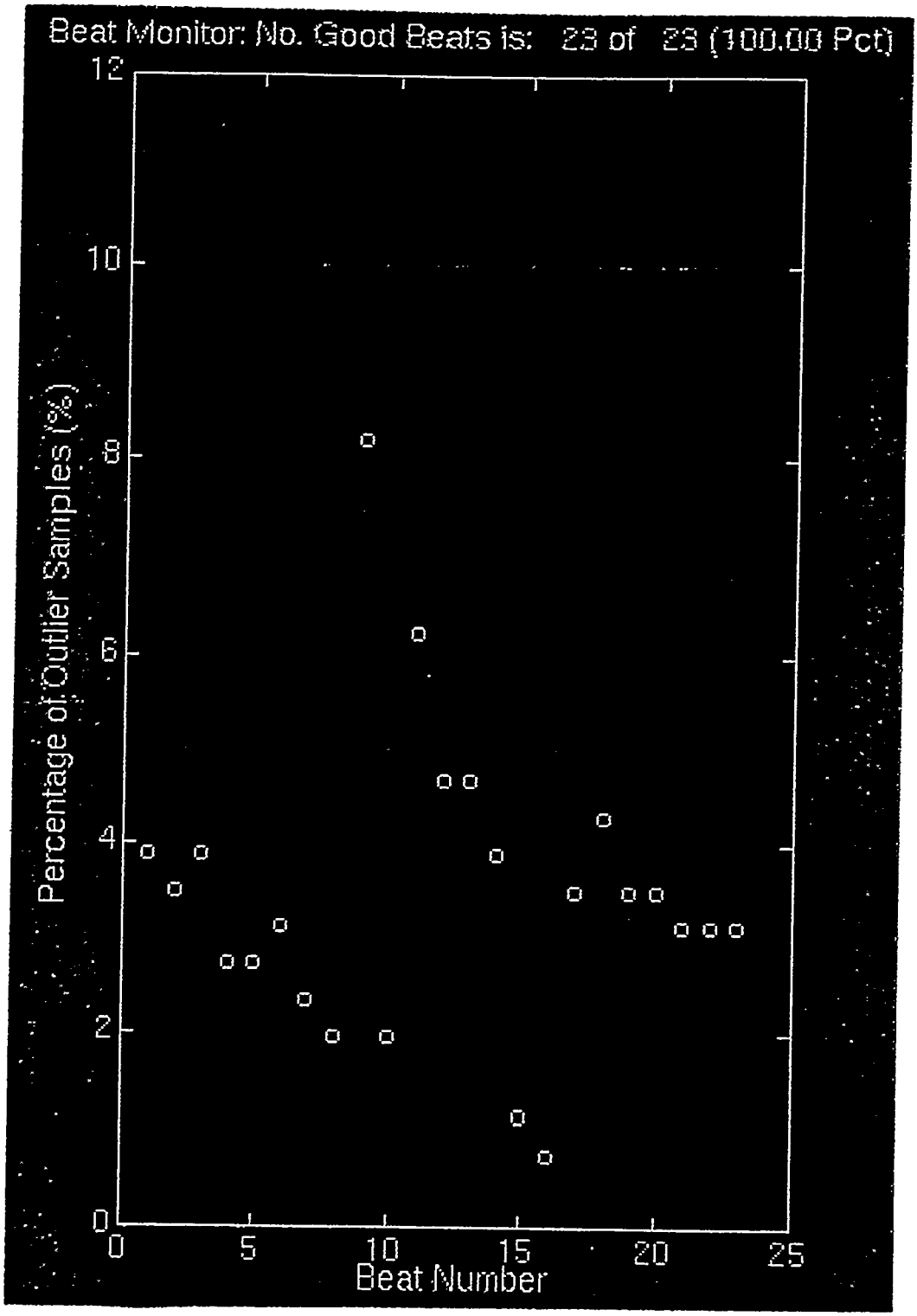

Figure 7 Beat Monitor Screening Results.

agreement assuring that the major spectral properties of the heart valve sound have been captured by the parametric model.

Utilizing this design, each irregular beat is processed by the estimated model and if tested statistically white, the model fits the beat and it is deemed acceptable, then we know that these beats which occur during irregular beat patterns due to atrial fibrillation have the same spectral content as normal beats.

V. Summary

After separating irregular opening patterns from normal patterns and comparing their spectral content it has been observed that the spectral signature of a valve is unaffected by atrial fibrillation. The spectral signature is not dependent upon the regularity of the opening and closing of the valve. At this point three valves have been studied with atrial fibrillation and all have confirmed this result. In conclusion atrial fibrillation will not have an adverse effect on the spectrogram of a given valve. It should be noted, however, that careful attention must be given not to mistake noise, a small closing signal or other anomalous events for an irregular beat pattern. To select opening events the ECG was of primary use to determine the validity of a suspected irregular pattern.

This work was performed under the auspices of the Department of Energy by the Lawrence Livermore National Laboratory under contract W-7405-Eng-48.

References

1) Berne, Robert M., *Cardiovascular Physiology*, The C.V. Mosby Company, 1986.

2) Braunwald, Eugene, *Heart Disease: A Textbook of Cardiovascular Medicine*, W. B. Saunders Co., 1992.

3) Chandler, J. G., "Broken Heart Valves," *Emergency Medicine*, Cahners Pub, 1992.

4) Candy J. V., Jones H.E., "Processing of Prosthetic Heart Valve Sounds for Single Leg Separation Classification," *LLNL-Report*.

CAFE: Computer Aided Fabric Evaluation

James Sims

Jackson State University

Lawrence Livermore National Laboratory
Livermore, California 94550

5/11/94

Prepare in partial fulfillment of the requirements of the Science and Engineering Research Semester under the direction of **Jose E. Hernandez**, Research Mentor, at the Lawrence Livermore National Laboratory.

* This research was supported in part by an appointment to the U.S. Department of Energy Science and Engineering Research Semester (hereinafter called SERS) program administered by LLNL under Contract W-7405-Eng-48 with Lawrence Livermore National Laboratory.

CAFE: Computer Aided Fabric Evaluation

James E. Sims

Jackson State University

Engineering Research Division

ABSTRACT

With the intent of automating the inspection of color printed fabrics for defects, the Engineering Research Division of the Lawrence Livermore National Laboratory in addition with several other national labs, in conjunction with the textile industry has initiated the CAFE project. The projects objective is predicated on the development, implementation and testing of an algorithm for the inspection of color printed fabrics. We attempt to take advantage of the wide ranging applications possible with Computer Vision in order to achieve this. The first job of the algorithm is to teach the computer the 'correct' printed patterns by using a defect-free repeat from the pattern. Once this is learned the computer, using the 'correct' repeat as the reference, tests the remaining repeats in the pattern. There are two different ways to go about doing the first job and with this paper we will describe both methods.

Introduction

The U.S. texitle industry, in order to become more competitive with foreign textile interests, needs measures to reduce overall costs of production. One area of focus is now the inspection process. The success of the project will enable two things. First, it will enable consistent inspection and second, it will allow errors in manufactoring to be corrected using process control.

There is a fundamental sturcture with fabrics which allows the possibility of such an application.. In all fabrics, any particular pattern will repeat itself thruout the length of the fabric. This concept is what the development of the project itself is based upon.

We develop an algorithm which is categorized under two modes, learning mode and inspection mode. In writing the code for the learning mode, we looked at creating an algorithm for determining the reference image, which will be used as the 'ideal' image during the inspection mode. For the inspection mode we develop code, which compares the 'repeat' images of the fabric to the reference image.

We employed a VISION [1] system to carry out the image processing tasks. The code for this work is written in Common Lisp, while the numerical algorithms are written in C. The Vision system interacts with a Data Cube system which digitizes the images taken from a CCD camera. The camera scans an area of the fabric. In this case it is scanning a pattern repeat.

General Approach

The digitized images from the camera had a resolution of 512 x 512..We were working with a gray scale of 256. The first step we had to make was to teach the computer the model for the repeats in the fabrics. With the understanding that there would rarely be an occasion where the gray values for the pixels would be exactly the same every time thruout the fabric, due to certain nuances which occur during printing, it was necessary to set an upper and lower bounds by determining what deviance would be allowed. This is one example where dialogue with people from the textile industry was very important, where we were given by them the guidelines we needed in order to help establish certain parameters. The pixels thruout the images must then be registered. Once we set the bounds we could then test the 'ideal' image with other repeats in the fabric. Those pixels whose grey levels fall outside of the bounds set can be then flagged.

Methods

During the learning mode, n frames were taken of a 'defect-free' portion of the fabric. The fabric was manually moved out and back into position again after each frame. This was done in order to simulate the real-time process where the fabric is on a roller and the camera is taking frames of each repeat thruout the fabric. The images had to be registered to compensate for the misalignment which occured in moving the fabric. We used several of the images as the reference image in order to find the smallest offset. P.D.F.'s of several reference images are shown in Figure 1. One problem we had in moving the fabric manually was that there was sometimes a rotational shift in some of the images. We did not develop the algorithm to compensate for the shift since rotation of images will not occur in real-time due to the hardware of the station that will be used. The main focus of the registration was on the alignment of the pixels.

For each pixel thruout the n frames, the gray level is collected and from these a template for the mean and standard deviation image is created. The mean image is taken to be the 'ideal' image and the sigma represents the allowed deviation for each pixel. Taking the sigma and multiplying it by a factor alpha, the program proceeds to set the lower and upper bounds for the pixels in the image by subtracting and adding the value to the mean. These values are set and once the inspection mode begins any value that does not appear within those particular bounds will then be taken as being a defect.

$$\mu_{x,y} = \frac{1}{N}\sum_{1}^{N} I_{x,y}(i) \qquad \sigma_{x,y} = \frac{1}{N-1}\sqrt{\sum_{1}^{N} (I_{x,y}(i) - \mu_{x,y})^2}$$

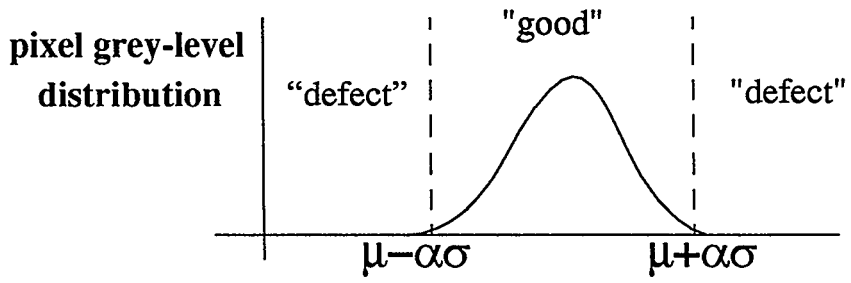

Figure 1. Histograms of Registered Images

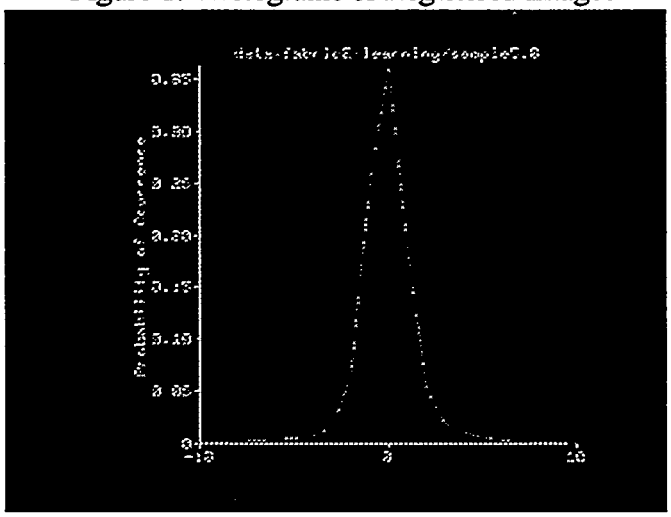

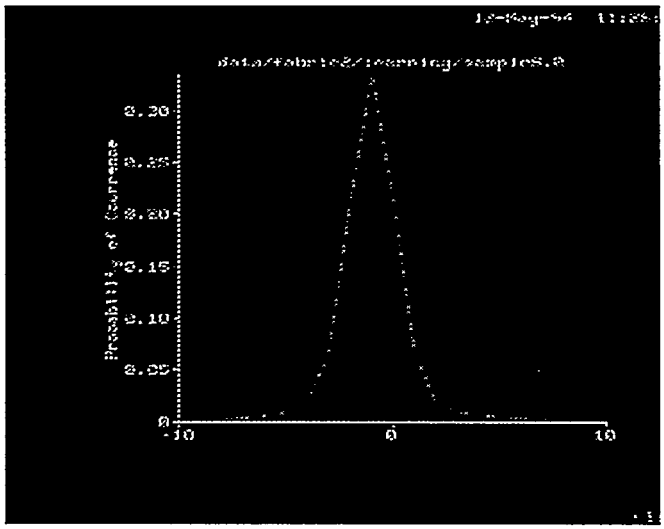

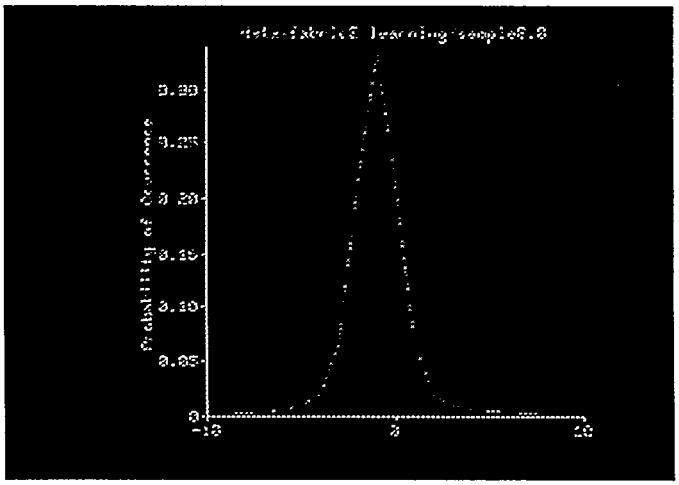

During the inspection mode the pixels from the repeat test images are registered. The images are then compared with the 'ideal' reference image by image subtraction [2] to check for any defects. A binary image highlights pixels that were out of the bounds set for those particular pixels in the learning mode.

Another technique was then used for setting the bounds. This time, instead of computing the mean and sigma value for each pixel, we go through the n frames and save the minimum and maximum grey level values for each pixel. These two values are then used to set the bounds for the grey levels.

Results

Several different fabrics were used to test the algorithm. With one of the fabrics there were already obvious defects that we could work with. In the case of one of the other fabrics, defects were placed arbitrarily upon repeats along the fabric. While the defects that were integrated into the fabric were not specifically made to be a certain size, the resolution of the individual pixels will be an important parameter once the automation is complete. Assuming success, the algorithm will be able to detect a defect as small as one-half millimeter (the size of each pixel). In using the mean/sigma method we looked at its efficiency using different fabrics. We have an example of one of the fabrics with the original 'ideal' and test image, along with a difference binary image is shown in Figure 2 a, b and c. We enhanced the sigma image, which represents the allowed deviation, with a bounding technique in order to get rid of any noise interpreted as defects by the computer. We then used the min/max method with the same fabrics. A binary image using this method is shown in Figure 2d. The image uses the same images from 2a and b.

Conclusions

The method using the mean and sigma for setting the thresholds the grey level values appeared to accurately distinguish defects from noise. We used several different fabrics to test the algorithm and also incorporated different types of defects, from discoloration in the fabric to simple foreign objects being placed along the repeats. With the method using the minimum and maximum values for setting the threshold, we did not get as accurate results as with the other method. One possible reason for the discrepancies is that there were only a handful of frames taken which didn't allow for possible larger deviations that might have come up had more been taken.

Figure 2a. Ideal Image

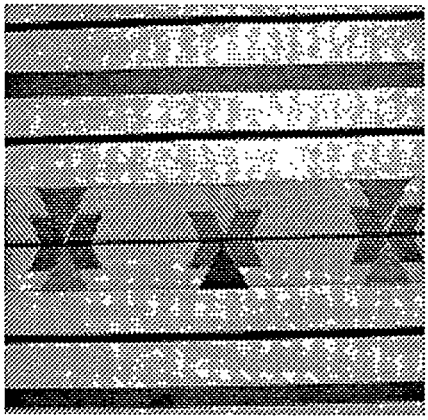

Figure 2b. Defect Image

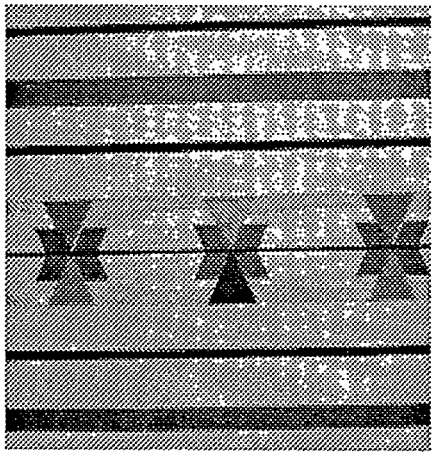

Figure 2c. Mean/Sigma binary image

Figure 2d. Min/Max binary image

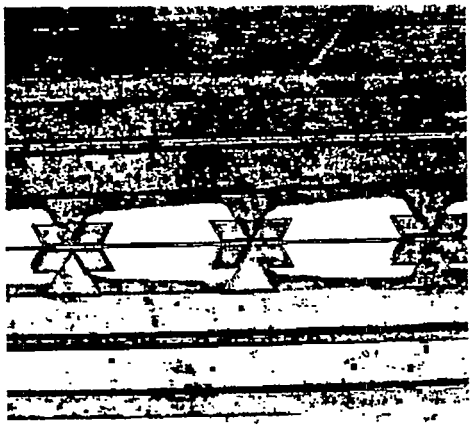

Future Work

So far with the methods used for setting the thresholds we have come up with promising results. We will look into trying the min/max method again, this time using more frames to come up with the bounding values. We will also be looking at possible other ways to attack the problem. In further developing the algorithm, we will be looking to incorporate methods of feature extraction. 3

Acknowledgments

The author would like to thank Jose E. Hernandez, who mentored him during the work on the project, for the extra time, energy and resources he put into helping the development of the author along. Also, thanks goes to everyone in the Engineering Research Division at the Lawrence Livermore National Laboratory.

Bibliography

1. J.E. Hernandez, "Using Vision: Object-Oriented Environment for Data Understanding" Lawrence Livermore National Laboratory, Livermore, California, draft(1993).

2. L.J. Galbiati, Jr., *Machine Vision and Digital Image Processing Fundamentals* Printice-Hall, (Englewood Cliffs, New Jersey) 1990.

3. T.E Weymouth and A.A. Amini "Visual Perception Using a Blackboard Architecture" Image Analysis Applications, R. Kasturi and M.M. Trivedi (eds.),Marcel Dekker,Inc., New York (1990) pg. 240.

Chromium Removal from Ground Water by Ion Exchange Resins

Panagiotis Skiadas

University of Florida

Lawrence Livermore National Laboratory
Livermore, California 94550

May 11, 1994

Prepare in partial fulfillment of the requirements of the Science and Engineering Research Semester under the direction of Maureen Ridley, a Research Mentor, at Lawrence Livermore National Laboratory.

* This research was supported in part by an appointment to the U.S. Department of Energy Science and Engineering Research Semester (hereinafter called SERS) program administered by LLNL under Contract W-7405-Eng-48 with Lawrence Livermore National Laboratory.

Chromium Removal from Ground Water by Ion Exchange Resins

Panagiotis Skiadas
University of Florida
Environmental Restoration Division

ABSTRACT

The ground water at several monitoring wells at LLNL has been found to exceed the Surface Water Discharge Limits for Cr(VI). Ion exchange resins have been selected for its removal. A research study is underway to determine which commercial resin is preferred for LLNL's ground water. The choice of an appropriate resin will be based on Cr(VI) exchange capacity, regeneration efficiency, and pH stabilization. A sequestering agent must also be selected to be used for the elimination of scaling at the treatment facilities. The chemistry of ion exchange resins, and instrumentation and procedures are explained and described in the following paper. Comparison of the different resins tested lead us to the selection of the most effective one to be used in the treatment facilities.

INTRODUCTION

This report describes the study conducted for the Environmental Restoration Division, to determine performance characteristics of ion exchange resins to be used for Cr(VI) removal from ground water. Cr(VI) exists in solution as CrO_4^{2-} (chromate) in the Lawrence Livermore National Laboratory (LLNL) ground water system. The results obtained from this study will assist LLNL in operating their treatment facility C (TFC), which is currently using an ion exchange resin, in a more efficient manner and to determine the most effective resin for use in future facilities.

SCOPE OF THE STUDY

The goal of the study is first to determine the most effective resin to be used on future treatment facilities. That decision will be based on the resin's performance for that well's chromate concentration--as we will see, each resin's performance varies with chromate concentration--and regeneration characteristics. Second, to determine the mechanics: flow rate, bed volumes (BV) of regenerant required, direction of flow to estimate the most efficient regeneration process. Third, using the lab study as a model, predict TFC's *breakthrough* point (See Section on Ion Exchange Chemistry). And fourth, determine if the use of a sequestering agent will affect the resin's performance.

BACKGROUND OF THE PROBLEM AND ITS SIGNIFICANCE

ERD's role

The Environmental Restoration Division (ERD) of the LLNL has the responsibility of restoring the ground water at the lab site to levels below established drinking water standards. The contamination originated in the 1940s when the site was a Navy aviation training base. Many of the Volatile Organic Compounds (VOCs) used at LLNL in the 1940's, such as trichloroethylene (TCE), perchloroethylene (PCE) were released into ditches and storm drains. These releases were done before their hazardous long-term effects were known. As they were found to be carcinogenic later on, LLNL was declared a Superfund site and clean up operations were initiated.

Chromium (VI)

In the process of pumping the water to the surface to treat it so it could be discharged to the city's sewer, the concentration of Cr (VI) was found to exceed the state' s surface water discharge limit of 11 parts per billion (ppb). Cr (VI) concentrations ranges from 10 to 150 ppb. Cr (VI) is known to be toxic and carcinogenic to plant and animal life (the drinking water standard is 50 ppb). The hexavalent form of chromium is usually very unstable but due to the oxidizing environment of the ground water (Eh range of 350 to 400 mV which indicates high levels of dissolved oxygen) and the basic pH (average pH is 7.8), the Cr (VI) maintains its oxidation state. The discharge limit for Cr(III) is 50 ppb. It is not clear as to why the Cr (VI) levels are so high but it is suspected that the geological characteristics of the region are responsible. The fractions of the subsurface sediment that contain the most Cr (VI) and Cr (III) also contain MnO_2, a natural oxidizing agent for the conversion of Cr (III) to Cr (VI) (Bartlett and James, 1979; Malati and Sear, 1989). The oxidation of Cr (III) has been suggested as (Ridley and Martinelli, 1992):

$$Cr^{+3} + 1.5\,MnO_2 + 6\,H^+ \rightarrow Cr^{+6} + 1.5\,Mn^{+2} + 3\,H_2O$$

Possible anthropogenic additions exist from: 1) chromic acid waste discharges to an unlined pit by a local manufacturing company and from 2) blow down releases from cooling towers at LLNL using chromate solution as a bacterial inhibitor. Given the nature of the water (see Table I) and the extremely low discharge limits, ion exchange resins were selected for the removal of chromate.

TABLE I

Water characteristics (Average)

pH	7.8
Cr Concentration	0.03 ppm
Sulfate	30 ppm
Nitrate	10 ppm
Calcium	75 ppm
Magnesium	35 ppm
Bicarbonate alk (as $CaCO_3$)	400 ppm
TDS	600 ppm
VOCs	0.05 ppm

ION EXCHANGE CHEMISTRY

Process

Ion exchange is a water treatment process in which a pre-saturant ion, the *absorbent*, is exchanged for an unwanted ion in the water. In our case the *absorbent* is Cl^- and the unwanted ion is CrO_4^{2-}. The reaction that takes place is shown (R_4N^+ is the active ingredient explained in the Resin Chemistry section):

$$R_4N^+Cl^- + CrO_4^{2-} \rightarrow (R_4N^+)_2CrO_4^{2-} + 2Cl^-$$

Water flows through the resin bed until the resin's ability to exchange CrO_4^{2-} is reduced to the point where the effluent has reached unacceptable discharge levels. This discharge level is called the *breakthrough* point. This is a result of the occupation of exchange sites by CrO_4^{2-} and other anions (SO_4^{2-}, HSO_4^-, NO_3^-, HCO_3^-). To restore the resin's exchange capacity, regeneration is performed by *washing* the resin with an excess of the pre-saturant ion (NaCl). The reverse of the above reaction takes place and this allows the resin to be used many times before being discarded because of irreversible fouling or attrition losses.
The resins have different affinities for each ion. The binary separation factor α_{ij}, common in chemical engineering practice, describes the exchange equilibria (Clifford, 1990):

$$\alpha_{ij} = \frac{\text{distribution of ion i between phases}}{\text{distribution of ion j between phases}} = \frac{y_i/x_i}{y_j/y_j}$$

where

y_i = equivalent fraction of ion i in resin
x_i = equivalent fraction of ion i in water

Table II lists the selectivity sequence for a strong base anion resin. As we see, the resin prefers CrO_4^{2-} 100.0 times over Cl^- but anions such as SO_4^{2-} and NO_3^-, although less preferred, they pose a problem as they overwhelm the resin with their presence . They are found in concentrations 1000 times higher than CrO_4^{2-} and occupy exchange sites therefore reducing the resin's capacity to

remove CrO_4^{2-}. The performance of the resin therefore depends on the water's concentration of competing anions.

Table II

Anion i	α_{i/Cl^-}
CrO_4^{2-}	100.0
SeO_4^{2-}-	17.0
SO_4^{2-}	9.1
HSO_4^-	4.1
NO_3^-	3.2
Br^-	2.3
Cl^-	1.0

Resins generally are preferred over other treatment methods because the effluent has essentially zero level of contaminant while creating very little waste. Resins are relatively insensitive to flow variations under 5 gpm/ft^3 of resin and can operate on demand. Flows over 5 gpm/ft^3 can cause stresses that exceed the resin's bead strength.

Resin Chemistry

All resins consist of a cross-linked polymer matrix on which different charged functional groups are attached covalently. The matrix is polystyrene cross-linked with divinyl benzene for structural stability (Dorfner, 1991). There are two categories of anion exchange resins based on the functional group: strong base anion (SBA) and weak base anion (WBA). The functional group in SBA resins is quaternary amine [--$N(CH_3)_3^+$] which is so strongly basic that it is ionized and is therefore useful over the entire pH range (Clifford, 1990). SBA resins are the most commonly used resins and three of these resins were tested in this study. With respect to the polymeric structure of the network, SBA resins are designated as gel, macroporous, and isoporous. Table III displays chemical and physical characteristics, as specified by the manufacturer, for two of the SBA resins tested.

Table III

	A600	A500
Matrix structure	gel	macroporous
Physical appearance	amber spheres	opaque spherical beads
Ionic form	Cl	Cl
pH limitations	none	none
Swelling (Cl-->OH)	20%	10%
Water retention	43-48%	53-58%
Screen size, US Std. Mesh (wet)	16-50	16-40
Mechanical strength(grams)	500	300

The gel type generally has no pores, is elastic in nature, and regenerates easily (two gel type resins were tested). The macroporous type has a porous matrix with large internal surfaces (one macroporous type resin was tested). The surface areas of the macroporous resin can have up to 100 m^2/g (Dorfner, 1991). Extended cross-linking is required to avoid collapse of the structure. The macroporous resins are generally harder to regenerate. The isoporous type is modified in a way to obtain polymers with a uniform pore size. They are not as commonly used (none were tested). The functional group in WBA resins is a tertiary amine [--$N(CH_3)_2$]. It is useful only in the acidic pH and it is relatively ineffective in the pH range, (6.5 to 8.5 inclusive as defined by the discharge limits) required for operation (Clifford, 1990), of LLNL treatment facilities. WBA resins are less commonly used with higher pH solutions. One WBA resin was tested.

PROCEDURE

Resin Performance Testing

The available materials at the lab allow us to duplicate the treatment process of TFC to a reasonable extent. Characteristics such as flow rate, pH, and of course the water are all similar to that of TFC's. The water velocity, the pipe material, (steel at TFC, teflon at the lab) and the dimensions of the columns differ, however. Therefore the lab study can only be used as a guide and further considerations have to be made before applying the data from the lab to TFC.

The water is delivered to the lab in 55 gallon interior plastic coated drums. Eighteen liters of water are then drained into a 20 liter polypropylene container which is where the water is prepared for the column tests. First, the water is air-stripped, to remove the VOCs, by bubbling air in the ratio of 25:1 (air: water) by volume at a rate of 10 cfh (4.72 L/min.). This simulates the air-stripping done at TFC. During the air-stripping process, the pH of the water increases as the air drives out the CO_2 along with the VOCs. The pH of the water increases to approximately 8.5. The increase in pH causes two problems for TFC. The first problem is that scaling occurs as Ca^{+2} and Mg^{+2} precipitate out with CO_3^{2-}. The pipes and the pump eventually plug up, therefore creating the need to replace them which is very costly. Scaling can also plug up the flow through the resin. The second problem is the pH is dangerously close to the discharge limit of 8.5. The pH is therefore adjusted to about 7.8 by bubbling CO_2 into the water at a rate of 3 cfh for about 15 seconds. Because of the open system we have at the lab, pH adjustment is required every 2-3 days as CO_2 continuously escapes and pH increases.

Experimental apparatus and set-up is the same for all the resins. Each resin column is consisted of a 10 ml plastic syringe barrel in which precisely 6 ml of resin is packed. The measurement is done using the specific gravity of the resin and measuring the resin's weight . From the weight we can then determine the volume. This method is preferred over eye-balling because air-pockets are held between the resin beads, therefore showing more volume than what it actually is. On top and the bottom of the resin there is approximately 0.5 ml of glass wool that serves as a filter on the influent side (top) and as a resin support on the effluent side (bottom). The tubing that transports the water from the 20 L container to the column is plastic and goes through a plastic sample port and a control valve. Some columns that were started by the SERS student from last semester have been found to have their volume erroneously measured and the results we receive from those columns may have to be duplicated. The water is pumped at a rate of 2.4 ml/min. (3-5 gpm/ft^3 of resin depending on the BV of the resin) by a peristaltic pump. The water flows through the column by gravity and is collected at the bottom in liter or gallon containers.

Total chromium analysis is performed using a Perkin Elmer atomic absorption (AA) spectrophotometer equipped with a graphite furnace. Its limit of detection

is 0.1 ppb and has range up to 60 ppb. Its range can be increased by decreasing the sample size (15µL) but that will cause a loss of sensitivity in the lower range. Calibration curves must have a correlation coefficient of at least 0.999. They are performed at least every two weeks or every time a graphite tube is replaced. The curve is checked with a standard every morning to ensure its credibility. A minimum of four replicates of each sample are analyzed at the instrument's default specifications for chromium analysis.

Cr(VI) analysis is performed by EPA method 7196, Colorimetric Determination of Hexavalent Chromium. Concentrations are about the same for both methods which proves that most of the chromium in the water occurs as Cr(VI). This method is ideal for regenerant analysis, as the high salt content of the regenerant does not interfere with the detection of the chromium as it does with AA analysis. After the column reaches its *breakthrough* point the flow is stopped and the resin is regenerated using five BVs of 2 M NaCl which are collected for analysis by the EPA method 7196. They are then treated as hazardous waste. Five additional BVs of deionized water are run through the resin to wash off any salt residue. Down flow regeneration was first used. Dorfner suggests that counter current regeneration is preferable because it has the advantages of lower leakage and improved effluent quality, lower regenerant, and reduction in the quantity of regenerant waste. Counter current regeneration will be employed next time regeneration is performed.

Sequestering Agent Testing

Sequestering agents are chemicals added to water to complex the Ca^{+2} and Mg^{+2} to prevent them from interacting with other compounds in the water (Jenkins and Snoeyink, 1980). They are mainly polyphosphates which quickly become orthophosphates in solution. A test was conducted to determine whether the sequestering agent of interest, JP7, would affect the resin's performance. The test was done only with the A600 resin since this is the resin presently in use at TFC. Original air-stripped TFC water was used for the test. The required concentration of JP7 in the water was 13.4 ppm as determined based on the total hardness, plus iron and manganese concentrations.

RESULTS

A500

The A500 is a macroporous SBA resin. The column was started last semester and continued on into this semester and was regenerated after having treated 11100 BVs before *breakthrough* occurred The average influent chromate concentration was 30 ppb. Regeneration was not done properly and regeneration data will be obtained after the completion of the current test. The current test will be completed during the summer of 1994. So far it has treated 7200 BVs and the effluent has 4.6 ppb chromate. The influent is from monitoring well # 361 (MW-361) contains about 15 ppb chromate. An additional amount of chromate was added(a spike) to the MW-361 well water. The well water was spiked with potassium dichromate to establish an average concentration of 38 ppb chromate. The transition from 0 to 4.6 ppb chromate in the effluent has not been very gradual, which is a disadvantage, because *breakthrough* could be reached to quickly to allow for the TFC operators to appropriately react.

A600

The A600 is a gel-type SBA resin. The column was started last semester and continued on into this semester. So far it has treated 32700 BVs and the effluent has 6.5 ppb chromate. The influent is from MW-361. The transition from 0 to 6.5 ppb chromate in the effluent has been very gradual.

A600 and JP7

The JP7 test was done with water from TFC that has about 35 ppb chromate. This test was completed, and 7530 BVs were treated before it reached *breakthrough.* Its transition is shown in Graph I. This transition is not very gradual and TFC would need to shut down probably once 8-9 ppb chromate were detected in the effluent. Regeneration has not been performed yet.

A300

The A300 is a gel-type SBA resin. The column was started last semester and continued on into this semester and was regenerated after having treated 10135 BVs before breakthrough. The well water had an average influent chromate concentration was 30 ppb. Regeneration was not done properly and regeneration data will be obtained after the completion of the current test. The current test

will be completed this summer. So far it has treated 6900 BVs and the effluent has 3.5 ppb chromate. The influent is from MW-361 but it is spiked to an average of 38 ppb chromate. The transition from 0 to 3.5 ppb chromate in the effluent has been very gradual.

AMB

The AMB is a macroporous WBA resin. Two columns were prepared for testing: one treating water with about 15 ppb chromate and one with about 38 ppb chromate. In both cases the pH was held at 7.8 as done with all the tests and the resins reached breakthrough just after 500 BVs and 450 BVs respectively.

CONCLUSIONS

The study is not complete as some of the resins have not reached *breakthrough* yet. Based on what we have, however, we can conclude the following:

- The A500 resin has high chromate exchange capacity when the influent chromate concentration is ≥30 ppb. Its transition from 0 to 4.6 ppb chromate is not very gradual.

- The A600 resin has very high chromium absorbance capacity when the influent chromate concentration is ≤15 ppb. Its transition from 0 to 6.5 ppb chromate is very gradual. Previous tests have shown that the A600 has relatively poor capacity to exchange chromate when the influent chromate concentration is ≥30 ppb.

- The sequestering agent JP7 does not have any noticeable short-term effects on the A600 resin. The performance of the resin treating water with JP7 gave similar results with the resin treating water without JP7.

- The A300 resin has high chromium absorbance capacity when the influent chromate concentration is ≥30 ppb. Its transition from 0 to 3.5 ppb chromate is very gradual.

- The AMB resin, at the pH of interest, failed. The AMB resin did not perform nearly as well as the rest of the resins in terms of BVs treated.

- Close attention has to be paid to the pH of the effluent when a new A600 is used. The pH for the first 30 BVs was under 6.5 therefore violating discharge limits.

- The water will flow through the points of least resistance in the resin. That may create some pathways that the water flows through leaving a portion of the resin untouched by the water. That may be avoided, in the lab tests, by shaking the column every 1000 BVs. At TFC it is suggested that regeneration is done counter current and flow through the resin is regulated at the bottom of the tank in such a way as to assure that there is a layer of water on top of the resin surface. That will assure that all of the resin is in contact with water.

FUTURE WORK

Once the resins currently tested reach *breakthrough* their regeneration efficiency will be determined. The number of BVs of regenerant required to reclaim all, if possible, of the chromate will be determined for each resin. The regeneration efficiency will directly affect how much hazardous waste will be created.

Because of the uncertainty involved in the measurements of some of the resin BVs started in the past, some of the tests may need to be duplicated.

The resins performance will be compared with other treatment methods such as reduction of Cr(VI) to Cr(III) by chemical additions. The most efficient technology will be used in future treatment facilities.

GRAPH I

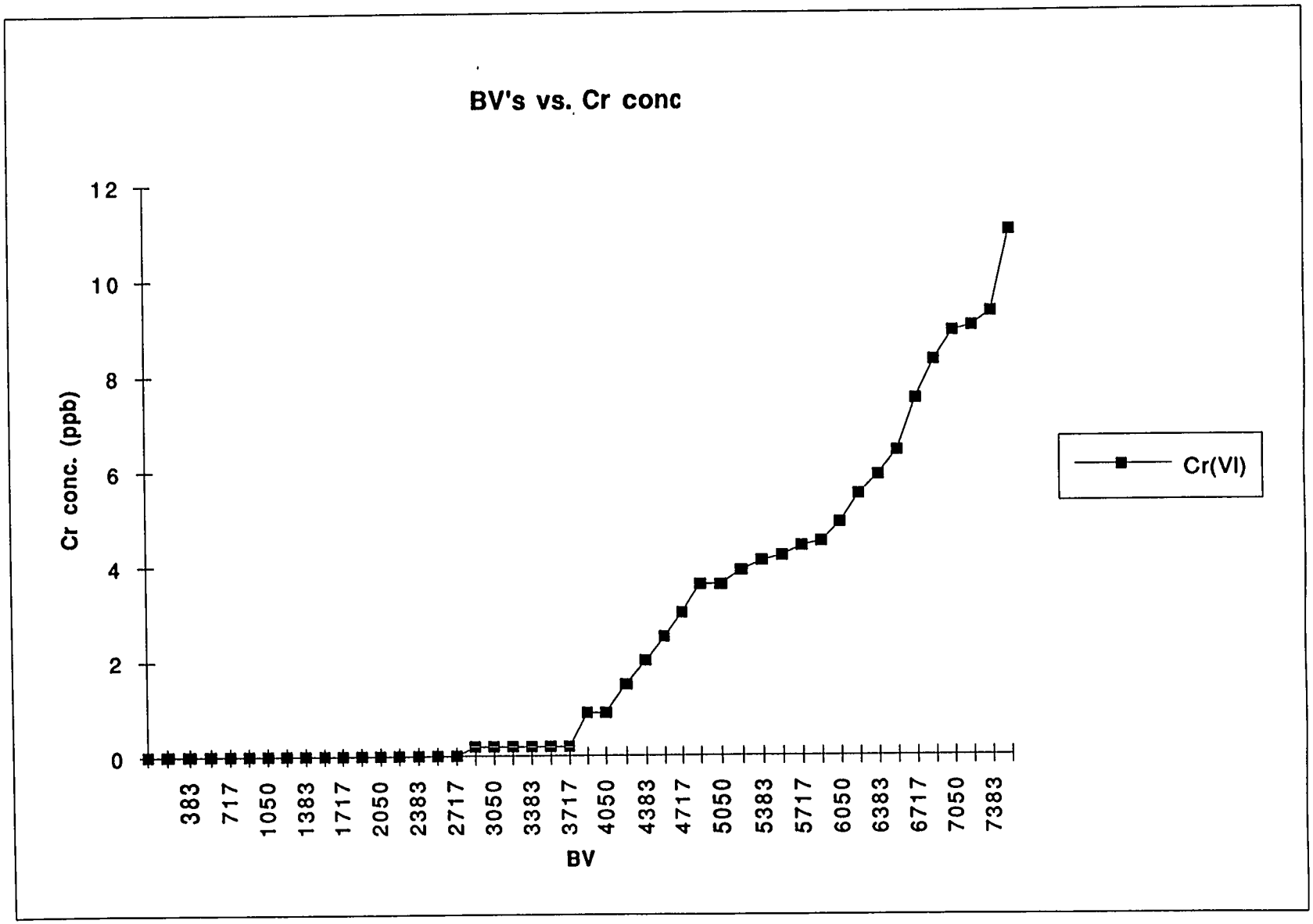
BV's vs. Cr conc
Cr conc. (ppb)
12
10
8
6
4
2
0
383
717
1050
1383
1717
2050
2383
2717
3050
3383
3717
4050
4383
4717
5050
5383
5717
6050
6383
6717
7050
7383
BV
Cr(VI)

REFERENCES

Bartlett, R. and James, B. 1979." Behavior of Chromium in Soils: Oxidation" *J. of Environmental Quality* 8:31-35

Clifford, D.A. Ion Exchange and Inorganic Adsorption. in Pontiu, F.W.,ed. *Water Quality and Treatment*. New York, McGraw-Hill, 1990

Dorfner, Konrad. *Ion Exchangers* Berlin, de Gruyter, 1991

Jenkins, D. and Snoeyink, V.L. *Water Chemistry* New York, Wiley, 1980

Malati, M.A. and Sear, A. 1989."Oxidation by Manganese(III)-Oxidation of Chromium(III)". Polyhedron. 8:1874-1875

Martinelli, R.E. and Ridley, M. 1992. "Chromium Characterization and Treatment at LaWrence Livermore National Laboratory" Unpublished, LLNL

Genetic Algorithms using SISAL Parallel Programming Language

Sheila Tejada
June 16, 1994

Abstract

Genetic algorithms are a mathematical optimization technique developed by John Holland at the University of Michigan [1]. The SISAL programming language possesses many of the characteristics desired to implement genetic algorithms. SISAL is a deterministic, functional programming language which is inherently parallel. Because SISAL is functional and based on mathematical concepts, genetic algorithms can be efficiently translated into the language. Several of the steps involved in genetic algorithms, such as mutation, crossover, and fitness evaluation, can be parallelized using SISAL. In this paper I will discuss the implementation and performance of parallel genetic algorithms in SISAL.

1 Introduction

Genetic algorithms are an optimization technique that is inspired by biological evolution. Solutions for a given problem are encoded as chromosomes or binary strings. For example, if the given problem was to maximize the function x^2, then a solution might look like this : 101101011100011. Genetic algorithms maintain a population of solutions and use operators, such as, mutation and crossover, to alter these solutions. In later sections I will describe the procedure and the characteristics of a genetic algorithm in further detail.

SISAL and its role in creating parallel genetic algorithms will also be discussed. SISAL is a high level functional programming language which "hides the complexity of parallel programming, expedites parallel programming development, and guarantees determinacy."[2] Since SISAL is a functional language, SISAL programs are more concise and portable than programs in conventional languages.[3] In section 4 more information on SISAL is provided. Section 5 describes the implementation and analysis of the parallel genetic algorithms; and, section 6 discusses how work with genetic algorithms can extend into genetic programming.

2 Background

In 1975 at the University of Michigan John Holland developed a search technique called genetic algorithms. Holland's objective in developing this technique was to understand the adaptive ability of natural systems in order to create an artificial system which possessed the important mechanisms of natural systems.[1] The key issue for Holland was the *robustness* of the search. "Genetic algorithms are theoretically and empirically proven to provide robust search in complex spaces." [1] Other characteristics of genetic algorithms are that they are computationally simple and do not require restrictive assumptions about the search space.

SISAL was designed in 1983 as a joint venture between Colorado State University (CSU), the University of Manchester, Digital Equipment Corporation (DEC), and Lawrence Livermore National Laboratory (LLNL). The objective was to determine the potential for using the functional programming style when there were no assumptions of the special hardware support for the execution model. The mathematical foundation of the language was believed to provide many opportunities for concurrency.[3]

3 Genetic Algorithms

Genetic algorithms are search methods based on the principles of natural selection(survival of the fittest) and genetics. A genetic algorithm is a randomized, yet directed search through a problem space. The first step of the procedure is to create an initial population of solutions or chromosomes. These solutions are generated randomly. In the example of maximizing the function x^2 , the population of solutions would be a set of binary strings. The next step would be to generate new solutions from the initial population using the crossover and mutation operators. After the new child solutions are produced then their fitness is evaluated; and they are placed into the population. Those chromosomes with unsatisfactory fitness values are discarded. The cycle continues on with a new generation of solutions being created using crossover and mutation (see diagram 1) until the values of the solutions converge upon a certain number.

3.1 Crossover Operator

If the population of chromosomes consists of binary strings, then the crossover operator would chose two chromosomes from the population as parents and combine or mate them in order to produce two child binary strings or chromosomes. To combine two parent solutions they both are split at the same position and then spliced back together again, creating two new solutions as in diagram 2.

How a Genetic Algorithm Works

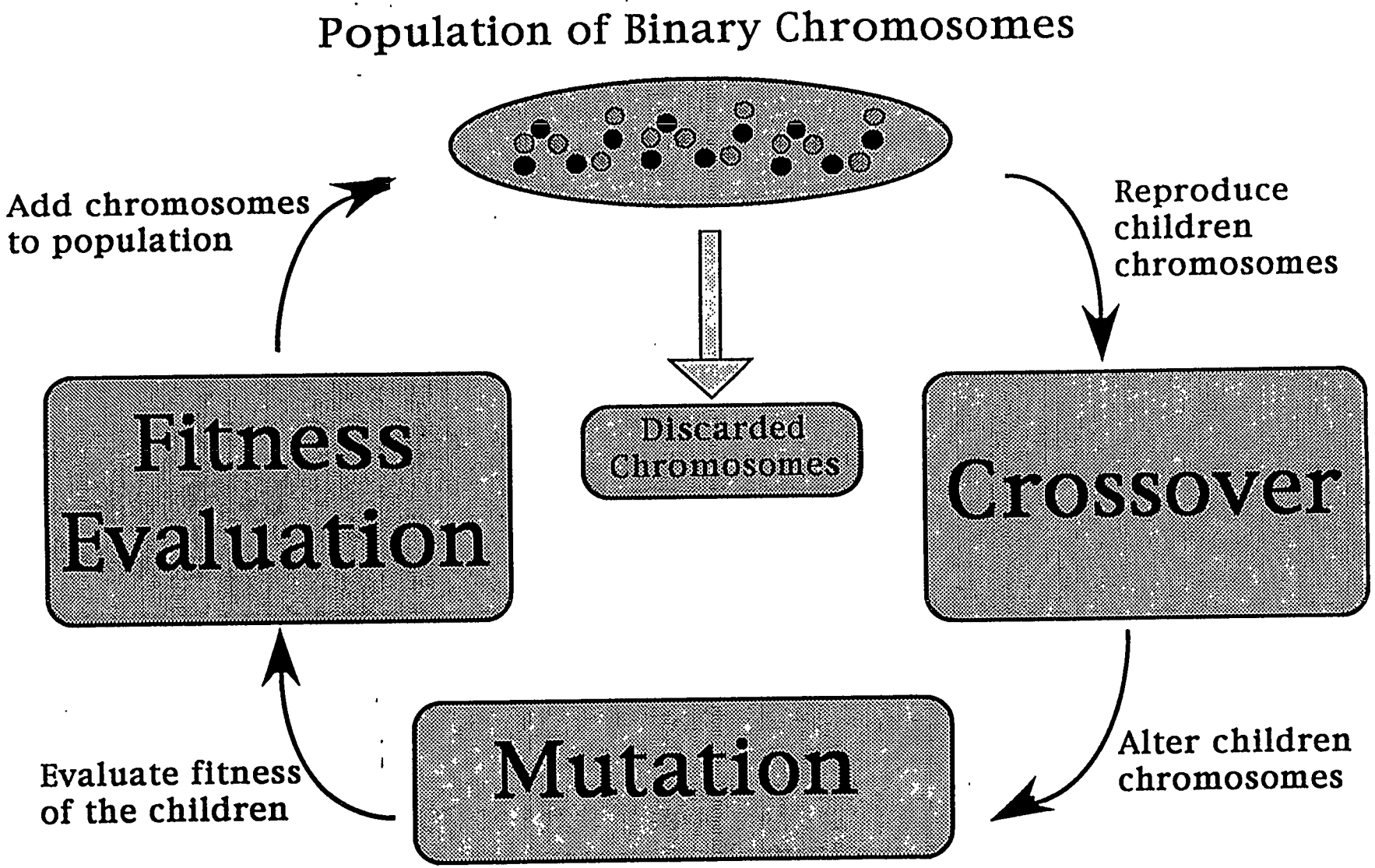

Crossover

Population of Binary Chromosomes

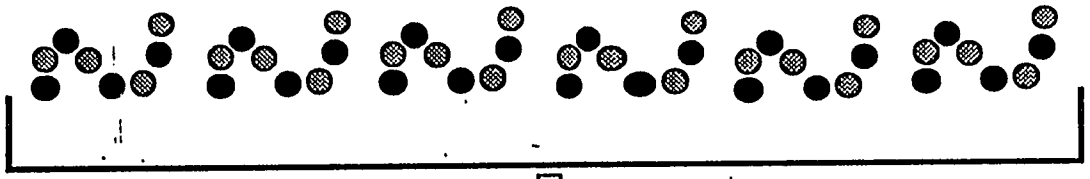

Select two parent chromosomes

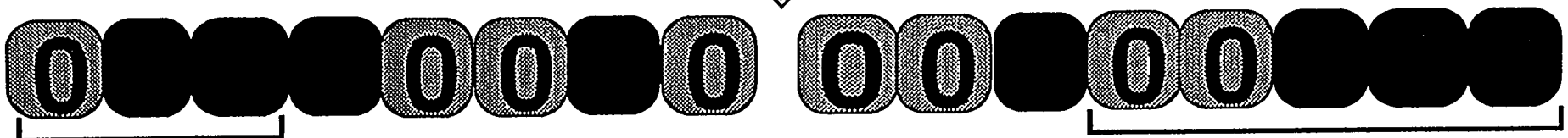

Splice pieces of the parents together

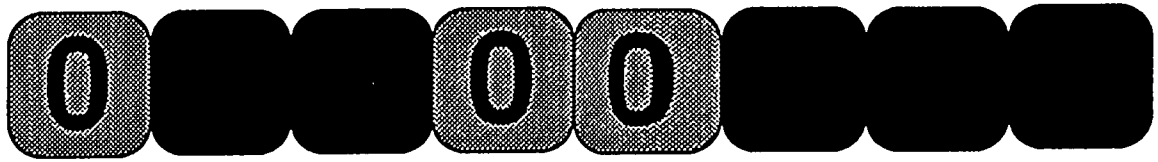

3.2 Mutation Operator

The mutation operator chooses one chromosome from the population, and then selects a position on that binary string. The value of the position that it has chosen is then altered as shown in diagram3.

3.3 Fitness Evaluation

The fitness evaluation is an important step in the genetic algorithm. Each solution is evaluated using a specific fitness function associated with the given problem. For example, if the problem was to maximize the function x^2, then the fitness function could be x^2, where x is the decimal representation of the binary string.

4 SISAL

One of the most important features of the SISAL programming language is the for expression:

```
for <range generator>
      <loopbody>
returns <return clause>
end for
```

The for expression is a parallel loop form. "The expression's syntax and semantics guarantee that the instances of the loop body are data independent." [3] This looping construct provides the concurrency for the language without having it directly specified by the user. This construct is used heavily in my implementation of a parallel genetic algorithm.

Mutation

Population of Binary Chromosomes

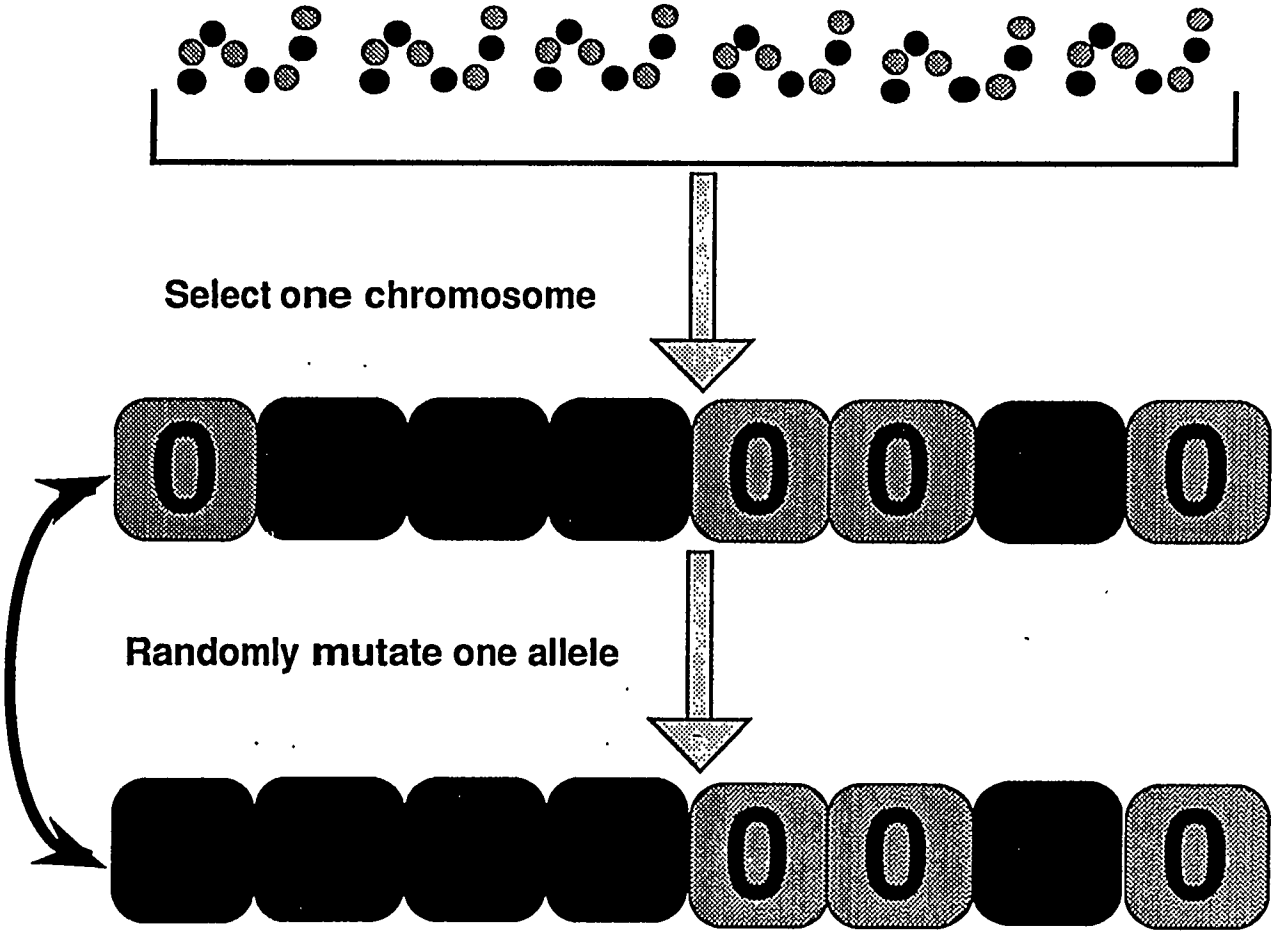

5 Parallel Genetic Algorithms

Genetic algorithms are inherently parallel. There are several steps in a genetic algorithm which can be performed in parallel. The first step is the generation of the initial population. Each of the chromosomes in the initial population can be created at once. The next step to parallelize is the reproduction (crossover) step. The population of chromosomes can be mated in parallel creating new children chromosomes. This can also be done with the mutation phase. Each of the chromosomes to be altered can be mutated at the same time. The fitness evaluation of each of the chromosomes can also be executed in parallel.

5.1 Implementation

I attempted to parallelize the steps of the genetic algorithm using SISAL. The problem that I chose to solve was maximizing the function x^2, where x is equal to 2^{15}. The two main data structures are two arrays - one for the fitness values of the solutions, and the other to hold the population of chromosomes (solutions). The length of the binary chromosome is 16 bits, and the size of the initial population is 50 chromosomes which remains constant throughout the generations.

For the crossover function two parent chromosomes are chosen at random and mated with probability p_{cross} . If the parents are not mated then the children take the values of the parents unaltered. The children chromosomes are altered by the mutation operator with probability $p_{mutation}$. The fitness of the children chromosomes are evaluated and are put into the population, replacing the chromosomes with the worst fitness values. This was repeated for 25 generations at each trial.

5.2 Analysis and Results

I conducted 9 experiments in which I varied the probabilities of mutation and crossover. There were three different sets of probabilities which I ran for 0, 5, and 10 generations. In figure 1, the probabilities are p_{cross} .99, $p_{mutation}$ .01. The probabilities for figure 2 are p_{cross} .75, $p_{mutation}$ .25, and for figure 3 are p_{cross} .50, $p_{mutation}$ .50. For this problem the population of solutions converge rather quickly upon the answer. The experiments with the greater probability for crossover converge faster than the other experiments. The performance of the genetic algorithm surprisingly was constant, and did not change with more workers added. I believe it probably is due to my replacement function.

6 Further Work

The principles of genetic algorithms can be extended to not only generating bit string solutions, but also whole programs. This technique, where a program can be evolved without explicitly being designed by a programmer, is called genetic programming. The method used to evolve these program solutions is the same as the one used in genetic algorithms. But, the crossover and mutation operator as well as the fitness function will be manipulating program graphs instead of binary strings.

7 Conclusions

Because many of the steps involved in genetic algorithms can be parallelized, genetic algorithms fit well with the features of SISAL. Since SISAL is based on familiar mathematical concepts the genetic algorithm was easily translated into a SISAL program. From the experimental results the effects of crossover and mutation on the generation of new solutions was demonstrated. The crossover

operator seemed to be the more dominate operator in guiding the creation of better solutions.

Acknowledgments

This work has been conducted at Lawrence Livermore National Laboratory. I would like to thank my mentors John Feo, Thomas DeBoni, and Rao Vemuri for their guidance and support.

References

1. Goldberg, David E. Genetic Algorithms in Search, Optimization and Machine Learning. Addison-Wesley Publishing Company, Inc., 1989.

2. McGraw, J. Parallel Functional Programming in Sisal: Fictions, Facts, and Future. Lawrence Livermore National Laboratory, Livermore, CA, July 1993.

3. Deboni, Thomas and J. Feo. et. al. Implementation and Performance of Domain Decomposition Algorithm in Sisal. *Hawaii International Conference on System Sciences,* Maui, HI, January 1994.

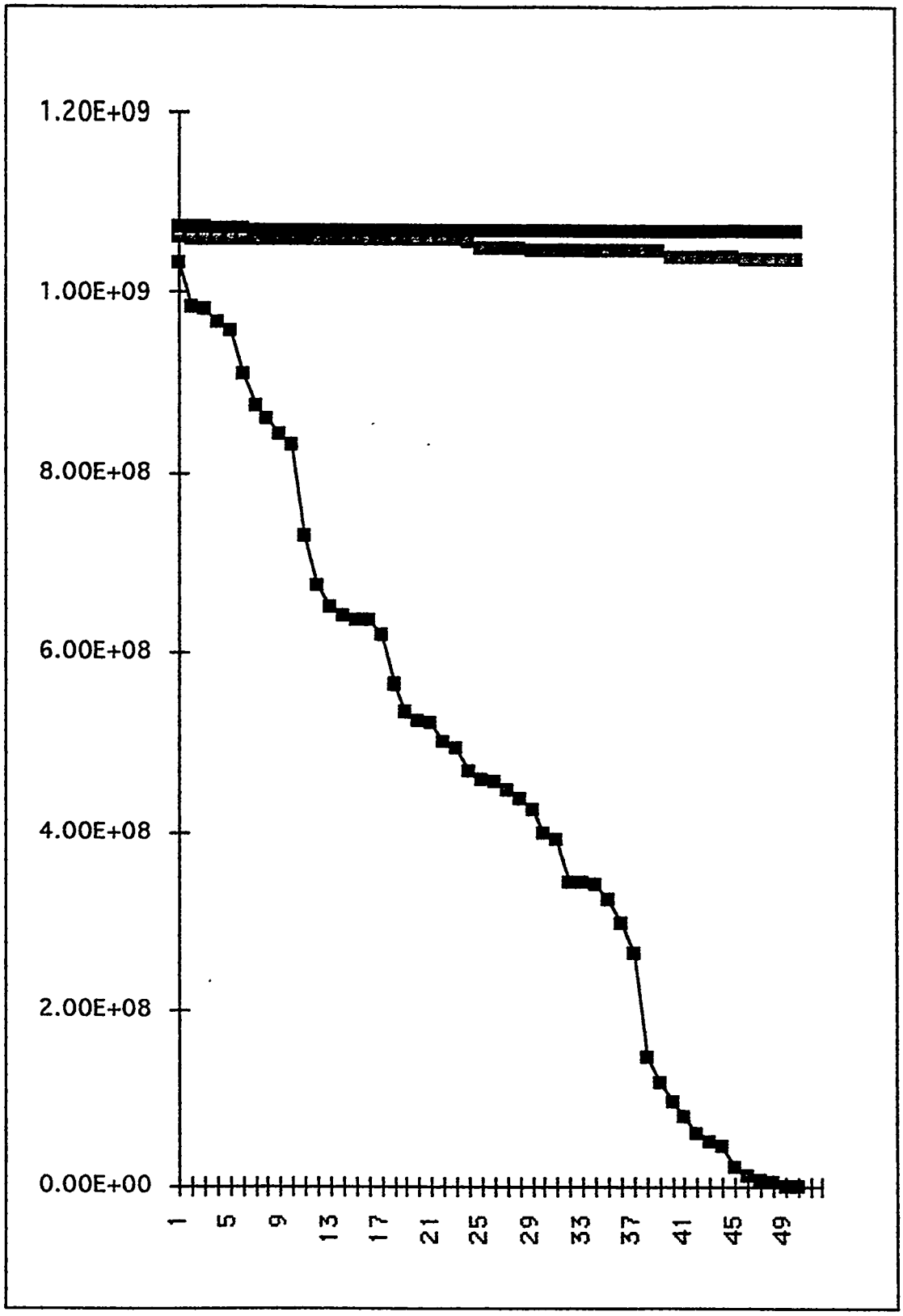
1.20E+09
1.00E+09
8.00E+08
6.00E+08
4.00E+08
2.00E+08
0.00E+00
1
5
9
13
17
21
25
29
33
37
41
45
49

Figure 1

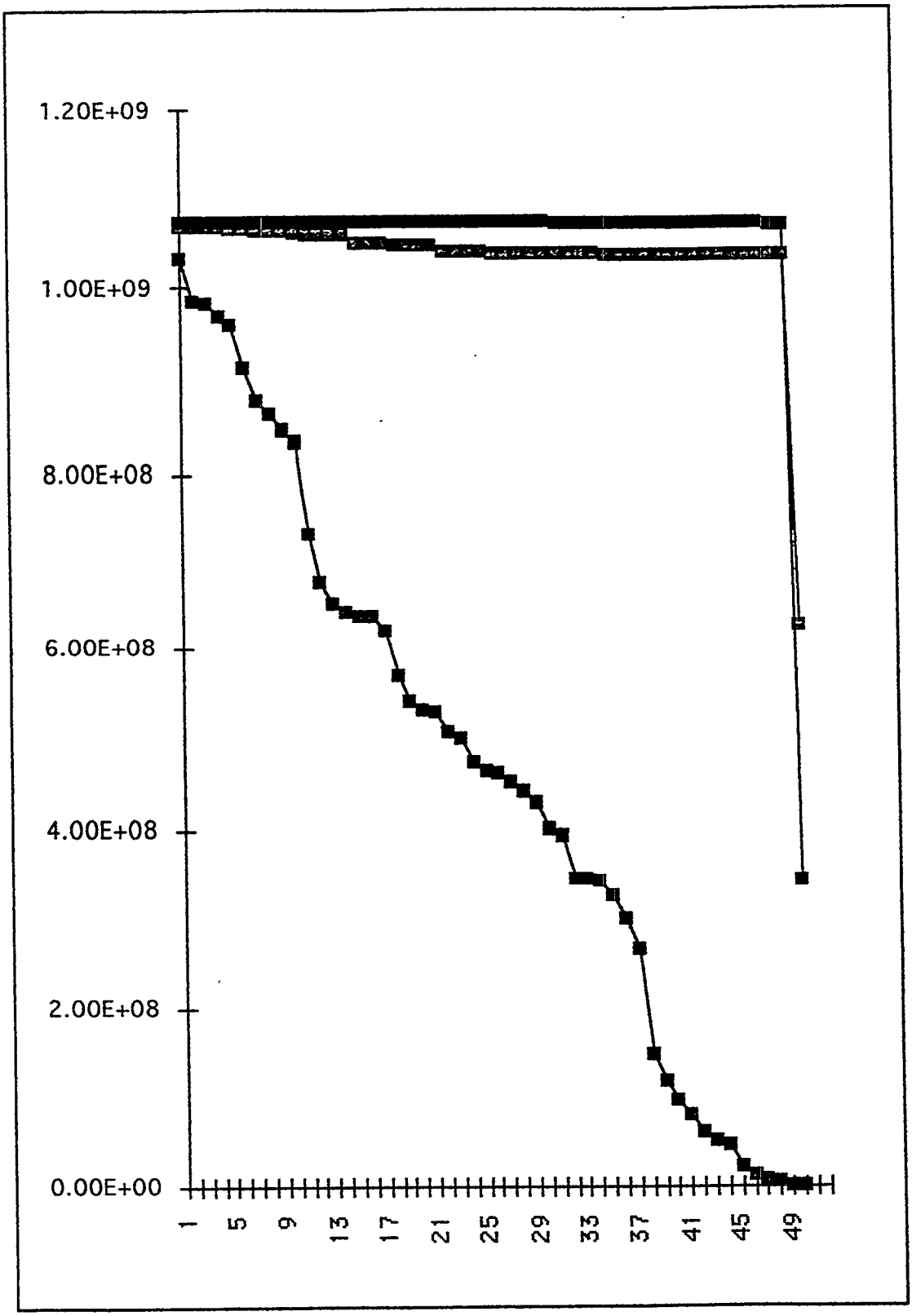
1.20E+09
1.00E+09
8.00E+08
6.00E+08
4.00E+08
2.00E+08
0.00E+00
1
5
9
13
17
21
25
29
33
37
41
45
49

Figure 2

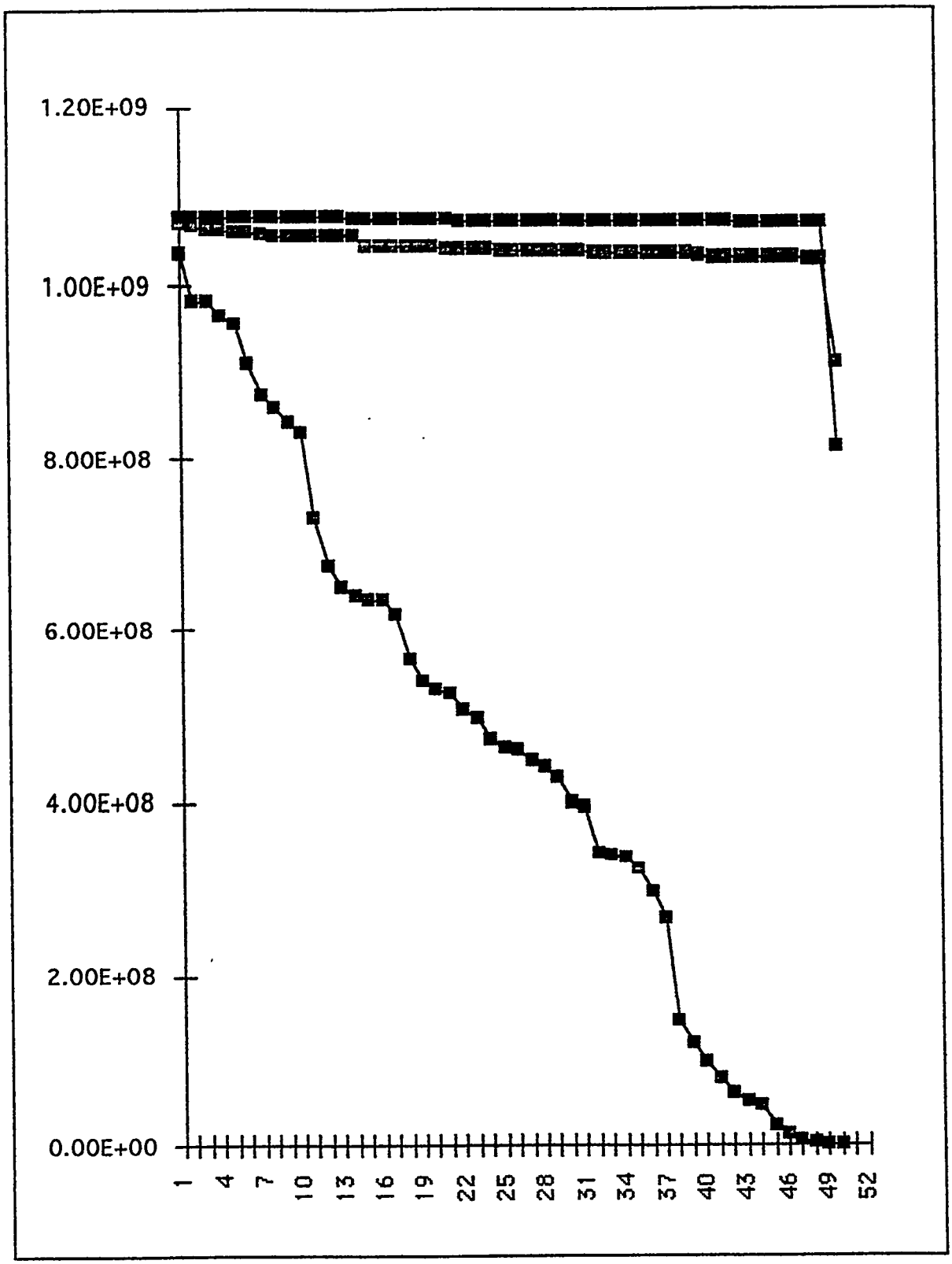
1.20E+09
1.00E+09
8.00E+08
6.00E+08
4.00E+08
2.00E+08
0.00E+00
1
4
7
10
13
16
19
22
25
28
31
34
37
40
43
46
49
52

Figure 3

BEAMLET DIAGNOSTICS *

Mitchell Theys

Purdue University
Lawrence Livermore National Laboratory
Livermore, California 94550

May 11, 1994

Prepare in partial fulfillment of the requirements of the Science and Engineering Research Semester under the direction of Scott Burkhart, Research Mentor, in the Lawrence Livermore National Laboratory.

* This research was supported in part by an appointment to the U.S. Department of Energy Science and Engineering Research Semester (hereinafter called SERS) program administered by LLNL under Contract W-7405-Eng-48 with Lawrence Livermore National Laboratory.

Beamlet is a high power laser currently being built at Lawrence Livermore National Lab as a proof of concept for the National Ignition Facility, or NIF for short. Beamlet is testing several areas of laser advancements, such as a 37cm Pockels cell, square amplifiers, and propagation of a square beam. The diagnostics on beamlet tell the operators how much energy the beam has in different locations, the pulse shape, the energy distribution, and other important information regarding the beam. This information is being used to evaluate new amplifier designs, and extrapolate performance to the NIF laser.

In my term at Lawrence Livermore National Laboratory I have designed and built a diagnostic, calibrated instruments used on diagnostics, setup instruments, hooked up communication lines to the instruments, and setup computers to control specific diagnostics.

Calibration is extremely critical on the diagnostic packages. Since there are multiple diagnostics on the system, the results must be consistent with each other. To ensure consistent similar results, calibration of integrating spheres, energy diagnostics, calorimeters, and imaging diagnostics is essential. The integrating spheres and calorimeters each have a coefficient associated with them that relates the output voltage from the device to an energy getting into the device. These coefficients can be determined in different ways, and in the case of the calorimeters was done in different ways, to verify the precision of the coefficients. By obtaining the coefficients by two different means, in the case of the calorimeters, we are able to better defend the data that we get from the instrument. If the data also matches what the integrating spheres obtain, then we have a well rounded set of data that is hard to argue with. The imaging diagnostics calibration was different than the previous calibrations. Neutral density filter glass is used to limit the amount of light that enters a camera or other light sensor. The amount of light it lets through is what we are trying to

determine, so that we can backtrack and determine how much energy the main beam of the laser has.

A calorimeter is a device that gives a voltage out which is proportional to the amount of energy shining inside the device. A calorimeter also contains a heater so that we can calibrate the device. By placing a known amount of current in the heater, which has a known resistance, we can calculate the amount of energy inserted into the device, see Figure A. By looking at the output from the calorimeter and the calculated energy in, we get a constant with units of J/V. This is our constant of proportionality. To verify that this number is accurate we then calibrated the calorimeters optically. This setup involved a NIST standard, assumed accurate, a splitter and a laser, see Figure B. The laser hit the splitter and part of the energy went to the NIST standard, and part went to our calorimeter. By taking the energy reading on the NIST, and the voltage out from our calorimeter we got a ratio, $C_1 = \frac{V_p}{NistEnergy} > K$. We then swapped the positions of the two calorimeters and got a similar ratio, $C_2 = \frac{V_p}{NistEnergy} < K$. Our constant K, was found from these two constants thus eliminating the need to know the exact split of the splitter, $K = \sqrt{C_1 C_2}$. The constants obtained from the optical and electrical calibration turned out to be extremely close in most cases. This verified the calibration techniques and provided the constants we needed. See Figure C for sample output from a calorimeter.

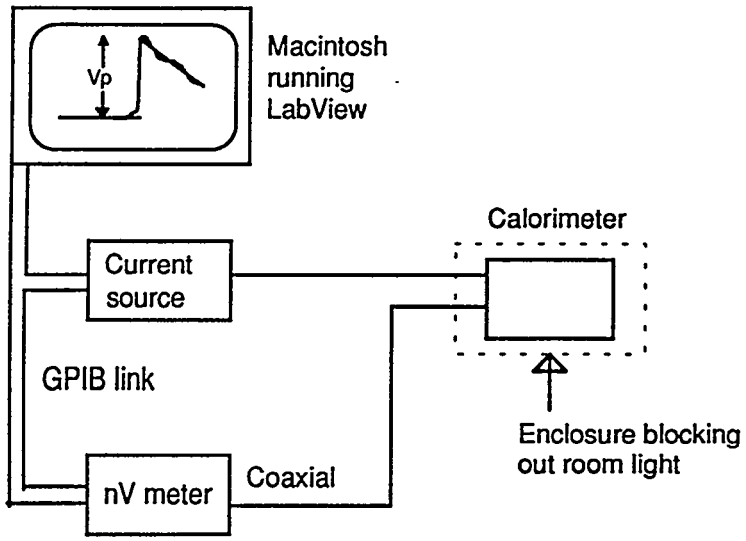

Figure A -- Electrical Calorimeter Calibration

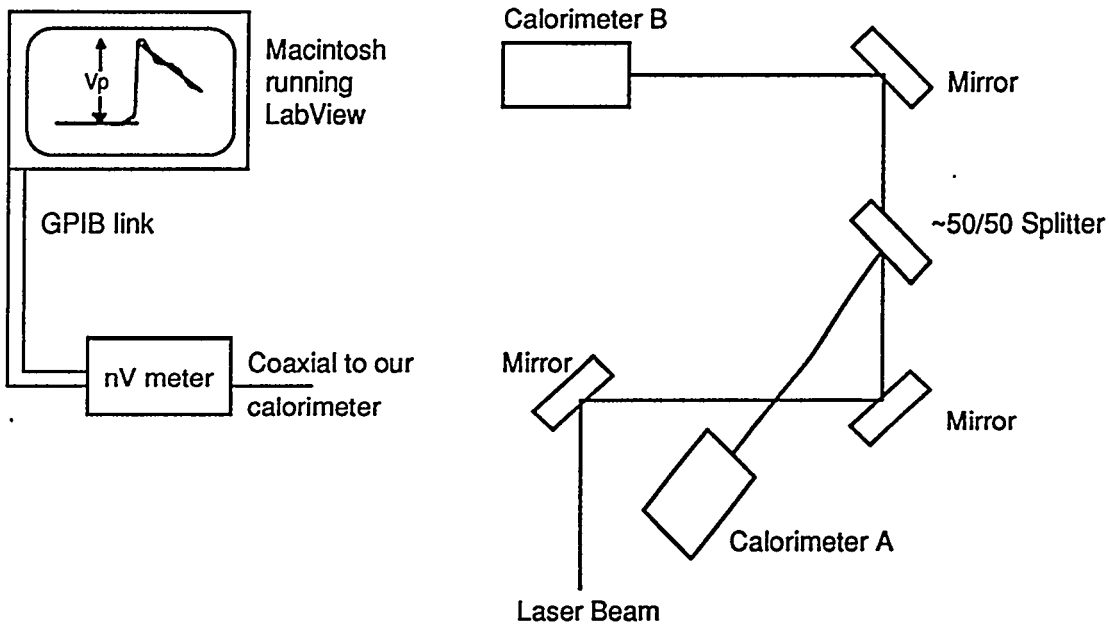

Figure B -- Optical Calorimeter Calibration

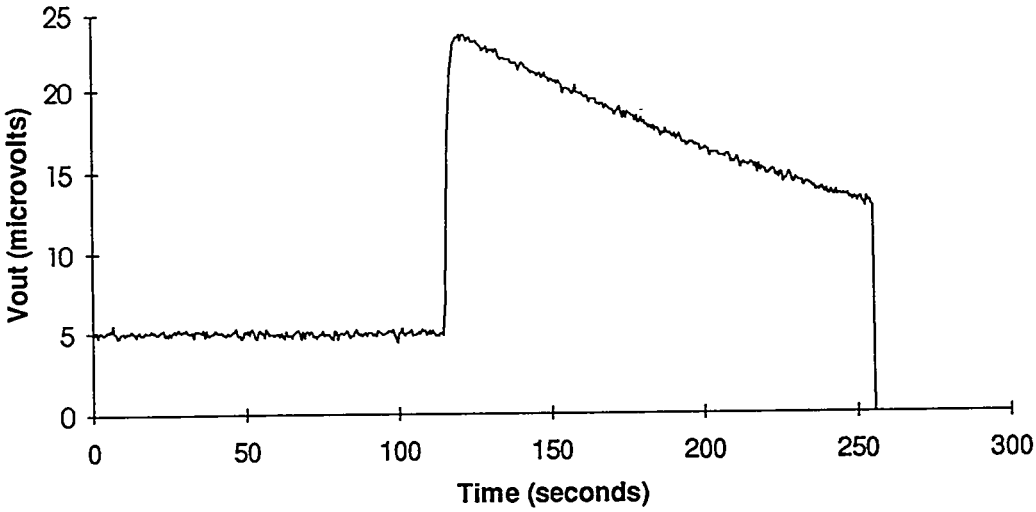

Figure C -- Sample Output from a Calorimeter

Data collection from the instruments has come a long way from the ways of the past. In the old days paper printouts were the only means of collecting data from instruments. Now we can send the information over a data line hooked up from the instrument to a computer, and transfer the data easily. Not only do we not have the large collection of paper associated with this new method, but we also have access to any instrument from one centralized location. Part of my stay at Livermore was used to hook up these data links from the instruments to the control room. All of the fiber optic cables had already been run, and my task was to hook up a GPIB-extender to each end of the fiber. One GPIB extender was then hooked up to the instruments and the other GPIB-extender was hooked up to the computer. After this had been accomplished a verification of the communication link was done, basically sending and receiving noise. In most cases the links worked on the first try, in other cases I had to try other optical fibers, other configurations of the GPIB-extenders, and determine why the link would not work.

The major project to which I applied most of my time involved the design and construction of a bandwidth diagnostic. Laser light normally has a very narrow bandwidth which is useful for most application. However at very high fluences developed in the Beamlet laser system, parasitic processes after frequency conversion such as stimulated Brillouin scattering (SBS) are strongly driven by the light intensity contained within a narrow band. SBS removes energy from the propagated laser beam, and at high enough intensities has the capability to damage system optics. It has been determined on experiments using the NOVA laser that a bandwidth of at least 1.3 GHz between side bands is necessary such that SBS growth is driven by each side band independently. For that reason, bandwidth is added to the injected seed laser beam, and it is necessary to determine the state of the laser bandwidth at the system output.

To measure the output bandwidth, I used an adjustable Fabry Perot etalon which was configured as a Fizeau interferometer. This is basically a pair of highly reflecting flats which are slightly tilted relative to one another, and which transmit the beam for the condition $m\lambda = 2d$ where m is an integer, λ is the wavelength and d is the plate spacing. Scanning across the Fabry Perot normal to the tilt axis yields the bandwidth information within the limit of the Fabry Perot free spectral range. The beam to be analyzed is a collimated sample of the output laser, which was relayed into the center of the etalon, and the interference lines were read out using a standard CCD camera.

Part of the challenge of this system was to relay the "image plane" to the center of the Fabry Perot etalon. The "image plane" referred to is that which is present at the Beamlet cavity mirrors, and at the frequency converter location. It is optically relayed twice within the diagnostics package, and I had to relay it one more time to the Fabry Perot.

The design came together quickly after knowing the basics involved, see figure D. A 1:1 relay was chosen to relay the image plane to the Fabry Perot, and a simple lens was used to focus the fringe pattern of the Fabry Perot onto the CCD camera. The focal length of this focusing lens was easily determined by: $\frac{1}{s_1}+\frac{1}{s_2}=\frac{1}{f_3}$. The 1:1 relay was adjustable and had to be varied depending upon the distance between the image plane before the splitter and the interferometer. $\frac{D}{4}=f_1$. Because of my space limitations a second level was added to the table. The 1:1 relay and the interferometer were placed on the main table, then two mirrors relayed the spatial information to the second level where the focusing lens and the camera were located. This location for the

camera helped eliminate the space limitations I was forced to deal with and also provide easy access to the camera, so that it could be changed out easily.

As the semester came to an end I was in the process of setting up this diagnostic. Due to the test schedule of the laser I was unable to get the diagnostic on line before completion of this report. The diagnostic is planned to be on-line before I leave for the semester.

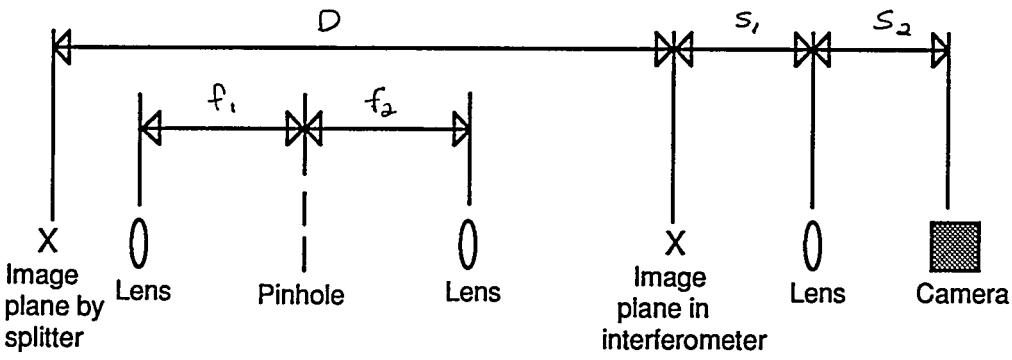

Figure D -- Interferometer Design Requirements

NONTHERMAL PLASMA REACTORS FOR TREATMENT OF NOx AND OTHER HAZARDOUS EMISSIONS*

Debbie S. Thomas

University of Illinois at Urbana-Champaign

Lawrence Livermore National Laboratory
Livermore, California 94550

July 27, 1994

Prepare in partial fulfillment of the requirements of the Science and Engineering Research Semester under the direction of George Vogtlin, Research Mentor, in the Lawrence Livermore National Laboratory.

* This research was supported in part by an appointment to the U.S. Department of Energy Science and Engineering Research Semester (hereinafter called SERS) program administered by LLNL under Contract W-7405-Eng-48 with Lawrence Livermore National Laboratory.

Nonthermal Plasma Reactors for Treatment of NOx and other Hazardous Gas Emissions

Debbie S. Thomas
University of Illinois at Urbana-Champaign
Defense Sciences Engineering Division

ABSTRACT

The 1990 Clean Air Act Amendments passed by the United States government has prompted a great deal of interest in reducing the amount of hazardous pollutants released into the air. Of particular interest to Lawrence Livermore National Laboratory is the reduction of NOx produced by mobile diesel engines. The use of nonthermal plasma technologies is employed in the effort to reduce the amount of toxins present in diesel exhaust.

INTRODUCTION

In Title II of the 1990 Clean Air Act Amendments, Congress has tightened mobile source emissions standards by requiring automobile manufacturers to reduce tailpipe emissions. In fact, tailpipe emissions of NOx [nitrogen oxides including nitric oxide (NO) and nitrogen dioxide (NO_2)] must be reduced by 60% in all vehicles sold in the year 1996 and beyond. This legislation has prompted many new technologies in an effort to pursue the most efficient way to reduce the amount of NOx and other toxins, including hydrocarbons, volatile organic compounds (VOCs), and soot, that are released into the environment by diesel exhaust. Lawrence Livermore National Laboratory is interested in using nonthermal plasma technologies to chemically reduce the amount of NOx that is generated in mobile diesel sources.

A plasma is considered nonthermal when the majority of energy applied is used in the production of energetic electrons rather than heating the gas. These energetic electrons then react with the bulk gas to produce radicals. These radicals have long life times and under favorable conditions, react selectively with the harmful constituents of the diesel exhaust to produce harmless products. Figure 1 illustrates the plasma chemistry necessary to reduce the hazardous emissions.

While the chemistry has been modeled, physical constraints place limitations upon constructing a processor that is 100% efficient. To maximize the removal of NOx, the amount of the right radical production must be maximized. Thus, the key to success is to build a nonthermal reactor in which the majority of electrical energy is utilized in the production of energetic electrons, which in turn will produce these radicals. To increase the number of electrons, the voltage and frequency of the pulsing must also be maximized. In addition to the impracticality of building a mobile processor that can generate such

energy levels, as these parameters increase so does the temperature of the gas. When the temperature of the gas reaches a certain threshold, breakdown occurs. Breakdown is counterproductive to the experiment because it produces NOx, the one product which is to be minimized. Therefore, the most efficient processor will generate a great number of radicals with the least amount of energy input into the system.

LEARNING TO PROGRAM AND USE LABVIEW

LabVIEW is a program development application distributed by National Instruments Corporation. LabVIEW differs from other applications because it uses a graphical programming language, called G. Programs are created in block diagram form and are called virtual instruments (VIs) because their appearance and operation mimic actual instruments. LabVIEW contains application-specific libraries for data acquisition, GPIB and serial instrument control, data analysis, data presentation and data storage.

The Pulsed Plasma Processing VI emulates the functions of a Tektronix oscilloscope with additional mathematical analyzing capabilities. Our VI reads in the voltage and current being supplied to the plasma processor. When the system reaches steady-state, a reading is taken. The VI digitizes the voltage and current waveforms to calculate the amount of energy that is being deposited into the gas. In lab we measure the total current which consists of both the discharge and capacitive current. The capacitive current is C dV/dT where C is the capacitance of the processor. The pulse energy is the product of the discharge current minus the capacitive effect and the voltage, integrated over time. In the experimental setup, LabVIEW is now the primary source of data acquisition and manipulation. Figure 2 shows a block diagram of the current calculation.

Since February, the test stand for the pulsed plasma processor has been operated under varying conditions. In addition to such system parameters as, voltage, pulse rate, water content, temperature of the gas and flow rates, three different processors have been tested; pulsed corona, alumina dielectric barrier and a dielectric packed with alumina beads. Using LabVIEW, I have been able to assist in collecting experimental data. The voltage and frequency are raised until breakdown is detected on the oscilloscope. When the oscilloscope is in the triggering mode, breakdown is noted in the current waveform. However, if the oscilloscope is in the averaging or stopped mode, breakdown might go undetected.

SOUND SYSTEM FOR BREAKDOWN

In order to have a more reliable and independent way to detect breakdown, I designed and constructed a circuit that would sound an alarm whenever breakdown should occur. See Figure 3 for a circuit diagram.

The photodiode detects the light from the breakdown at the window of the processor. The 10 K potentiometer provides the sensitivity adjustment so that the diode reacts to the light from a breakdown and not the discharge. The two capacitors and the 1 K resistor were chosen to create a time delay of 1 second, giving the alarm enough time to detect the breakdown. The 10 K resistor keeps the timer off until the output of the op-amp goes high.

OPERATING MAXWELL 2D

Maxwell 2D Field Simulator is an interactive software package created by Ansoft Corporation that uses finite element analysis to solve electromagnetic problems. It allows a

user to create the geometry of a modeling problem, specify the material's properties and boundary conditions, and generate, analyze and store the solution.

In the continuing effort to reduce NOx by using a nonthermal plasma, an electron beam processor is currently being implemented. Within this configuration, two magnetic coils are used to control the direction of the electron beam through the processor. The electron beam can be guided by the magnetic fields created by the current flowing through the coils. The magnetic field needed was empirically calculated and then simulated using Maxwell 2D. As shown in Figure 4, I modeled the two, 2 x 2 cm coils, 2 cm apart, each with 10,000 turns and 100 mA running through them. Using Maxwell 2D, I calculated the magnetic flux lines and the flux density at various points and plotted the flux density along the center line vs. the distance from the edge of the processor (Figure 5). From these simulations, we were able to determine the necessary conditions needed to generate the correct magnetic field, which in turn will produce the desired results.

SUMMARY

Although the desired results have not yet been realized, much headway has been made in understanding the removal of NOx with the use of nonthermal plasma technologies. Continuing efforts on this project involve implementing a new processor, the electron beam, and using the diesel engine rather than simulating the diesel exhaust from bottled gases.

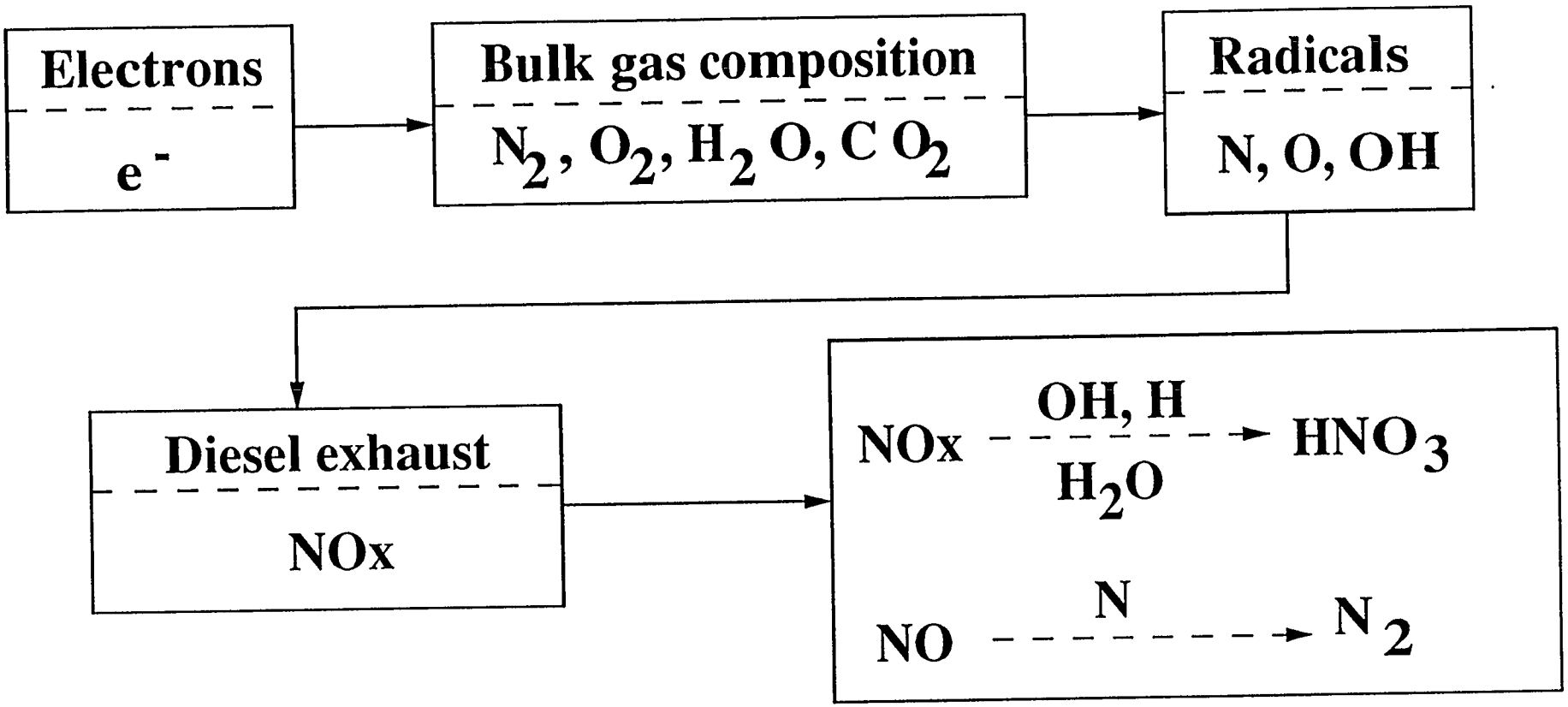

- Energetic electrons react with the background gas to form radicals, which in turn react with the toxins to create non-hazardous products under favorable conditions.

Plasma Chemistry
Figure 1

Block Diagram

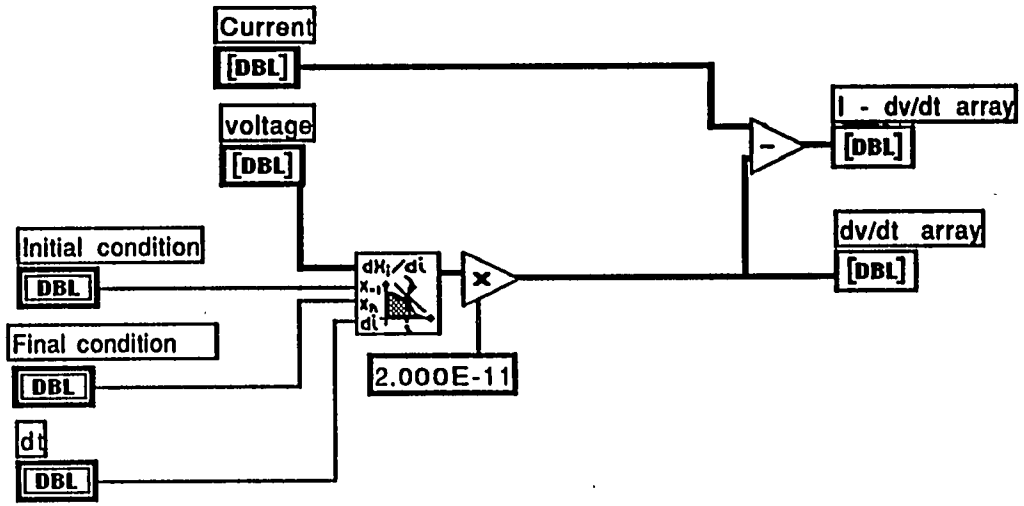

Block Diagram
Figure 2

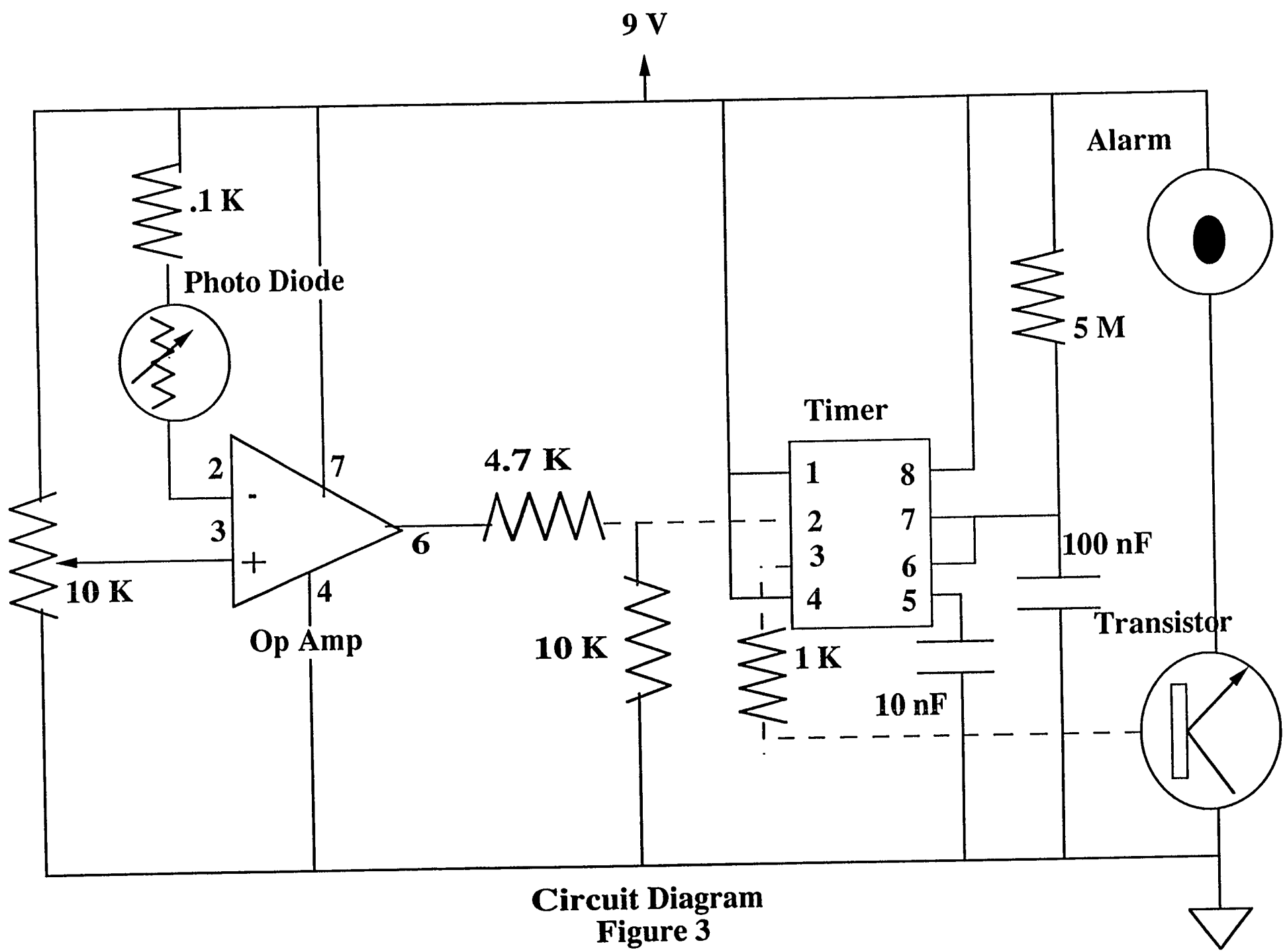

Circuit Diagram
Figure 3

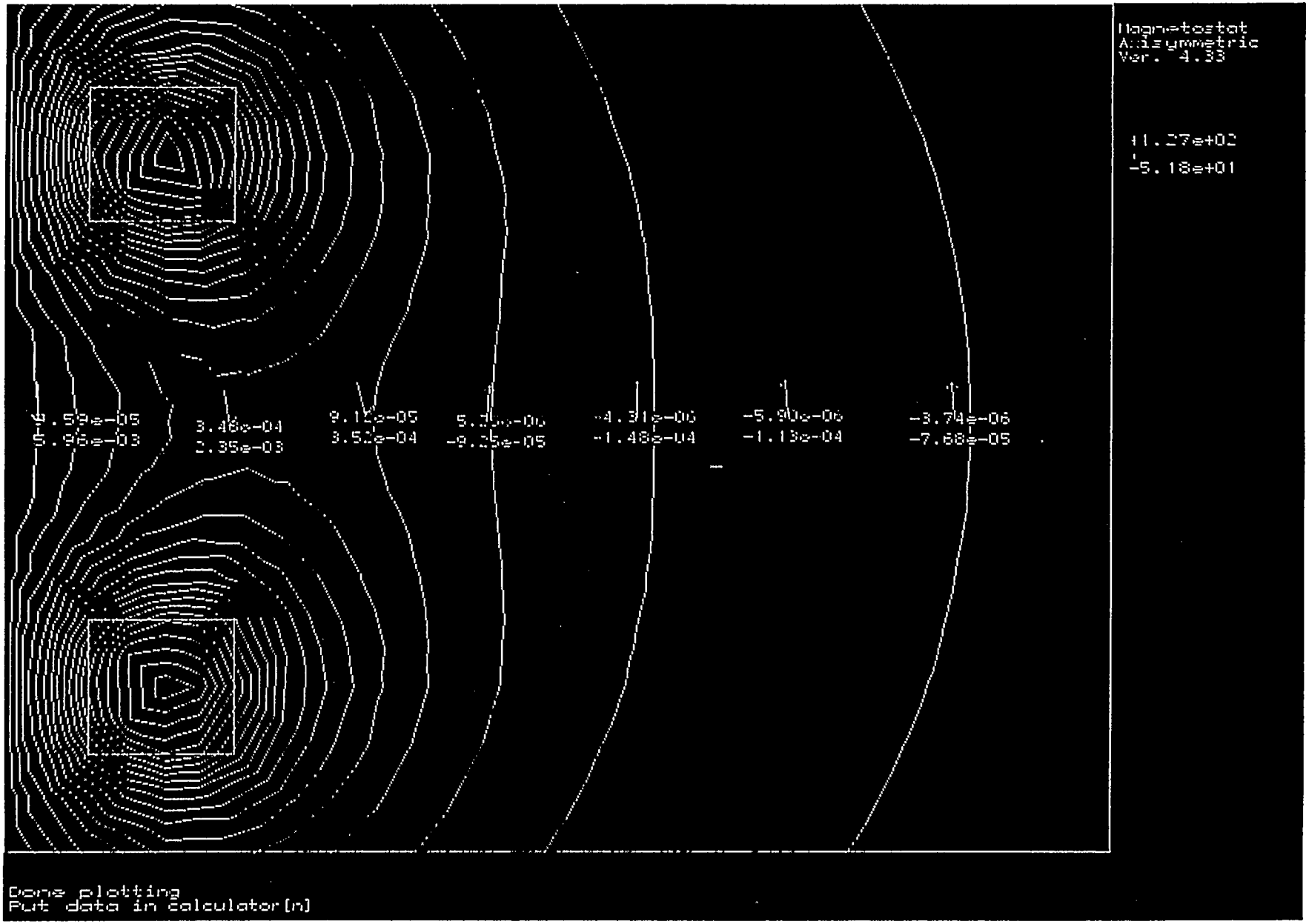

Computer Modeling

Figure 4

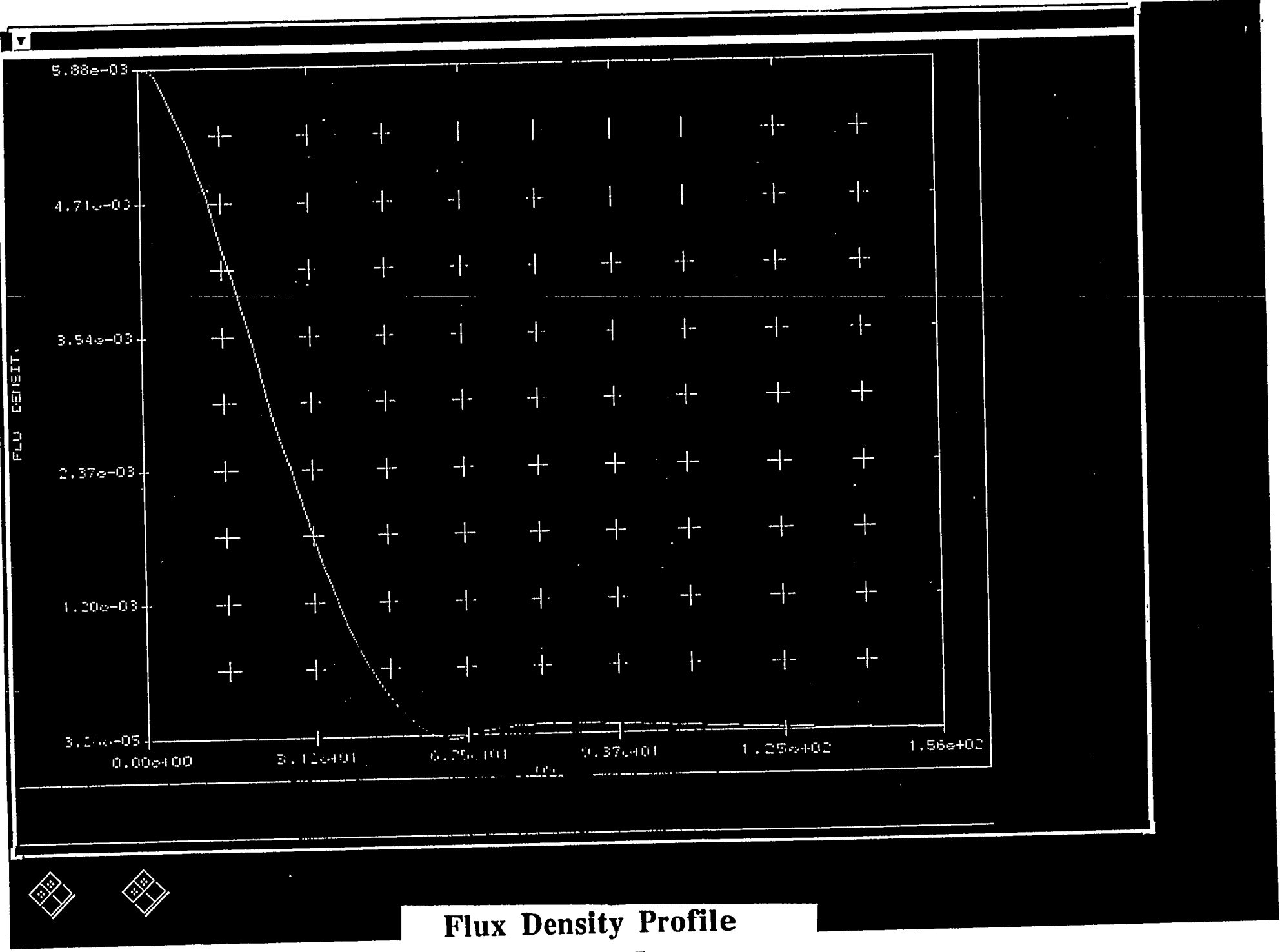

Flux Density Profile

Figure 5

BIBLIOGRAPHY

"Amendments to Title II of Clean Air Act" in Laws of 101st Congress, 2nd Session, 1990 West Publishing Co., St. Paul, MN.

LabVIEW for Macintosh User Manual, National Instruments Corporation, 1993.

Maxwell 2D Field Simulator, Ansoft Corportation, 1991.

Penetrante, Bernie M. "Nonthermal Plasma Reactors for Treatment of NOx and Other Hazardous Gas Emissions," Lawrence Livermore National Laboratory, 1993.

Creating an Automated Tool for Measuring Software Cohesion

John M. Tutton

California State University, Sacramento

Lawrence Livermore National Laboratory
Livermore, California 94550

May 10, 1994

Prepared in partial fulfillment of the requirements of the Science and Engineering Research Semester program under the direction of Professor Lin Zucconi, Research Mentor, in the Lawrence Livermore National Laboratory.

* This research was supported in part by an appointment to the U.S. Department of Energy Science and Engineering Research Semester program administered by L.L.N.L. under Contract W-7405-Eng-48 with Lawrence Livermore National Laboratory.

Creating an Automated Tool for Measuring Software Cohesion

John M. Tutton
California State University, Sacramento
Department of Computer Science and Engineering
jtutton@nes.nersc.gov

Lin Zucconi, Ph.D.
Lawrence Livermore National Laboratory
Computation Division
zucconi@llnl.gov

Abstract

Program modules with high complexity tend to be more error prone and more difficult to understand. These factors increase maintenance and enhancement costs. Hence, a tool that can help programmers determine a key factor in module complexity should be very useful. Our goal is to create a software tool that will automatically give a quantitative measure of the cohesiveness of a given module, and hence give us an estimate of the "maintainability" of that module. The Tool will use a metric developed by Professors Linda M. Ott and James M. Bieman. The Ott/Bieman metric gives quantitative measures that indicate the degree of functional cohesion using abstract data slices [3].

1 Introduction

1.1 The Importance of Functional Cohesion

A major problem with computer programs is complexity. Large programs are probably the most complicated entities ever created by humans. Because of this complexity, programs are prone to error, and software errors can be expensive and even life-threatening [2].

A fundamental task of program design is the partitioning of a large program into smaller units known as modules. This is done not only to reduce the complexity of the programming problem, but also to facilitate changes to the program which may be required after the initial implementation. Software developers have long realized that the decomposition into modules has a critical effect on properties of the finished software product, such as reliability and modifiability. In view of this, designers have looked for criteria to be used in guidelines for evaluating modularity. These criteria have ranged from rough gauges of module size or structure, to more sophisticated complexity and difficulty metrics [1].

One of the most useful of these criteria is based on a property known as "cohesion" (first described by Constantine [10]). Cohesion is a module attribute that expresses the degree of functional unity of a module [1]. Constantine and Yourdon define seven grades of cohesion. The most beneficial is considered to be "functional cohesion." In a completely

functionally cohesive module, every element of processing is an integral part of, and is essential to, the performance of a single function [10].

Therefore, we can state that a large complex program is more reliable, more easily constructed, understood, and maintained when broken down into smaller functionally cohesive modules [10].

1.2 Abstract Data Slices

"Abstract data slices" are sets of statements related by their flow of data [8]. Program slicing is a method of program decomposition based on data-flow analysis [9] introduced by Professor Mark Weiser (Comp. Sci. Dept., Univ. Maryland). Tracing backwards from a particular variable in a particular statement to identify all possible sources of influence on the value of that variable often reveals that many statements in the program have no influence [8]. Code not having to do with the variable of interest is ignored [10]. Data-flow analysis can find all the program code which might have influenced the specified variable [10] when taking into account the "uses" and "used by" data relationships [4]

1.3 A Technique for Measuring Cohesion

Professor Linda M. Ott (Dept. of Comp. Sci., Mich. Tech. Univ.) and Professor James M. Bieman (Dept. of Comp. Sci., Col. State Univ.) devised a metric which examines the functional cohesion of procedures using a abstract data slices. Their analysis identifies the data tokens that lie on more than one slice as the "glue" that binds separate components together. Cohesion is measured in terms of the relative number of "glue tokens," tokens that lie on more than one data slice, and "super-glue tokens," tokens that lie on all data slices in a procedure, and the "adhesiveness" of the tokens [3].

2 Overview of the Automated Tool

The Tool will parse the source code of a C function, recording data tokens and a series of attributes associated with each token. It will then create abstract data slices which are related to each output variable in the function. Measures of functional cohesion will be calculated using the Ott/Bieman metric.

The Tool is applied to a single C source code function and shall assume the following conditions are satisfied for any function we consider:

i. The function has a single entry point and a single exit point.
ii. All variables are assumed to be uniquely named.

3 The Parser

The C source code of the function to be examined should be stored in the file "Test.c." The Parser will identify reserved words and types by comparing them to lists read from text files called "res.txt" and "type.txt." The Parser will divide the function into "data tokens,"

which are instances of variables and constants. For every instance of each data token, the Parser will determine and record the following attributes associated with that token instance:

i. the character string representation of the token
ii. the "token number" corresponding to the location in which this instance appears in the function
iii. the "statement number" of the statement in which this instance appears
iv. the token type (i.e. output variable, regular (non-output) variable, or constant)
v. whether this instance is found in a variable declaration
vi. whether this instance is an Lvalue (a variable on the left of an assignment operator, and therefore being assigned a value)

A report will be generated showing a list of all of the tokens in the function and their attributes.

4 The Slicer

The Slicer will take the list of all tokens in the function and divide it into "slices." A slice is a list of the tokens which contribute to the value of an individual output variable. There will be one slice for each output variable. Each slice will contain the instances of all tokens which directly affect the value of the output variables, and the instances of all tokens that directly affect the value of those tokens, and so on. This will continue until all tokens are included in the slice which directly or indirectly affect the value of the output variable. This slicing is accomplished using a recursive function.

The Slicer will generate a report showing a data slice for each output variable.

5 The Measurer

The Measurer will compare the data slices for each output variable. It will use the Ott/Bieman metric for measuring the functional cohesion of a module. It will determine the number of "glue tokens," those tokens that are included in more than one data slice. It will determine the number of "super-glue tokens," those tokens that are included in every data slice. The Measurer will then calculate the "strong functional cohesion" of the function, which is the ratio of "super-glue tokens" to the total number of data tokens in the function. It will calculate the "weak functional cohesion" of the function, the ratio of the number of "glue" tokens" to the total number of data tokens. The "adhesiveness" of each token will be calculated by dividing the number of slices which include that token by the total number of slices in the function. The "overall adhesiveness" of the function is calculated as the average "adhesiveness" of the data tokens in the function.

A functional cohesion measures report will be generated by the Measurer, showing the "adhesiveness" of each token in the function as well as the "strong functional cohesion," "weak functional cohesion," and the "overall adhesiveness" of the function.

6 Conclusion

The Tool has been used on several small C functions, and has generated correct outputs and accurate measures of functional cohesion (please see figures). However, several modifications to the Parser must be made before it can be considered "fully functional" for measuring "real-world" C functions. Among these needed modifications are:

i. Global variables whose values are changed in the function should be considered output variables.
ii. Functions called in the examined function which contain passed parameters should be considered Lvalues.
iii. Parameters passed by value to "Lvalue functions" should be considered contributing to the value of the "Lvalue function."
iv. Variables passed by reference to "Lvalue functions" should be considered Lvalues.
v. Functions called in the examined function that do not contain passed parameters should be considered constants.
vi. Types defined in #include files should be added to the type list.
vii. Global variables declared in #include files may be added to the token list.

7 Future Work

7.1 Validating the Metric

We will use the Tool to determine the validity of the Ott/Bieman metric. To do this we will measure the cohesion of a significant number of functions with varying sizes and varying "degrees of cohesion." We will then make a "humanistic" measurement of each function's cohesion. We will compare the results from of the humanistic measurement with those given by the Tool. If the Ott/Bieman metric is valid, the ranking of the modules' cohesion should be similar in both instances.

The humanistic measurement we will apply to the functions is based on a method described by Yourdon and Constantine [10] and Page-Jones [6]. It is a method of determining a module's cohesion by translating the module's operation into a single English sentence and examining that sentence. If the translation is not a compound sentence containing more than one verb, does not contain words relating to time or sequence, and contains a single specific object following the verb, then it may be considered functionally cohesive [10].

7.2 Parsing Other Programming Languages:

Due to the modularity of the Tool, it can be readily modified to work on other programming languages. The Parser module is the only part that needs to be changed for the tool to work on another language. We plan to modify the Parser to work on FORTRAN.

7.3 Code Optimization

Future work may also include work on a code optimization module which would "rewrite" source code to give it a higher cohesion rating.

Acknowledgments

The authors wish to thank the Department of Energy for funding this project under the Science and Engineering Research Semester program. We also wish to thank Lawrence Livermore National Laboratory for providing the facilities required for this project.

References

[1] T. J. Emerson. A discriminant metric for module cohesion. *Proc. 7th Int. Conf. on Software Engineering*, pages 294-303, 1984.

[2] R. Lafore. *Object Oriented Programming in Turbo C++*. Waite Group Press, 1991.

[3] L. M. Ott and J. M. Bieman. Effects of software changes on module cohesion. *Proc. Conf. on Software Maintenance*, November 1992.

[4] L. M. Ott and J. M. Bieman. Technical report CS-93-109 Dept. Computer Science, Colorado Sate Univ., June 1993.

[5] L. M. Ott and J. J. Thuss. Slice based metrics for estimating cohesion. *Proc. IEEE-CS Int. Software Metrics Symp.*, pages 71-81, 1993.

[6] M. Page-Jones. *The Practical Guide to Structured Systems Design*. Yourdon Press, 1988.

[7] M. D. Weiser. Program slicing. *Proceedings of the 5th International Conference on Software Engineering*, pages 439-449, 1981.

[8] M. D. Weiser. Programmers use slices when debugging. *Communications of the ACM*, 25(7):446-452, 1982.

[9] M. D. Weiser. Program slicing. *IEEE Trans. Software Engineering*, 10(4):352-357, 1984.

[10] E. Yourdon and L. Constantine. *Structured Design*. Prentice-Hall, 1979.

```
/*****************************************************************
*   "SumAndProduct.c"
*   This function contains two output variables that are somewhat related procedurally.
*   Intuitively, we would expect it to have a mediocre functional cohesion rating.
*****************************************************************/

        void SumAndProduct(int N, int *SumN, int *ProdN)
        {
            int I;

            *SumN = 0;
            *ProdN = 1;
            for ( I =; ++I <= N; )
            {
                *SumN =SumN + I;
                *ProdN =ProdN * I;
            }
        }
```

Figure 1. Source code listing of "SumAndProduct" function

Token List for SumAndProduct Module:

Token	Token#	Stmnt#	TokenType	Declr	Lvalue
I	15	7	reg	FALSE	FALSE
ProdN	14	7	reg	FALSE	FALSE
ProdN	13	7	reg	FALSE	TRUE
I	12	6	reg	FALSE	FALSE
SumN	11	6	reg	FALSE	FALSE
SumN	10	6	reg	FALSE	TRUE
N	9	5	reg	FALSE	FALSE
I	8	5	reg	FALSE	FALSE
I	7	5	reg	FALSE	TRUE
ProdN	6	4	reg	FALSE	TRUE
SumN	5	3	reg	FALSE	TRUE
I	4	2	reg	TRUE	FALSE
ProdN	3	1	output	TRUE	FALSE
SumN	2	1	output	TRUE	FALSE
N	1	1	reg	TRUE	FALSE

Figure 2. Token list report for "SumAndProduct" function

Slice On Output Variable ProdN:

Token	Token#	Stmnt#	TokenType	Declr	Lvalue
ProdN	6	4	reg	FALSE	TRUE
ProdN	14	7	reg	FALSE	FALSE
I	4	2	reg	TRUE	FALSE
I	8	5	reg	FALSE	FALSE
N	1	1	reg	TRUE	FALSE
N	9	5	reg	FALSE	FALSE
I	7	5	reg	FALSE	TRUE
I	15	7	reg	FALSE	FALSE
ProdN	13	7	reg	FALSE	TRUE
ProdN	3	1	output	TRUE	FALSE

Figure 3. Data slice report for "ProdN" output variable

Slice On Output Variable SumN:

Token	Token#	Stmnt#	TokenType	Declr	Lvalue
SumN	5	3	reg	FALSE	TRUE
SumN	11	6	reg	FALSE	FALSE
I	4	2	reg	TRUE	FALSE
I	8	5	reg	FALSE	FALSE
N	1	1	reg	TRUE	FALSE
N	9	5	reg	FALSE	FALSE
I	7	5	reg	FALSE	TRUE
I	12	6	reg	FALSE	FALSE
SumN	10	6	reg	FALSE	TRUE
SumN	2	1	output	TRUE	FALSE

Figure 4. Data slice report for "SumN" output variable

Functional Cohesion Measures:

Token#	#Slices in	Glue	SuperGlue	Adhesiveness
1	2	True	True	1.0000
2	1	False	False	0.5000
3	1	False	False	0.5000
4	2	True	True	1.0000
5	1	False	False	0.5000
6	1	False	False	0.5000
7	2	True	True	1.0000
8	2	True	True	1.0000
9	2	True	True	1.0000
10	1	False	False	0.5000
11	1	False	False	0.5000
12	1	False	False	0.5000
13	1	False	False	0.5000
14	1	False	False	0.5000
15	1	False	False	0.5000

Strong Functional Cohesion = 0.3333
Weak Functional Cohesion = 0.3333
Overall Adhes. of Module = 0.6667

Figure 5. Cohesion measures report for "SumAndProduct" function

Isotope Labeled ImmunoAssay for Environmental Chemical Detection

Marilyn M. Velez
SERS-Spring, 1994 student
Mentor- John S. Vogel

Biology and Biotechnology Research Program, Lawrence Livermore National Laboratory, Livermore, California 94550

Atrazine, one of the most heavily used agricultural pesticides in North America, has been identified as a major groundwater contaminant in the U.S. Research provides evidence that under certain conditions atrazine and some of its derivatives may prove to be carcinogenic and mutagenic.

Immunoassays are one of the most powerful of all analytical immunochemical techniques. They employ a wide range of methods to detect and quantitate antigens or antibodies, and to study the structure of antigens. With the appropriate assay, they can be remarkably quick and easy, to yield information that would be difficult to determine by other techniques. The development of the appropriate assay; however, requires clean and precise separation of antigens bound to antibodies from those that remain free. Sensitive assays depend on quantification of these bound antigens at very low levels.

We are making direct and competitive immunoassays with atrazine and its antibodies using accelerator mass spectrometry (AMS) in order to obtain a sensitive immunoassay for atrazine in environmental samples.

Introduction

Immunoassays are immunochemical detection methods based on a reaction between a target analyte and a specific antibody. Quantification can be performed by monitoring a color change or by measuring radioactivity or fluorescence. Many immunoassays have been developed for environmental compounds that are difficult to detect by conventional methodologies.

Immunoassays can be performed in many ways. The essential elements include a labeled antibody or anylate, an equilibrium reaction of the antibodies and anylates, and then separation of bound antibodies and anylates from remaining unbound components. The amount of label separated with the bound fraction or left behind in the free fraction is quantified to determine the fraction of total bound anylate.

Researchers can use any assay label to design direct or competitive immunoassays. Direct assays demonstrate simple binding kinetics and can be used in developing assay protocols for new compounds. In a competitive assay, separating and quantifying the bound labels provide a measure of the non-labeled molecules also bound to the separated antibodies.

In this study were used direct and competitive assays to detect and measure the binds between the antibody and the labeled and non-labeled molecules. Atrazine was used as the anylate throughout all the experiments. The AMS is a sensitive tool for the detection of radio-isotopes, and because of its sensitivity at low levels, we used it in this study in order to obtain a sensitive immunoassay for atrazine.

Material and methods

Materials

QuantAffinity^{TM} Expoxide-Glass Beads were obtained from Rainin Instruments CO, Inc. (Batch # 3-44-4). We obtained antibodies (Ab 2005) to the ubiquitous herbicide, atrazine, from Chemicon, Temecula, USA. The isotope-labeled atrazine with activity of 7.8 mCi/mmol was obtained from SIGMA, St. Louis, USA. The non-labeled atrazine was obtained from researchers at UC Davis. The glass beads were coated with Protein A Extracellular Lot #123H68321 from SIGMA, St. Louis, USA. We used 0.4 M of ethanolamine 98% from SIGMA, St. Louis, USA plus 0.1 M of PBS in order to avoid the non-specific binding. We used the Phosphate Buffer Solution - Tween (PBS - Tween) described by A.E. Karu et al. in their paper "Monoclonal Immunoassay of Triazine Herbicide" (1991).

Methods

Direct Immunoassay :

The antibody is attached to a glass bead coated with Protein A (helps to glue the antibody to the beads), and isotope-labeled antigen is allowed to bind. The unbound antigens are removed by washing with a Phosphate Buffer Solution (PBS), and the assay is quantitated by measuring the amount of antigen that is bound.

Competitive Immunoassay :

The antibody and the non-labeled antigen are exposed to a glass bead coated with Protein A, and isotope-labeled antigen is allowed to compete with the non-labeled antigen for binding position of the antibody. The unbound antigens are removed by washing with PBS, and the assay is quantitated by measuring the amount of antigen that is bound.

For both assays, the Accelerator Mass Spectrometer (AMS) is used to measure the antigens bound to the bead.

Time Sequencing Test We made a direct assay using 40,000 fmol of labeled atrazine, and the beads were exposed to the antibody and the antigen for 1 hr.,

3 hrs., 6 hrs., 12 hrs., and 24 hrs. The Scintillation machine was used to quantify the antigens remaining on the glass bead by counting flashes of light produced by the decaying isotope label.

Titration of the antibodies Direct assays using the different concentrations of antibodies were measured against 10 fmol and 100 fmol of labeled atrazine in a 120 ul assay volume.

Competitive assay for atrazine We made a competitive assay using different levels of non-labeled atrazine (10,000 fmol - 1 fmol) against 100 fmol of labeled atrazine. The AMS was used for counting undecayed isotope labels in the titration of the antibodies and in the competitive assay.

Results

Time Sequencing Test

With this test we were investigating the maximum time that the beads should be exposed to the antibody and the antigen in order to obtain the optimum labeled atrazine detection percentage.

Fig.1 shows that the beads have to be exposed to the antibody and the antigen for at least 3 hrs. More than 3 hrs. will decrease the labeled atrazine detection percentage.

Titration of the antibodies

We made this test in order to understand the binding process with different concentrations of antibody and two different concentration of labeled atrazine. We were looking for the antibody that gave us a good range of binding. In higher concentrations of antibody the Bound and Bound/Free of labeled atrazine decrease (see Fig.2 and Fig.3).

Competitive assay for atrazine

We expected that in lower concentrations of non-labeled atrazine the binding of labeled atrazine would increase because the assay had more labeled atrazine to compete against the non-labeled atrazine. But the assay did not show that pattern (see Fig.4).

Discussion

As Fig.1 shows the optimum time for exposing the beads to the antibody and the antigen in order to obtain a maximum atrazine detection percentage is 3 hrs. Therefore, in the subsequent experiments we allowed the antibody and the antigen to bind to the beads for 3 hrs.

In the titration of the antibodies, using the solutions with the highest concentrations of antibody, the assay have more antibody than labeled atrazine. Therefore, the antibodies without atrazine are competiting for binding position against the antibody with labeled atrazine. And because the assays were saturated with antibodies the graphs (Fig.2 and Fig.3) show a decrease of

binding against the highest concentrations of antibodies. Therefore, it is necessary to dilute the antibody solutions in order to avoid saturation of the assay.

In the competitive assay, we expected that at lower concentrations of non-labeled atrazine against a standard concentration (100 fmol) of labeled atrazine the binding of labeled atrazine would increase. But we did not see this pattern because the beads did not have enough Protein A to bind the atrazine. For this experiment we used another batch of beads coated with Protein A, and we think we did not add enough Protein A to the beads. It is necessary to add 155 to 200 mg of Protein A per 100 beads in order to have a good solid support in the assay.

Fig.5 is an extrapolation of Fig.4; if we extrapolate the point that represent the concentration used in the competitive assay (Fig.2) and the beads have enough Protein A attached to them, the binding of labeled atrazine against the lower concentrations of non-labeled atrazine would increase. Therefore, we will have a sensitive competitive assay.

Acknowledgments

I would like to thank the U.S. Department of Energy for providing the funds for this project, Lawrence Livermore National Laboratory for allowing us to use the facilities, my mentor John S. Vogel for helping me in this project and Barry Goldman for giving me the opportunity to participate in the SERS program.

References

Jockers, R., Bier, F.F. and Schmid, R.D. (1993) Enhancement of immunoassay sensitivity by molecular modification of competitors. J. Immunol. Methods, 163, 161-167.

Karu, A.E., Harrison, R.O., Schmidt, D.J., Clarkson, C.E., Grassman, J., Goodrow, M.H., Lucas, A., Hammock, B.D., Van Emon, J.M. and White, R.J. (1991) Monoclonal Immunoassay of Triazine Herbicides. ACS Symposium Series; 451, 59-77.

Lucas, A.D., Jones, A.D., Goodrow, M.H., Saiz, S.G., Blewett, C., Seiber, J.N. and Hammock, B.D. (1993) Determination of Atrazine Metabolites in Human Urine: Development of a Biomarker of Exposure. Chem. Res. Toxicol., 6, 107-116.

Rosner, M.H., Grassman, J.A. and Haas, R.A. (1991) Immunochemical Techniques in Biological Monitoring. Environmental Health Perspectives, Vol. 94, 131-134.

Schmidt, D.E., Brooks, T.L., Mhatre, S., Junghans, R.P. and Khazaeli, M.B. (1993) An Advanced Solid Support for Immunoassays and Other Affinity Applications. BioTechniques, Vol. 14, No. 6, 1020-1025.

Schneider, P. and Hammock, B.D. (1991) Influence of the ELISA Format and the Hapten-Enzyme Conjugate on the Sensitivity of an Immunoassay for s-Triazine Herbicides Using Monoclonal Antibodies. ACS.

Ugazio, G., Burdino, E., Dacasto, M., Bosio, A., van't Klooster, G. and Nebbia, C. (1993) Induction of hepatic drug metabolizing enzymes and interaction with carbon tetrachloride in rats after a single oral exposure to atrazine. Toxicology Letters, 69, 279-288.

Van Emon, J.M. and Lopez-Avila, V. (January 15, 1992) Immunochemical Methods for Environmental Analysis. Analytical Chemistry, Vol. 64, No. 2, 79-88.

Vogel, J.S. and Turteltaub, K.W. (1992) Biomolecular tracing through accelerator mass spectrometry. Trends in Analytical Chemistry, Vol. 11, No. 4, 142-149.

Figures

Figure 1. Time Sequencing Test for the determination of maximum time that the Protein A-beads should be exposed to the antibody and antigen in order to obtain the optimum labeled atrazine detection percentage.

Figure 2. Titration of the antibodies using 100 fmol of labeled atrazine in a direct assay.

Figure 3. Titration of the antibodies using 10 fmol and 100 fmol of labeled atrazine in a direct assay.

Figure 4. Competitive assay using different levels of non-labeled atrazine (10,000 fmol to 1 fmol) against 100 fmol of labeled atrazine.

Figure 5. An extrapolation of Fig.4 that represents the concentration used in the competitive assay (Fig.2).

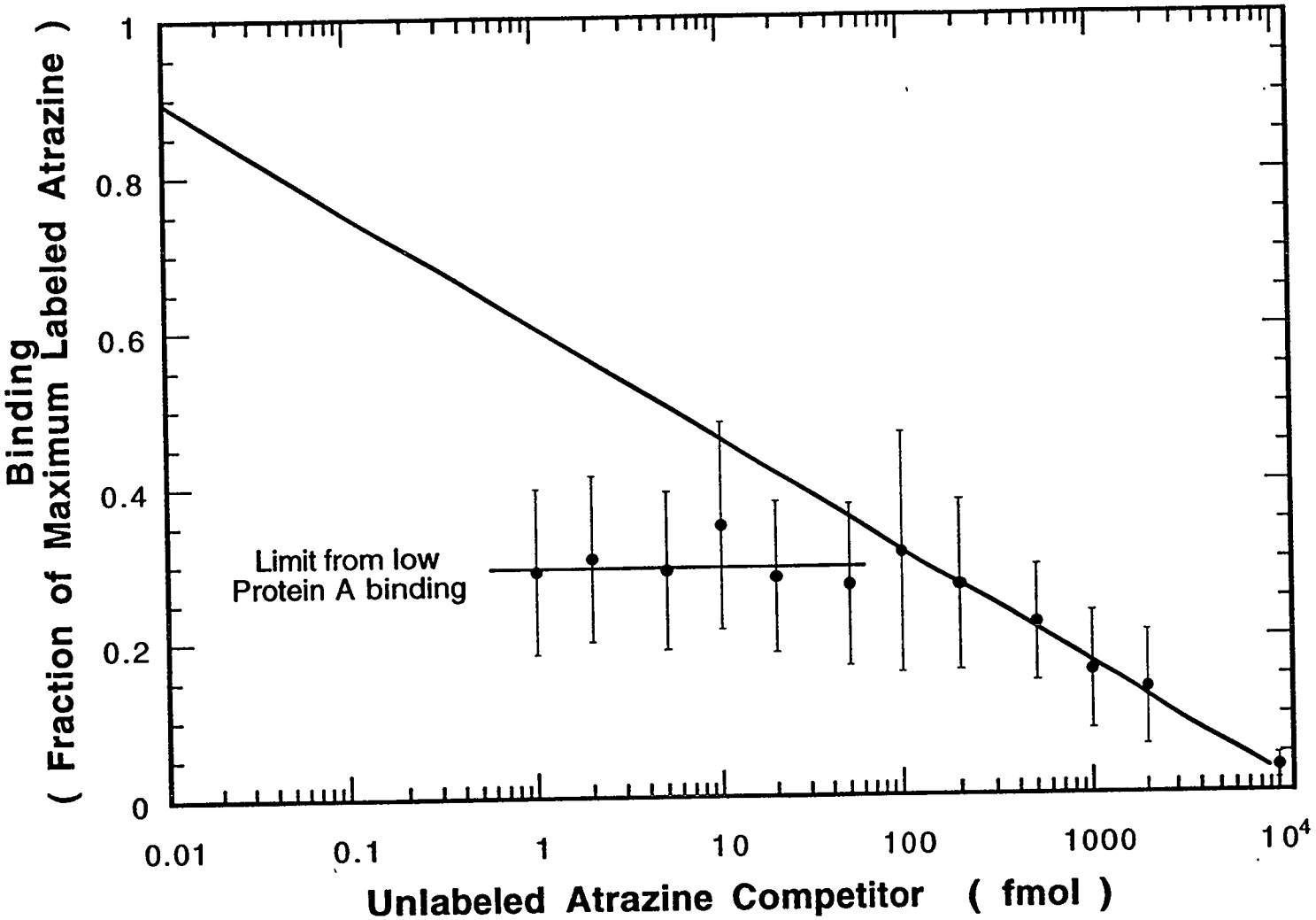
Binding
(Fraction of Maximum Labeled Atrazine)
1
0.8
0.6
0.4
0.2
0
Limit from low
Protein A binding
0.01
0.1
1
10
100
1000
10^4
Unlabeled Atrazine Competitor (fmol)

CA 04 28

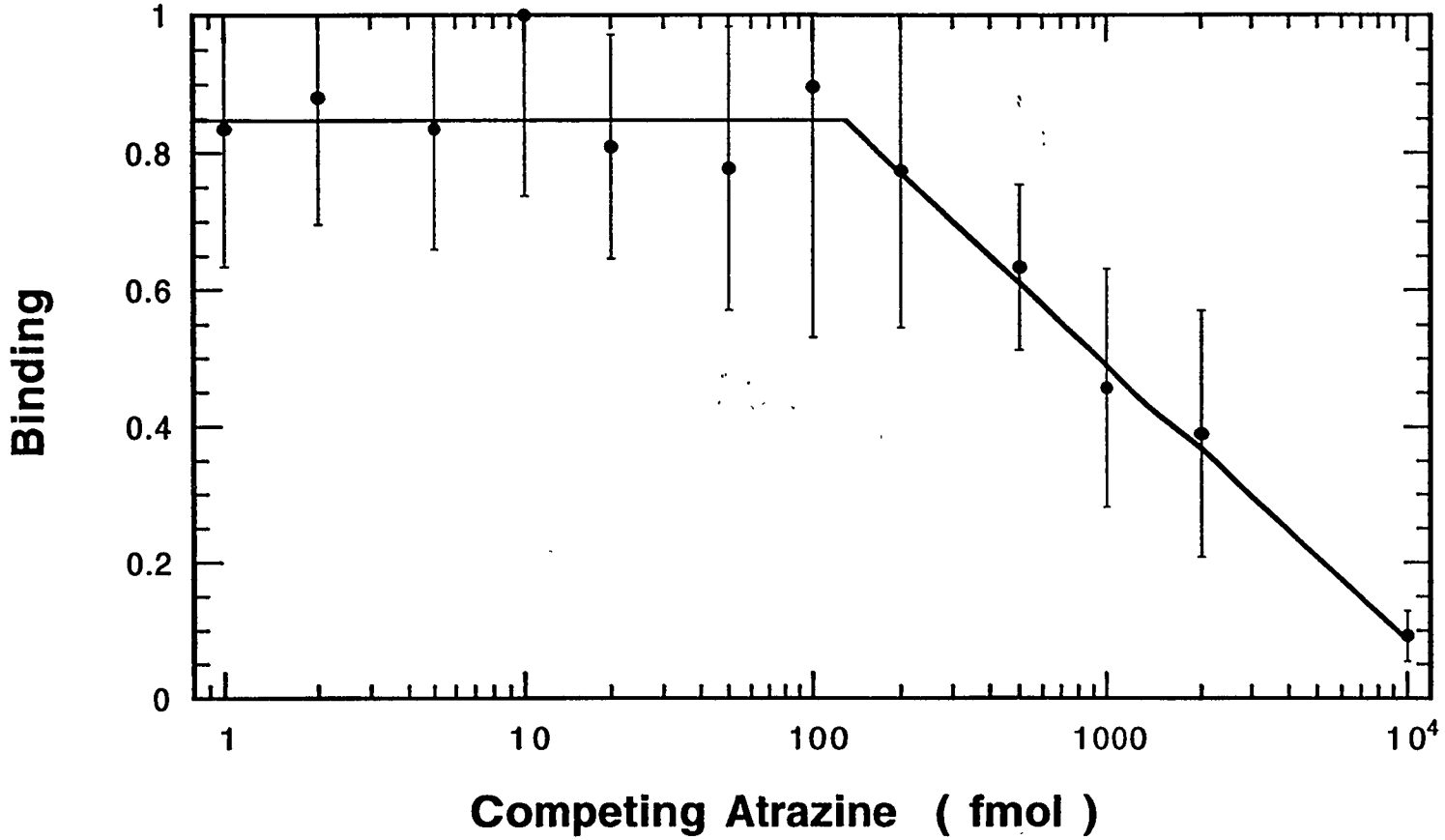
Binding
1
0.8
0.6
0.4
0.2
0
1
10
100
1000
10^4
Competing Atrazine (fmol)

CA 04 28

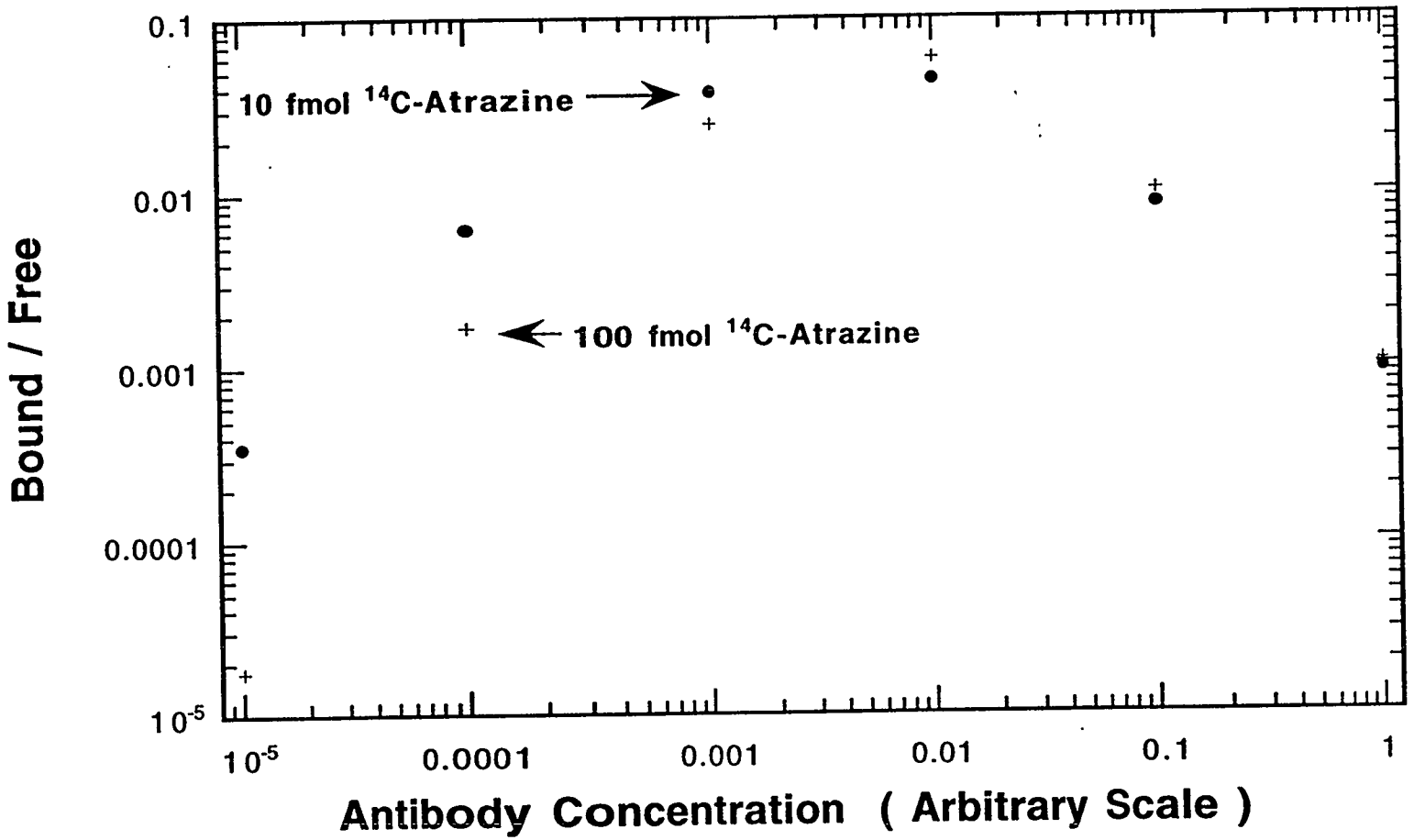

DA 0413
DA 0425

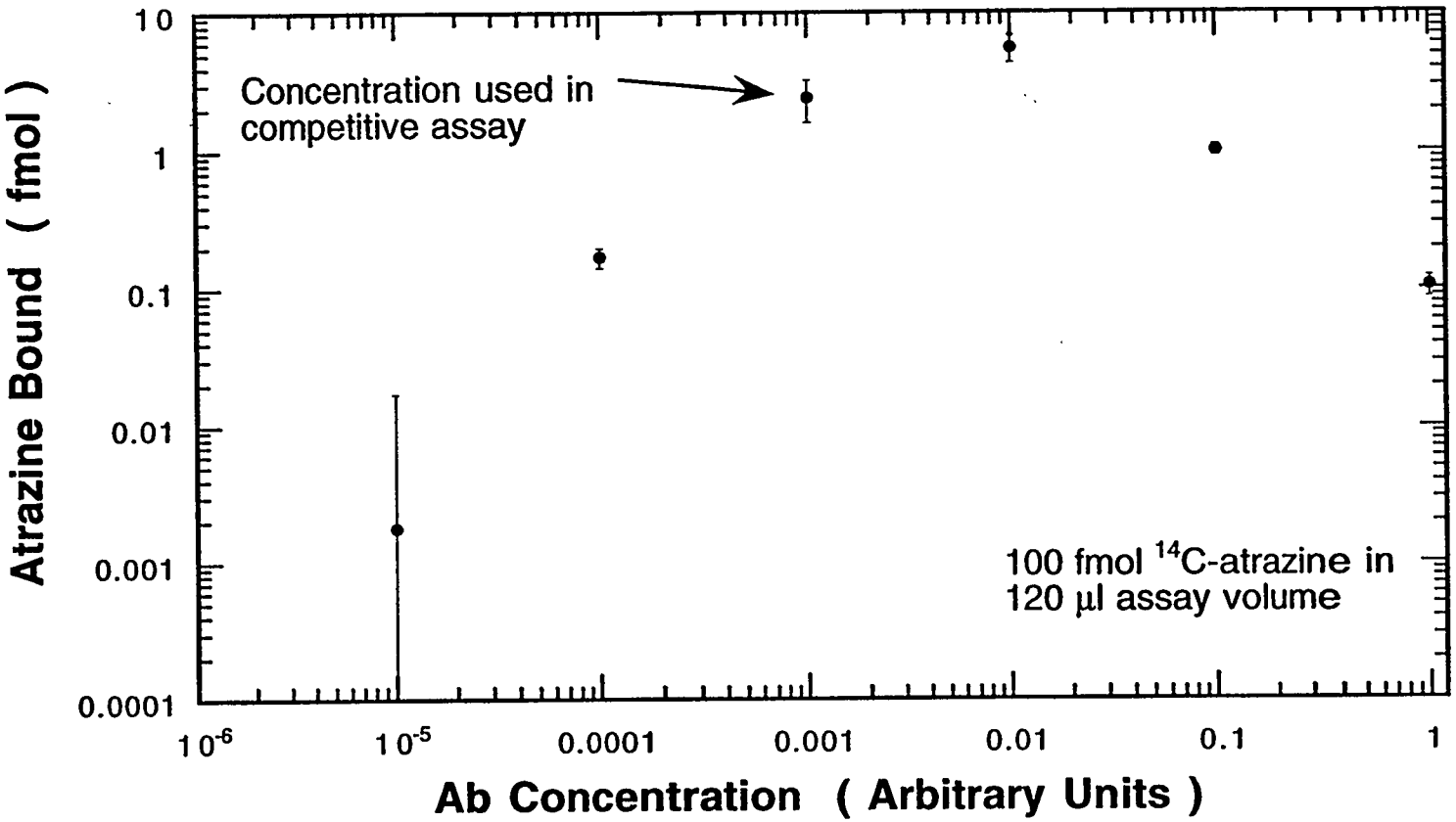
Atrazine Bound (fmol)
10
1
0.1
0.01
0.001
0.0001
Concentration used in
competitive assay
100 fmol ^{14}C-atrazine in
120 µl assay volume
10^{-6}
10^{-5}
0.0001
0.001
0.01
0.1
1
Ab Concentration (Arbitrary Units)

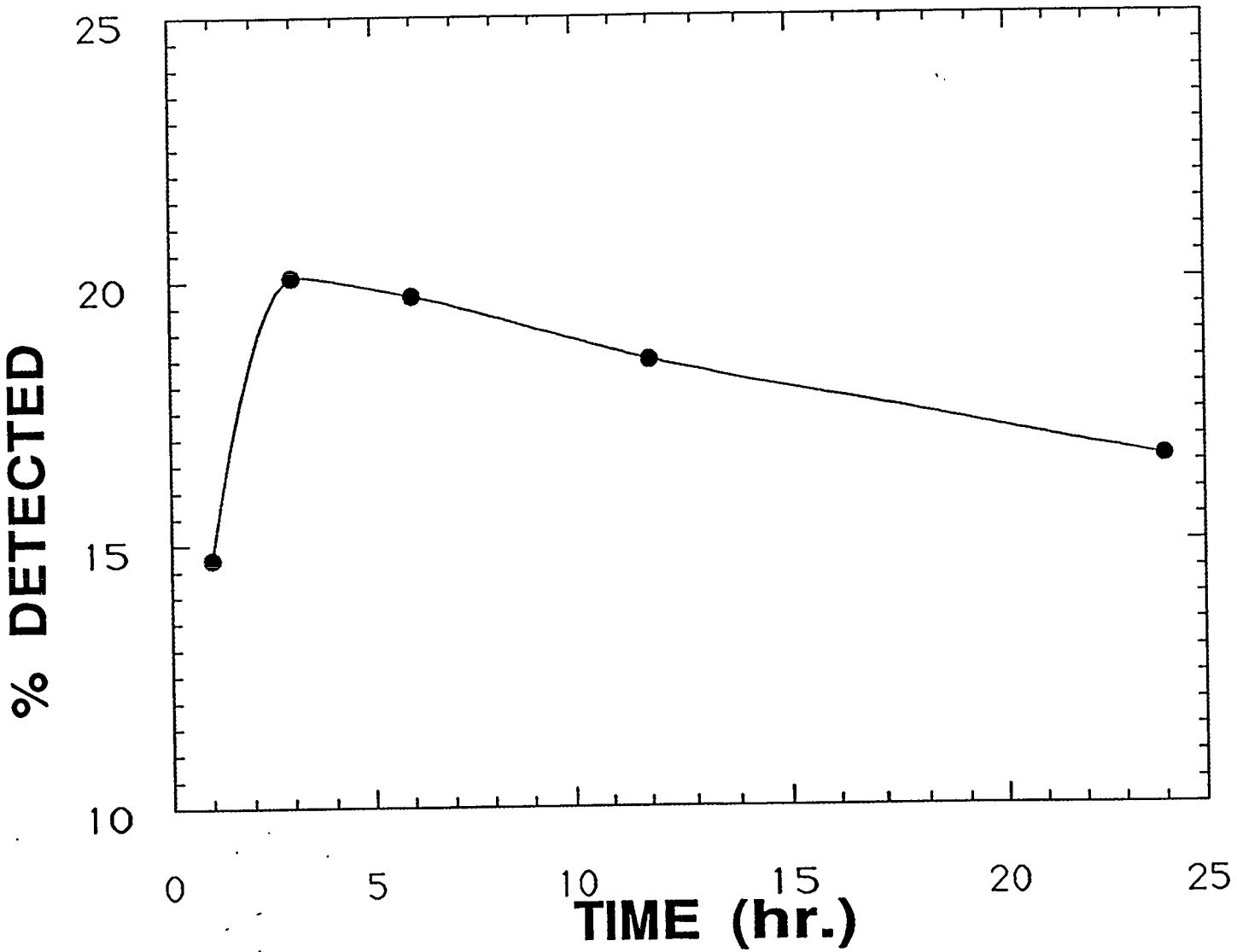
25
20
15
10
% DETECTED
0
5
10
15
20
25
TIME (hr.)

RELIABILITY OF THE NERVE CONDUCTION MONITOR IN REPEATED MEASURES OF MEDIAN AND ULNAR NERVE LATENCIES

Iris Alese Washington

Grambling State University
Grambling, Louisiana

Lawrence Livermore National Laboratory
Livermore, CA 94550

May 11, 1994

Prepared in partial fulfillment of the requirements of the Science and Engineering Research Semester under the direction of Dr. Stephen Burastero, Research Mentor, in the Lawrence Livermore National Laboratory.

*This research was supported in part by an appointment to the U.S. Department of Energy Science and Engineering Research Semester (hereinafter called SERS) program administered by LLNL under Contract W-7405-Eng-48 with Lawrence Livermore National Laboratory.

RELIABILITY OF THE NERVE CONDUCTION MONITOR IN REPEATED MEASURES OF MEDIAN AND ULNAR NERVE LATENCIES

Iris A. Washington
Grambling State University, Grambling Louisiana
Health Services

ABSTRACT

According to the Bureau of Labor Statistics, carpal tunnel syndrome (CTS), one of the most rapidly growing work-related injuries, cost American businesses up to $10 billion dollars in medical costs each year (1992) [1]. Because conservative therapy can be implemented and CTS is more reversible in its early stages, early detection will not only save industry unnecessary health care costs, but also prevent employees from experiencing debilitating pain and unnecessary surgery. In response to the growing number of cases of CTS, many companies have introduced screening tools to detect early stages of carpal tunnel syndrome. Neurotron Medical (New Jersey) has designed a portable nerve conduction monitor (Nervepace S-200) which measures motor and sensory nerve latencies. The slowing of these latencies is one diagnostic indicator of carpal tunnel syndrome. In this study, we determined the reliability of the Nervepace Monitor in measuring ulnar and median nerve latencies during repeated testing. The testing was performed on 28 normal subjects between the ages of 20 and 35 who had no prior symptoms of CTS. They were tested at the same time each day for three consecutive days. Nerve latencies between different ethnic groups and genders were compared. Results show that there was no significant daily variation of the median motor and ulnar sensory latencies or the median sensory latencies. No significant differences of latencies was observed among ethnic groups; however, a significant difference of latencies between male and female subjects was observed ($p < 0.05$).

INTRODUCTION

Many studies have evaluated the effectiveness of nerve conduction devices as diagnostic tools for detection of carpal tunnel syndrome. Formal nerve conduction studies are considered "gold standard" for CTS diagnoses and abnormality in nerve function is considered one of the earliest indicators of a developing compression neuropathy [3,5,6]. The Nervepace Nerve Conduction Monitor S-200 is one example of a portable nerve conduction machine that measures both motor and sensory nerve latencies of the ulnar and median nerves. The machine's portability and ease of use have made it potentially attractive for health and safety officers interested in conducting active surveillance in the field. In addition, the actual testing requires 15 minutes to complete as compared to 30 - 45 minutes using the standard nerve conduction machine, and the average cost per test is $35 as compared to up to $500 for the standard nerve conduction study.

The present study evaluated the test-retest reliability of the Nervepace Monitor over three consecutive days. The mean motor and sensory latencies of the median and ulnar nerves were examined over this time period as well as interindividual variability based on age, gender, and race.

METHODS

Twenty eight (28) healthy employees of the Lawrence Livermore National Laboratory were recruited for the study. Of the 28 subjects, 17 were women, and 11 were men. Of these subjects, 13 were Caucasians, 4 were African-Americans, 3 were Hispanics, and 8 were Asians. Their occupations ranged from research assistants to electrical engineers. They ranged in age from 20-35. The subjects had no prior diagnosis or symptoms of carpal tunnel syndrome, nor did they have occupational or avocational risk factors for CTS.

Prior to testing, subjects were asked to sign a consent form and to complete an occupational health questionnaire to assess prior occupational history, hobbies and pre-existing work environments. The subjects also underwent vibrometry testing, as well as Phalen's and Tinel's exams in addition to nerve conduction tests. Testings were conducted at the same time each day for three consecutive days.

For each test, the ground electrode was placed on the dorsal side of the dominant hand. Electrode placement were made according to the directions suggested by the manufacturer. In median motor latency measurements, the

active electrode was placed over the abductor pollicis brevis muscle and the reference electrode was placed on the radial volar aspect of the proximal phalanx of the thumb. In median sensory latency measurements, the active electrode was placed around the proximal interphalangeal joint of the index finger, with the reference electrode around the distal interphalangeal joint of the index finger. In ulnar sensory latency measurements, the active electrode was placed around the proximal interphalangeal joint of the fifth digit and the reference electrode was placed around the distal interphalangeal joint of the little finger [4]. Hand temperatures were checked prior to testing, and all fell within normal range. All testings were performed in an examination room with room temperature set at 70° F.

The stimulus probe was coated with conductive gel and a mild electrical stimulus was applied 3 cm proximal to the distal wrist crease. The nerve latency is measured in milliseconds as the time between the application of the stimulus and the resulting action potential of the distal muscle over which the electrodes are placed. Five consecutive readings within 0.2 milliseconds of each other were recorded and averaged for each test session for the motor and sensory nerve latencies of both the median and ulnar nerves for each subject. All testings were performed by one tester trained in the proper use of the instrument.

RESULTS

In comparing the test results between days, we found that the results showed a high degree of intrarater reliability. The four sets of readings included motor median, motor ulnar, sensory median and sensory ulnar nerve latencies. Among the four, Friedman's Test indicated no significant differences in the latency measurements for motor median latencies, sensory median latencies, or sensory ulnar latencies. However, there was a significant difference in motor latencies of the ulnar nerve ($p < 0.05$).

The Wilcoxon Signed Rank test indicated that there were no significant differences between measurements taken on successive days except for the motor measurements of the ulnar nerve. The coefficient of variation was less than 0.22 for all measurements, with the variation for the motor latency of the ulnar nerve being highest. This indicates a high degree of repeatability in intrarater measurements. (Figure 1)

The data was also compared among different ethnic groups and genders. We found no significant differences among the different ethnic groups, but we did observe higher mean latencies ($p<0.05$) in men than in women (Figure 2).

DISCUSSION

The purpose of this study was to determine intrarater reliability of the Nervepace Nerve Conduction Monitor S-200. Overall, the data showed a high degree of intrarater reliability. The coefficient of variation between days for each measurement was small, and no significant differences were detected except in motor latencies of the ulnar nerve. The design of this study included repeated measures testing of the motor and sensory nerve latencies of the median and ulnar nerves over a period of three consecutive days. Electrode placement was an important factor in obtaining accurate results because misplacement of an electrode would significantly affect the accuracy of the results. With proper validation, it may be a reliable tool for detecting carpal tunnel syndrome at an early stage when combined with clinical findings.

CONCLUSION

The objective of this study was to test the Nervepace Nerve Conduction Monitor S-200 for reliability in repeated testing. After completing tests on 28 normal subjects for three consecutive days and at the same times on those days, the results showed little differences in the latency averages over three days of testing. In measurements of motor latencies of the median nerves, sensory latencies of the median and ulnar nerves, no significant differences in the latencies were found. In addition, no significant differences in latencies were found when comparing ethnic groups. Therefore, the Nervepace Nerve Conduction Monitor has a high degree of intrarater reliability. Further research is necessary to validate its diagnostic sensitivity and specificity, especially when combined with clinical findings.

REFERENCES

[1] Bureau of Labor Statistics Report on Survey of Occupational Injuries and Illnesses in 1977-1989 (1990). Washington, DC, Bureau of Labor Statistics, US Department of Labor.

[2] Gelberman RH, Szabo RM, Williamson RV, Dimick MP. (1983) Sensibility testing in peripheral nerve compression syndrome, J Bone Joint Surg, 65A:632-8.

[3] Gelberman RH, Aronson D, Weisman MH, (1980). Carpal tunnel syndrome-Results of a prospective trial of steroid injection and splinting, J Bone Joint Surg, 62A:1181-84.

[4] Neurotron Medical (1992). Nervepace Nerve Conduction Monitor Model S-200 Operating Manual, pp. 7-12.

[5] Szabo RM, Gelberman RH, Dimick MP, (1984). Sensibility testing in patients with carpal tunnel syndrome. J Bone Joint Surg, 66A:60-4.

[6] Thomas JE, Lambert EH, Cseuz KA, (1967). Electrodiagnostic aspects of carpal tunnel syndrome, Arch Neur, pp. 635-41.

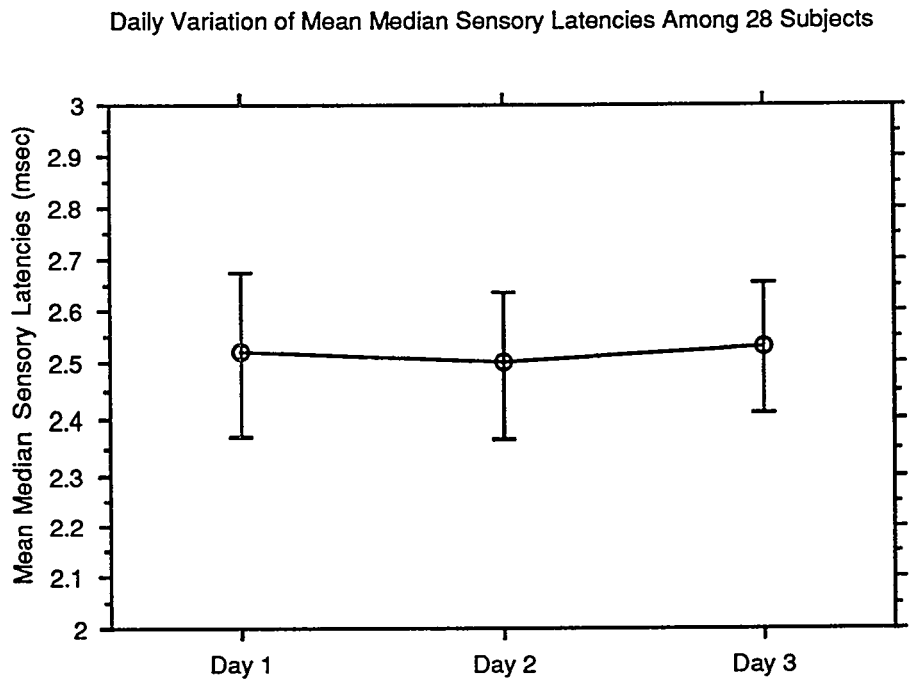

Figure 1: Results with 95% confidence error bars show no significant daily variation in the mean median sensory latencies among the 28 subjects tested.

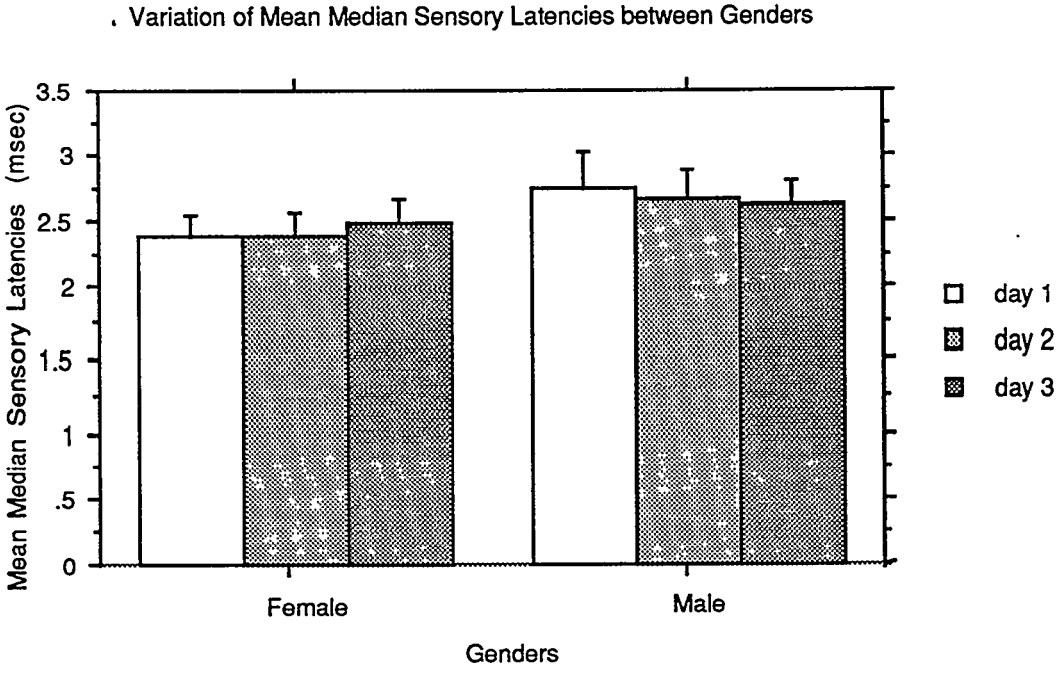

Figure 2: Results show a statistically significant difference in the mean median sensory latencies between males and females ($p < 0.05$)

The Contamination Analysis Unit (CAU)
Environmental Protection Department
Waste Minimization
Reasearch Report

Heidi K. Weber

May 1994

OUTLINE

I. Introduction

II. Background - Need for a Real-Time Contmination Analysis Unit
  A. Parts and Equipment cleaning - a major Quality-Assurance issue in all phases of Manufacturing
  B. Prestent Methods of High-Quality Cleaning
    1. expensive
    2. time-consuming
    3. impact production
    4. Examples: Overcleaning, Lab analysis - long turn around time
  C. Real-Time cleaning performance analysis provides potential financial benefits

III. Potential Applications for CAU
  A. TRW
    1. Contamination interferes with bonding of Pronted Board Assemblies
    2. Real-Time measurements could reduce work by identifying problems before bonding attempts
    3. Useful in failure analysis and troubleshooting
  B. Lockheed Fort Worth
    1. Contamination of organics and particulates interferes with adhesion of paint to primer on F-16 fighter planes
    2. Presently overcleaning everything to ensure quality
    3. Real-Time analysis would save time , money and materials
  C. Northrup
    1. Cleaning of composite substrates for aircrafts
    2. Potential to use this analysis in entire aerospace industry
  D. Support also shown by Boeing

IV. Analysis of Surface Contamination
  A. Hardware
    1. Placed against surface
    2. Volitized contaminants drawn into vaccuum (Rotary-Vane Pump, Turbomolecular Pump)
    3. Analyzed by Mass Spectrometer (Quadrupole)
  B. Software
    1. Compared to library to determine what contaminants are present (Real-Time, Modes (Analog, Bar, Table))

V. Future Stages of the CAU
  A. Shrink vaccuum chamber more
  B. Install laser or infrared beam source to volitize non-volitile contaminants.
  C. Install new and improved software based on LabView

VI. Conclusion

The Contamination Analysis Unit (CAU)

The Contamination Analysis Unit (CAU) is a new idea in Mass Spectrometry. The first of its kind, the CAU is a portable unit which will minimize waste in industry by developing an improved process to be performed on-site. Chemicals, labor, time, capital, and our environment are being wasted due to these old-fashioned procedures remaining at large industrial companies. The CAU is the new generation of instrumentation to avoid the waste in these areas.

Background - The Need for a Contamination Analysis Unit (CAU)

For years industry has been wasting precious resources due to a lack of proper instrumentation. More time, labor, capital and chemicals are spent than are actually needed because these industries do not have an on-site, real-time instrument to tell the workers that they have cleaned a given surface enough for Quality-Assurance. Pre-existent methods include over cleaning and lab analysis. Over cleaning wastes labor, chemicals, and capital. The overuse of these cleaning chemicals not only is a detriment to the company, but also the environment. The company not only has to clean their products, but they also have to pay for the disposal of these extra chemicals in a hazardous waste landfill. These costs add up quickly for these special wastes. The method of lab analysis is time consuming. Instead of cleaning the surface and moving on to the next level of production, the part must be transported to a laboratory to be analyzed and authorized by Quality Control. Extra costs associated with this method would be transportation costs, extra labor, and slowed production. A Contamination Analysis Unit (CAU) would relieve these problems by being able to analyze surfaces on-site and in a matter of minutes with no need for

over consumption of chemical cleaners.

One of the potential applications for the Contamination Analysis Unit would be at TRW. This company manufactures Printed Circuit Boards where contamination affects the assembly's overall performance. Contamination, such as flux, interferes with bonding of components to the board itself. The CAU would improve production in this area by taking real-time measurements and identifying problem contamination before bonding is attempted. Troubleshooting and failure analysis would also be made easier with the CAU.

Lockheed Fort Worth has also expressed interest in the CAU for their own purposes. The manufacturing of fighter planes requires precision and clean surfaces. The problem that the CAU could aid this industry with is organic and particulate contamination interfering with the adhesion of paint to the primer on the body of the plane. Presently, Lockheed is over cleaning everything to ensure a clean surface and successful adhesion. Real-time analysis would save the industry time, capital and material.

Lastly, Northrup is also in the aircraft industry, but they manufacture only composite substrates. This company has the same basic need for the CAU as Lockheed Fort Worth as far as needing a clean surface to ensure adhesion of paint to the primer surface. However, this surface being composite substrates opens up a new realm of products for the CAU to aid in the production processes. If the CAU can analyze these composites it has the potential to aid the entire aerospace industry.

The Contamination Analysis Unit (CAU)

The Contamination Analysis Unit is essentially the first compact vacuum chamber with a Mass Spectrometer inside. The fact that it is *portable* makes it unique to any other Mass Spectrometer made before. Portability is the key to this unit's success in the above mentioned applications. The CAU can be brought on-site for testing various surfaces with immediate results.

The procedure for operating the CAU is to bring the unit up to the surface that is to be analyzed. Place the opening against the surface and open the valve, making sure that the vacuum pressure is not decreased dramatically. The contamination is then brought up into the vacuum chamber and meets with the Mass Spectrometer. This is where the analysis is performed. The Quadrupole Mass Spectrometer determines the mass spectrum of the contaminants therefore determining the cleanliness of the surface. Each contaminant can be determined by the mass spectrum it produces. Key peaks in the spectrum are used to identify the contamination. For example, Trimsol can be identified by the peaks at masses 109, 111, and 180 m/z (see fig. 1). This procedure takes only a few minutes at the site, as opposed to the hours, possibly a full day, it took to determine the same results with the pre-existing procedures.

The software used for the CAU presently is a basic program that will produce a mass spectrum of the contamination in Analog and Bar modes. Bar mode is a way of seeing the intensity of each mass (up to 200 m/z). Analog views only the peaks of each mass intensity. Bar mode is what is used to determine the identifying spectrum for each contaminant, but Analog mode can be used thereafter for regular use. In either mode, the Electron Multiplier can be turned on. This feature bombards the sample with electrons and excites each element or compound. A smoother, more consistent spectrum is the result of using the Multiplier.

Tests and Results

Testing of the CAU and its abilities in the laboratory was performed in one general means. Samples of a known contamination were placed on a small slab of stainless steel and heated with a heat gun from behind the sample. This determined the optimum temperature to take sample spectra, which was narrowed to approximately 200 degrees Celsius. The sample spectra were then stored to a file within the software program on the hard drive of the PC. These files were then translated and transferred to Microsoft Excel © for analysis and plotting. The hard copies were then compared and contrasted to the results of the same contamination on a proven laboratory Mass Spectrometer (see fig. 1 & 2). The results coincided.

The next phase of testing was to determine if the CAU could pick up extremely small amounts of contamination on a given surface. Previous laboratory experiments tested various alternative solvents' performance by measuring the thickness of the layer of contamination remaining after cleaning. These layers were measured to only a few nanometers. Using the same procedure, these measured amounts of contamination were released into the CAU for analysis. The instrument picked up enough of the contamination to be identified easily on the mass spectrum. The key peaks were present and distinguishable even at such small amounts.

Future Stages of the CAU

The future holds several improvements for the CAU. Immediate changes include shrinking the vacuum chamber more to make it easier to handle. The present prototype weighs approximately forty to fifty pounds (see fig. 3). The next unit is expected to be closer to twenty pounds and be less cumbersome (see fig. 4). New changes will also include a laser or infrared source attached to the inside of the vacuum chamber for the purpose of heating the sample exactly where the contamination sits on the surface. The

present method in the laboratory would not be valid out on-site since most of the applications involve large surfaces, like airplane wings. Heating the back side of this massive piece of metal would not work as it does with the small samples in the laboratory. The last immediate change to be made on the CAU is the software program being used. The present software is operational but not very resourceful. The SQX software allowed for the start up and basic functions needed to prove that this unit works, but more is needed for the unit to progress to its more complex phases and be user friendly in the field. The new software being looked at presently is built on LabView© and is programmable for several various applications. It is believed that this software will progress the CAU to a higher level of convenience and complex functionality.

Conclusion

The Contamination Analysis Unit (CAU) is a revolutionary product for several industries. The ease and convenience of the process will save many companies across the country in many ways mainly through avoidance costs of disposal, transportation to laboratories, and labor. From an environmental standpoint, the CAU will save energy, wasted chemicals, and extend the life of hazardous waste facilities through minimizing industrial waste.

CAU Mass Spectrum of Trimsol Contamination

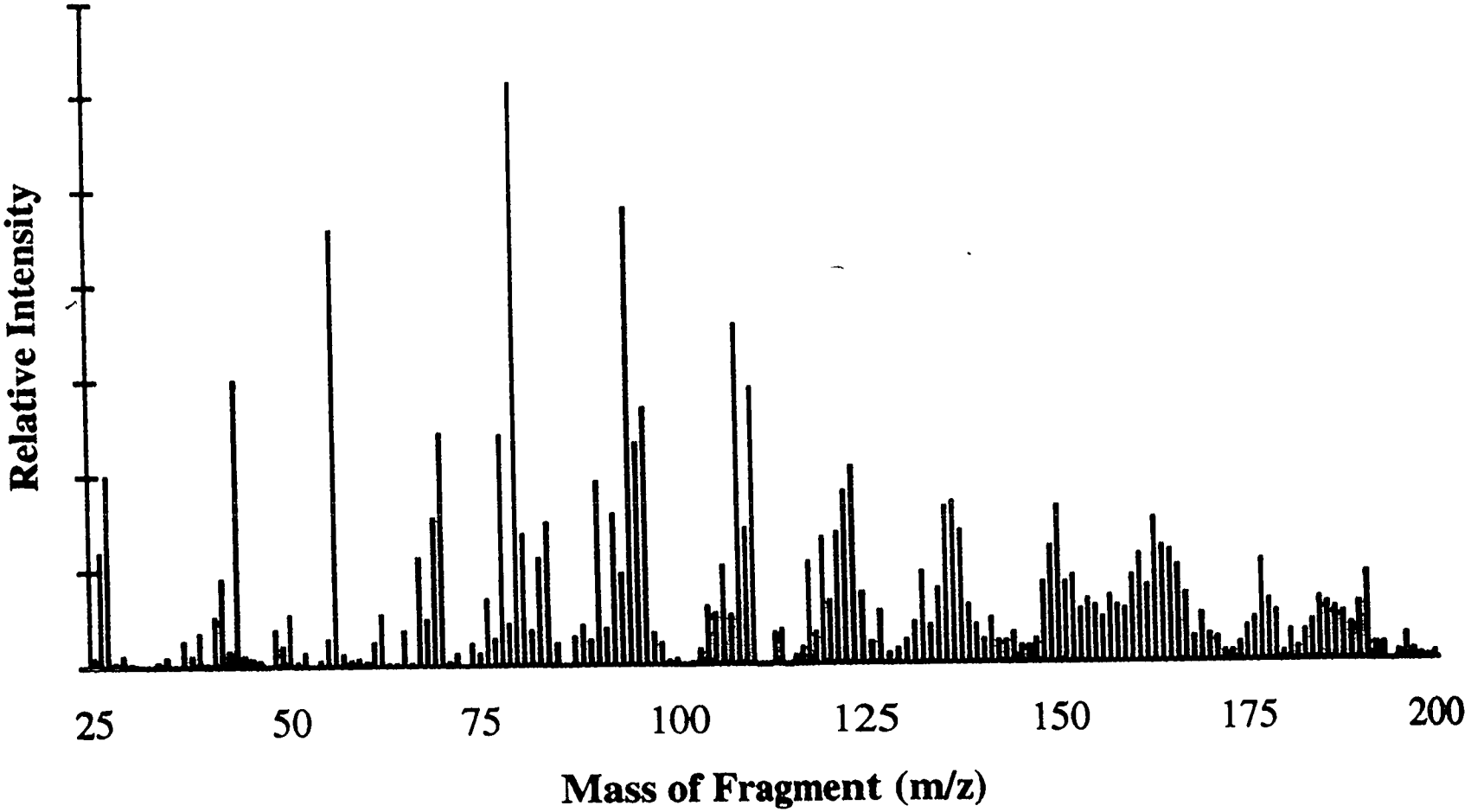

fig 2

Mass Spectrum of Trimsol Contamination @220°C

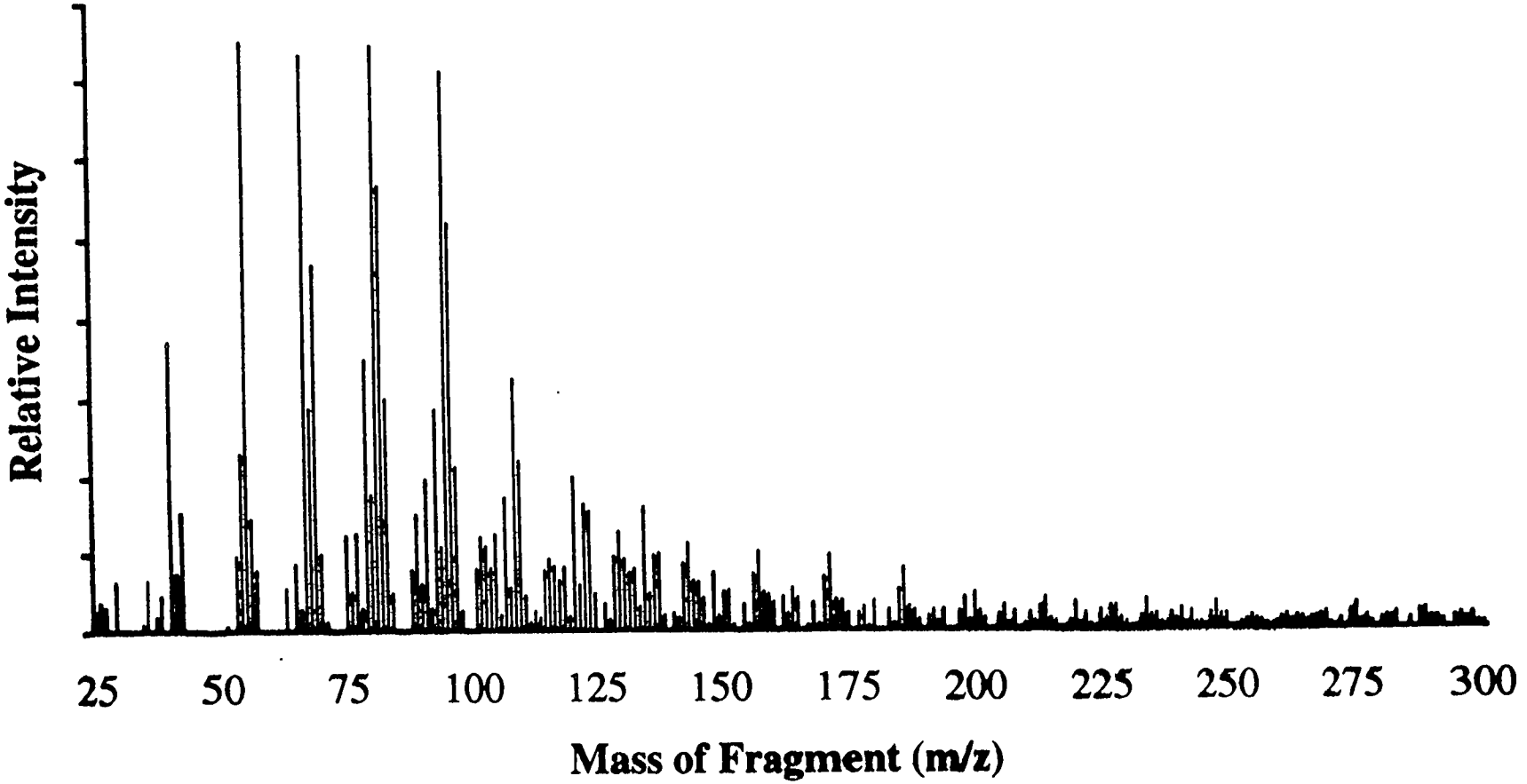

Phase I System: Portable Contamination Analysis Unit

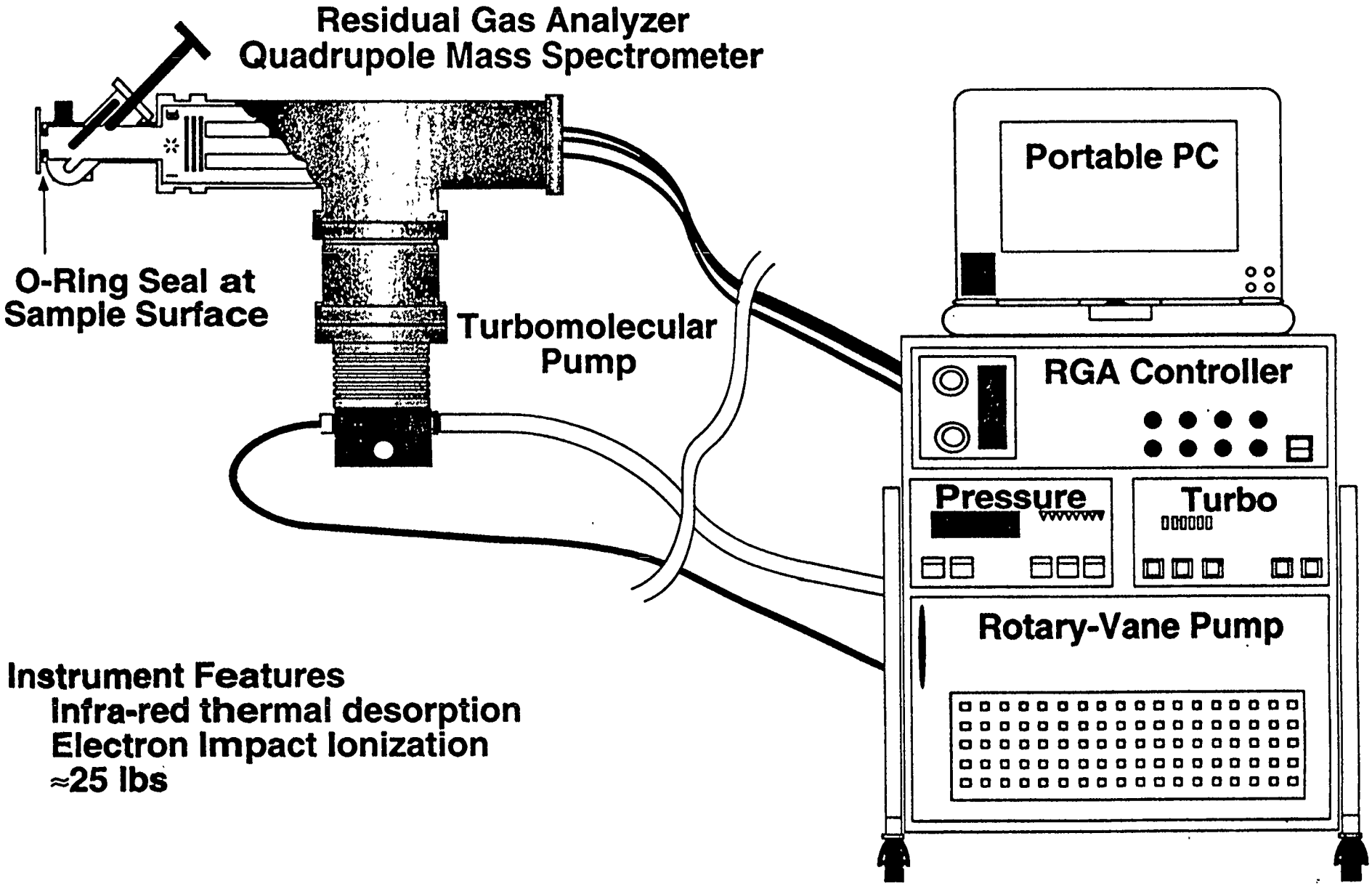

Instrument Features

- Infra-red thermal desorption
- Electron Impact Ionization
- ≈25 lbs

fig 4

Phase II System: Surface Analysis Mass Spectrometer

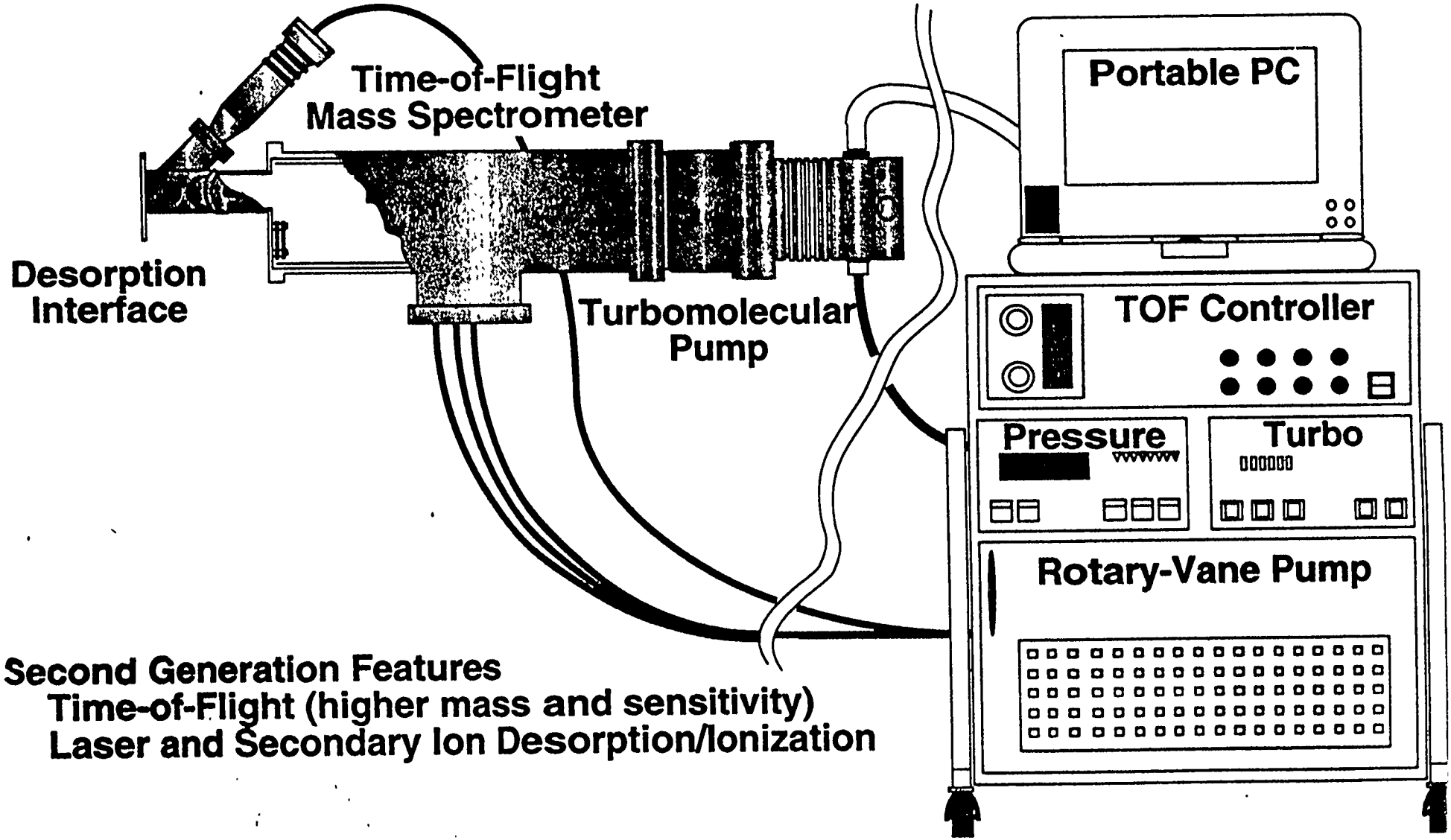

Second Generation Features

- Time-of-Flight (higher mass and sensitivity)
- Laser and Secondary Ion Desorption/Ionization